

AD-A105 088

PHYSICAL RESEARCH INC PALOS VERDES ESTATES CA

F/G 20/4

HIGH REYNOLDS NUMBER CYLINDER FLOW WORKSHOP, 27-28 NOVEMBER 197--ETC(U)

AUG 81 W C SHIH

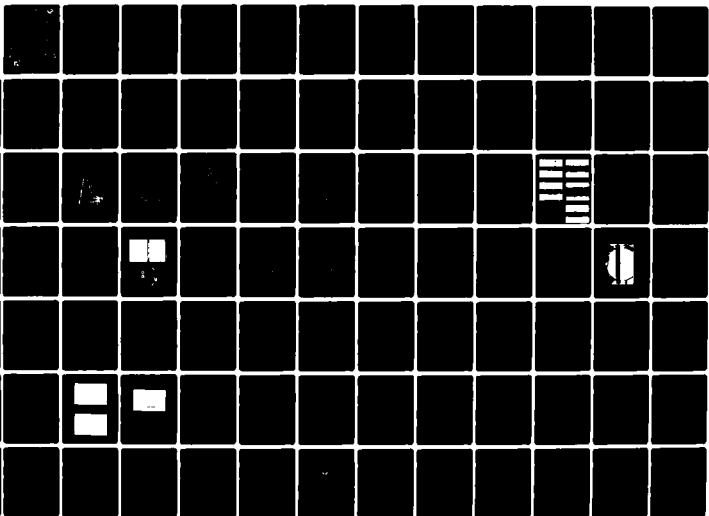
N00014-79-C-0893

PRI-LA-81-R003

NL

UNCLASSIFIED

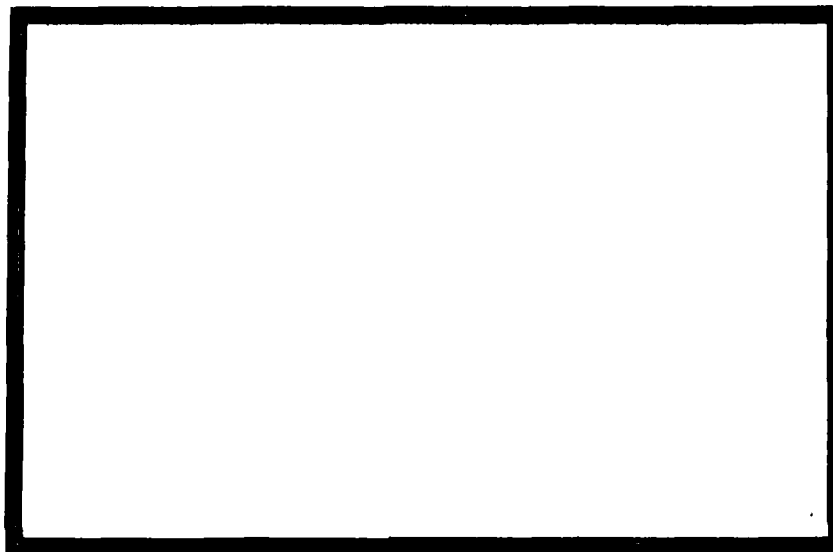
1 OF 2
ADA
105 088



LEVEL *II*

2

AD A105088



gm

DTIC FILE COPY

DTIC
ELECTE
OCT 6 1981
S D D



DISTRIBUTION STATEMENT A

Approved for public release;
Distribution Unlimited

Physical Research, Inc.

2668 Via Olivera, Palos Verdes Estates, California 90274 (213) 377-5845
2608 Hickory Flats Trail S.E. Huntsville, Ala. 35801 (205) 883-6659

X-4
81 10 5 016

Accession For		
NTIS GRA&I	<input checked="" type="checkbox"/>	
DTIC TAB	<input type="checkbox"/>	
Unannounced	<input type="checkbox"/>	
Justification		
By		
Distribution/		
Availability Codes		
Avail and/or		
Dist	Special	
A		

HIGH REYNOLDS NUMBER CYLINDER FLOW WORKSHOP

FINAL REPORT

17 AUGUST 1981

PR1-LA-81-R003

PREPARED FOR:

SCIENCE APPLICATIONS, INC.
101 CONTINENTAL BLVD.
EL SEGUNDO, CA 90245

AND

OFFICE OF NAVAL RESEARCH
OCEAN TECHNOLOGY PROGRAM
OCEAN SCIENCE AND TECHNOLOGY PROGRAM
800 NORTH QUINCY STREET
ARLINGTON, VA 22217

UNDER CONTRACT
N00014-79-C-0893

PHYSICAL RESEARCH, INC.

2668 VIA OLIVERA, PALOS VERDES ESTATES, CA 90274 (213) 377-5845
2608 HICKORY FLATS TRAIL S.E., HUNTSVILLE, AL 35801 (205) 883-6659

DTIC
SELECTE
OCT 6 1981
D

DISTRIBUTION STATEMENT A

Approved for public release;
Distribution Unlimited

412571

Unclassified

SECURITY CLASSIFICATION OF THIS PAGE (When Data Entered)

REPORT DOCUMENTATION PAGE		READ INSTRUCTIONS BEFORE COMPLETING FORM
1. REPORT NUMBER PRI-LA-81-R003 4	2. GOVT ACCESSION NO. AD-A305088	3. RECIPIENT'S CATALOG NUMBER
4. TITLE (and Subtitle) High Reynolds Number Cylinder Flow Workshop, 27-28 November 1979.	5. TYPE OF REPORT & PERIOD COVERED Final Report.	
7. AUTHOR(s) Dr. W. C. L. Shih	6. PERFORMING ORG. REPORT NUMBER PRI-LA-81-R003	
9. PERFORMING ORGANIZATION NAME AND ADDRESS Physical Research, Inc. 2668 Via Olivera Palos Verdes Estates, California 90274	8. CONTRACT OR GRANT NUMBER(s) N00014-79-C-0893	
11. CONTROLLING OFFICE NAME AND ADDRESS Office of Naval Research 800 N. Quincy Street Arlington, Virginia 22217	10. PROGRAM ELEMENT, PROJECT, TASK AREA & WORK UNIT NUMBERS	
14. MONITORING AGENCY NAME & ADDRESS (if different from Controlling Office) 12 98	12. REPORT DATE 17 August 1981	
	13. NUMBER OF PAGES 88	
	15. SECURITY CLASS. (of this report) Unclassified	
16. DISTRIBUTION STATEMENT (of this Report) Approved for public release; distribution unlimited		
17. DISTRIBUTION STATEMENT (of the abstract entered in Block 20, if different from Report)		
18. SUPPLEMENTARY NOTES		
19. KEY WORDS (Continue on reverse side if necessary and identify by block number) Cylinder Flow, Drag Coefficient, Lift Coefficient, Vortex Shedding, High Reynolds Number Flow, Turbulence, Roughness Effects, Spanwise Flow, Wind Tunnel Testing, Cylinder Wake Structure		
20. ABSTRACT (Continue on reverse side if necessary and identify by block number) The Office of Naval Research and NASA Ames Research Center sponsored a workshop on High Reynolds Number Cylinder Flows, held at Ames on 27-28 November 1979. The purpose of the workshop was to review the state of knowledge of high Reynolds number (incompressible) rigid cylinder flows, to identify problem areas, and recommend research for understanding these flow conditions. The recommendations are being incorporated into the design of a comprehensive experiment that is scheduled for Spring of 1982 in the Ames 12-foot pressurized wind tunnel.		

FOREWARD

The Office of Naval Research and NASA Ames Research Center sponsored a workshop on High Reynolds Number Cylinder Flows, held at Ames on 27-28 November 1979. The purpose of the workshop was to review the state of knowledge of high Reynolds number (incompressible) rigid cylinder flows, to identify problem areas, and to recommend necessary research work for the fundamental understanding of such flows. The recommendations are being incorporated into the design of a comprehensive experiment sponsored by ONR and NASA and scheduled for Spring of 1982 at Ames in the 12 Foot Pressurized Tunnel.

Dr. Eugene Silva was the Technical Monitor from ONR and Dr. Gerald Malcom of NASA Ames was the coordinator at Ames and made all the necessary arrangements for holding the meeting there. The overall coordinator was Dr. W.C.L. Shih of SAI now with Physical Research, Inc. We take this opportunity to express our appreciation to all the attendees who contributed to a very informative and interesting meeting.

ATTENDEES

<u>Name</u>	<u>Affiliation</u>	<u>Phone Number</u>
Clyde Allen	NASA/Ames	(415) 965-6258
Ben Cagle	ONR	(213) 795-5971
Brian Cantwell	Stanford Univ.	(415) 497-4825
Donald Coles	Cal Tech	(213) 795-6811 Ext. 1483
Doug Deffenbaugh	TRW	(213) 536-1547
Phil Engelauf	NASA/Ames	(415) 965-5876
Lars Ericsson	LMSC	(408) 743-2535
Cesar Farell	Univ. of Minnesota	(612) 373-2783
Duane Hove	SAI	(213) 640-0480
Joe Katz	NASA/Ames	(415) 965-6877
Earl R. Keener	NASA/Ames	(415) 965-6272
Frank Kmak	NASA/Ames-FAX	(415) 965-6701
Gerald Malcolm	NASA/Ames	(415) 965-6266
Mark V. Morkovin	IIT	(312) 383-0973
Kevin Owen	Self-Employed	(425) 327-9674
Bill Rose	Rose Engineering & Research Inc.	(702) 831-5094
Anatal Roshko	Cal Tech	(213) 797-7185
Dwight Sanderfer	NASA/Ames	(415) 965-6260
Lewis Schiff	NASA/Ames	(415) 965-6265
Dick Schwind	NEAR	(415) 968-9457
Steve Sheffield	TRW	(213) 536-1547
W.C.L. Shih	SAI	(213) 377-5845
E. A. Silva	ONR	(202) 696-7358
Murray Tobak	NASA/Ames	(415) 956-5398
G. H. Toebes	Purdue	(317) 749-2075

HIGH REYNOLDS NUMBER CYLINDER FLOW WORKSHOP

AGENDA

27-28 November 1979

27 November 1979

Opening Remarks	W. Shih	9:00-9:15am*
Welcome	G. Malcom	9:15-9:30
Overview	G. Silva	9:30-9:45
Navy Requirements	T. Ward	9:45-10:35
Break		10:35-10:45
Review of Flow Around Rigid Cylinders	A. Roshko/ D. Coles	10:45-11:35
Discussions		11:35-12:00
Lunch		12:00-1:00pm
Effects of Roughness and Stream Turbulence	C. Farell	1:00-1:50
Effects of Cylinder Motion	T. Sarpkaya	1:50-2:40
Analytical Models	D. Deffenbaugh	2:40-3:30
Effects of Spanwise Nonuniformities	D. Coles/ A. Roshko	3:30-4:20
Discussions		
Dinner Working Session	Holiday Inn, Sunnyvale	6:30-

28 November 1979

Tour of 12' Pressurized Wind Tunnel and View of Model	G. Malcom	8:30-9:30am
Proposed Cylinder Tests	W. Shih	
Discussion/Recommendations	Attendees	9:30-12:00n
Summary	W. Shih	

*Time includes 20-30 minutes for free discussions after or during each presentation.

TABLE OF CONTENTS

	<u>Page</u>
Opening Remarks	1
Welcome	1
ONR Overview.	1
Navy Requirements	2
High Reynolds Number Flow Regimes	2
Review of Flow Around Rigid Cylinders	4
NASA/ISU Experiments.	18
Near Wake Measurements.	23
Skin Friction Measurements.	35
Effects of Roughness and Stream Turbulence.	42
Freestream Turbulence in the 12-Foot Tunnel	49
Unsteady Flow About Bluff Cylinders	52
Analytical Models	52
Effects of Spanwise Nonuniformities	53
Effects of Cylinder Motion.	69
Proposed Cylinder Tests	75
Summary of Recommendations Made at the Workshop	85
References.	87

LIST OF TABLES

Table 1 - Run Matrix.	43
Table 2 - Proposed NASA Ames Test Matrix.	84

LIST OF FIGURES

<u>Figure</u>		<u>Page</u>
1	Flow Regimes for Flows Past Circular Cylinders . .	3
2	Pressure Coefficient at Rear Point of Circular Cylinder	5
3	Review of Cylinder Drag Coefficients	8
4	Vortex Shedding Frequency for Circular Cylinder (1) and 11-1/4 Degree Wedge (2).	9
5	Drag Coefficient Correlation with Base Pressure Coefficient.	11
6	Drag Coefficient - Strouhal Number Correlation . .	13
7a	Strouhal Number, Pressure Fluctuation-Separation Angle Correlation.	14
7b	Arrangement for Measuring the Value of Critical Circulation.	15
7c	The Critical Angle Difference to Stop Coherent Vortex Shedding.	16
7d	The Critical Amounts of Admissible Circulation Required to Prevent Coherent Vortex Shedding . . .	17
8	Fluctuating Lift Coefficient	19
9	Operating Characteristics of the Ames 12-Foot Pressure Wind Tunnel	20
10	Model Support and End-Plate Location for 15.24 cm Circular Cylinder.	21
11	Location of Instrumentation on the 31.65 on Circular Cylinder.	21
12	Variation of Crossflow Drag Coefficient with Crossflow Reynolds Number for Circular Cylinders at Crossflow Mach Numbers ≤ 0.4	22
13	Pressure Coefficient Distribution.	24
14	Outboard Pressure Distribution on 15.24 cm Circular Cylinder with End-Plates.	25
15	Outboard Pressure Distribution on 15.24 cm. Circular Cylinder with End-Plates.	26
16	Outboard Pressure Distributions on 31.65 cm and 45.16 cm. Diameter Circular Cylinders	28
17	15 Second Scope Traces of Kulite Output.	29
18a	Fluctuating Pressure Distribution.	30
18b	Fluctuating Pressure Distribution.	31

<u>Figure</u>		<u>Page</u>
18c	Fluctuating Pressure Distribution.	32
18d	Fluctuating Pressure Distribution.	33
18e	Fluctuating Pressure Distribution.	34
19	Photos of Buried Wires	36
20a	Calibration in Laminar Flow.	37
20b	Example of Data Obtained in Turbulent Flow	38
20c	Example of Data Obtained in Turbulent Flow	39
21	Surface Phenomena Inferred from Data	40
22	Example of Rough Surface Data.	41
23	Circular Cylinder Model in CalTech 10-Foot Tunnel.	44
24	Pressure Distributions From CalTech Tests.	45
25	Cylinder Spanwise Pressure Distributions from CalTech Tests	46
26	Drag Coefficient	47
27	Roughness Effect on Drag Coefficient	48
28	Power Spectral Density Plots of the Lift Coefficient	50
29	Effects of Relative Roughness on Strouhal Number in Reynolds Numbers Independence Regime.	51
30a	Discrete Vortex Model Early Time Flow Field Development.	54
30b	Discrete Vortex Model Wake Development $t=25.0$. . .	55
31	Discrete Vortex Model, Boundary Layer Separation Angle.	56
32	Discrete Vortex Model, Pressure Coefficient. . . .	57
33	Discrete Vortex Model, Drag Coefficient.	58
34	Discrete Vortex Model, Lift Coefficient.	59
35a	Wake Structure for Uniform Cylinder.	62
35b	Wake Structure for Tapered Cylinder.	63
35c	Wake Structure for Cylinder with a 2:1 Discontinuity in Diameter.	64
36	Vortex-Excited Displacement Response of a Flexible Cantilever (from equilibrium) in the In-Line Direction Plotted Against the Reduced Velocity $V/f_n D$. The Reduced Damping of the Structure is Denoted by k_s	71

<u>Figure</u>		<u>Page</u>
37	Cross Flow-Induced Vibration Displacement E/D and Frequency F of Three Circular Cylinders in Water, Plotted Against the Reduced Velocity V_r	72
38	Composite Stability Diagram for the First Three Normal Modes of a Flexible, Cantilevered Circular Cylinder as a Function of the Incident Water Velocity. Both In-Line and Cross Flow Instabilities are Shown	73
39	Maximum Vortex-Excited Flow Displacement $2Y_{EFF,MAX}$ of Circular Cylinders Plotted Against the Reduced Damping $\zeta_S/\mu = 2\pi St^2 (2m\delta/\rho D^2)$	74
40	The Excitation Component C_{LE} of the Lift Force Plotted Against the Vortex-Excited Cross Flow Displacement $2Y_{EFF,MAX}$ (peak-to-peak). The Legend for the Data Points is Given in Figure 39	76
41	A Comparison of the Full Scale and 1/27-Scale Model Results for Vortex-Excited In-Line Oscillations of a Flexible, Cantilevered Circular Cylinder. The Full-Scale Reynolds Number was about $6(10^5)$	77
42	Model Instrumentation at 0 Degrees Roll Angle	79
43	Hot-Wire Gauge Mount	81
44	Grommet and Safety Wire Screen Attachment Design.	83

Opening Remarks

W. Shih of SAI opened the Workshop with a brief discussion of the reasons for holding such a meeting which has already been summarized in the Foreword. To reiterate, the main output of the Workshop is to obtain inputs for the forthcoming test at Ames. After a few administrative details, an overall summary of the two-day program was presented. Free discussions of the presentations were encouraged so that the summary of the talks here will also include any relevant comments from the audience.

Welcome

G. Malcom of Ames welcomed the participants and gave a brief overview of how Ames became involved in high Reynolds number cylinder flow work. Initially the main motivation was in obtaining relevant data for missiles at high angles of attack. Some tests were conducted by James of Iowa State University with the support of Ames. At that time, ERDA expressed interest in high Reynolds number flows around cylinders because of concerns for hydrodynamic loads on the OTEC cold water pipe. Tests were scheduled at Ames making use of the model and some of the instrumentation that were made available from the ISU/NASA experiments. Unfortunately, tunnel problems delayed these tests by more than one year by which time the ERDA program had to be completed and the effort was redirected.

Because of the availability of the model and instrumentation at Ames, ONR expressed interest in sponsoring a fundamental study of high Reynolds number cylinder flows. This interest included the sponsorship of this meeting along with NASA Ames to help design a well conceived fundamental experiment.

ONR Overview

E. Silva of ONR gave an overview of the navy interests in high Reynolds number flow phenomena. The Navy has interest in large manned offshore structures to house bases and other test

facilities to minimize community encroachment resulting in need for design data at the anticipated high Reynolds numbers. Interest in the higher speed regimes also spell out the need for high Reynolds number flow data. Some large structure data exist in the Offshore community in the private sector; however, these are not generally available to the general scientific community since they are proprietary in nature. It is hoped that we take full advantage of the current opportunity to get the most out of this work to obtain both the needed engineering data as well as the scientific aspects of the problem.

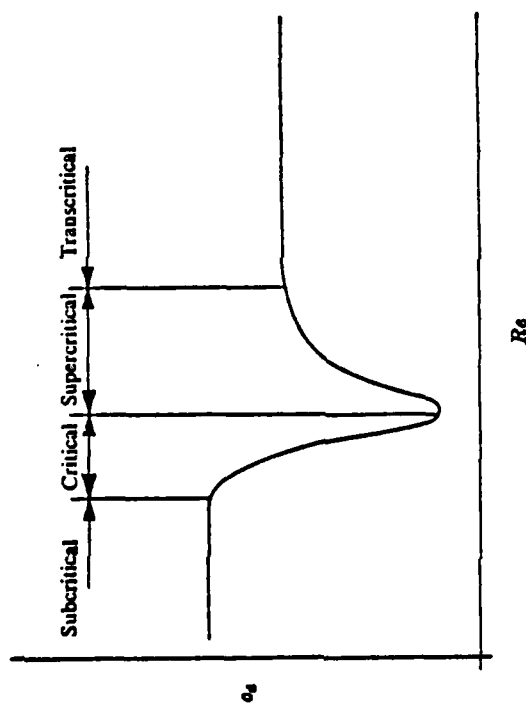
Navy Requirements

T. Ward of CEL in Port Hueneme was unable to attend the meeting due to Navy travel restrictions so that W. Shih summarized Mr. Ward's comments concerning his view of Navy requirements.

CEL has and is currently sponsoring research in areas dealing with flows about underwater cable arrays for Reynolds numbers less or equal to 10^6 ; guide towers in the range $Re \leq 10^7$; large ocean structures for $Re \leq 10^8$; and development of strumming suppression devices for reducing flow-induced oscillations. Present CEL needs include data for drag and lift coefficients on structures in the Re range of 10^6 - 10^8 including the effects of freestream turbulence and shear flows; drag and lift for arrays; effect of roughness and its distribution on vortex shedding; and correlation methods for assessing strumming suppression devices.

High Reynolds Number Flow Regimes

The various Reynolds number flow regimes as defined by Roshko are shown schematically in Figure 1 in terms of the behavior of the drag coefficient. The subcritical regime is associated with the region for which Re is less than that at which minimum drag (drag crises) occurs. The critical regime refers to the region where the drag coefficient undergoes a



Smooth Cylinders

Subcritical - $Re < 2 \times 10^5$

Critical - $2 \times 10^5 < Re < 5 \times 10^5$

Supercritical - $5 \times 10^5 < Re < 3.5 \times 10^6$

Transcritical - $Re > 3.5 \times 10^6$

FIGURE 1. Flow Regimes for Flows Past Circular Cylinders

sharp decrease toward the drag minimum; supercritical regime is in the upper transition region as the drag increases from its minimum value; and finally the transcritical regime where no significant new flow phenomena associated with transition is expected and the drag curve flattens out. The high Reynolds number region that we refer to here is the transcritical region.

Review of Flow Around Rigid Cylinders

Professor A. Roshko of CalTech presented a review of cylinder flow phenomena beginning with a description of the general parameters of interest which are C_D , $C_p(0)$, $C_L(t)$, $C_p(t)$, and S and are, respectively, the drag coefficient, pressure coefficient distribution around the cylinder, the time fluctuating lift and pressure coefficients and the dominant nondimensional vortex shedding frequency or Strouhal number. In general, these are functions of the Reynolds number, Re . In addition, external parameters are the relative roughness, k/D , freestream turbulence scale as well as intensity are important. Geometric parameters such as end configuration, and cylinder taper also contribute to the nature of the flow around the cylinder.

The flow about the cylinder undergoes significant changes as the Reynolds number is varied. The base pressure coefficient, Figure 2, is a more sensitive indication of the various Reynolds number ranges than the drag coefficient, since the latter is an integrated quantity.

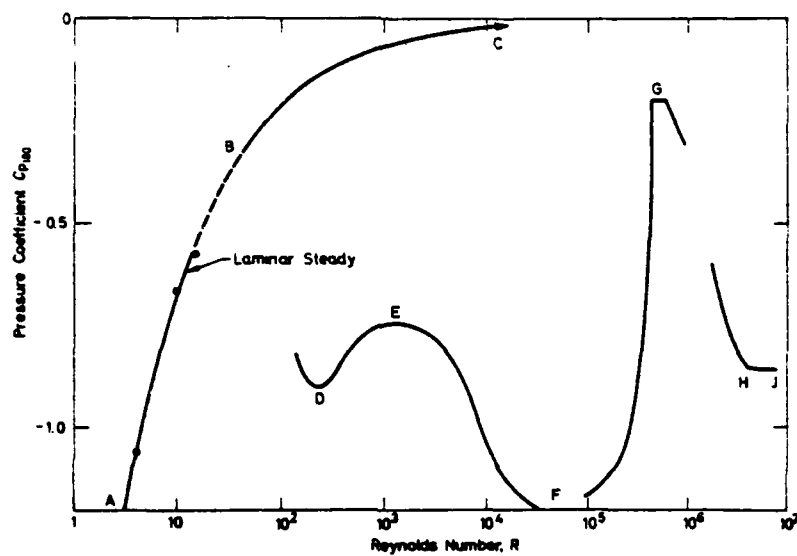


FIGURE 2. Pressure Coefficient at Rear Point of Circular Cylinder

Up to an Re of 50 the flow is laminar and steady and can and has been calculated with digital computers using the steady Navier-Stokes equations. Some results at the lower Reynolds numbers are shown in Figure 2 and the curve is drawn through these points. Previous calculations were reliable only up to an Re of 50 but more recently, Ohrenberg of CalTech has obtained results up to about Re of 400. Other calculations at higher Re have been shown to be dubious in nature. If the flow remained laminar and steady, the base pressure curve would be expected to follow along B-C in Figure 2. Actually, the wake becomes unstable and begins to oscillate at an Re of about 50, and the base pressure coefficient decreases with increasing Re . Up to about Re of 2×10^5 , regular periodic vortex shedding takes place with transition to turbulence starting in the wake and into the separated shear layers. This entire region, termed subcritical, can be characterized as a transitional region made up of a variety of modes as turbulent flow spreads in the separated region and separation of the laminar boundary layer occurs on the front portion of the cylinder. At Re between 2×10^5 and 5×10^5 , the critical region, the base pressure rises as the drag coefficient decreases drastically. This phenomenon was first explained by the Gottingen people in Germany who attributed the behavior to transition to turbulence of the boundary layer permitting it to support the adverse pressure gradient further back along the cylinder thereby delaying separation and resulting in a lower drag coefficient. It was actually discovered, years later, that separation still occurred at the same location as in sub-critical flow, but the transition in the wake had moved into the shear layer so close to the separation point that it allowed the boundary layer to

reattach thus forming a separation bubble. The combination of the bubble and reattached boundary layer can better withstand the pressure gradient than a boundary layer that has undergone transition on the cylinder surface thus explaining the very high base pressure coefficient and the resulting minimum in the drag curve. Further increases in Re causes the transition to move on to the cylinder surface and the boundary layer undergoes a transitional separation with an attendant upstream movement of the separation point and increase in the drag coefficient. The region where the drag coefficient levels off and the boundary layer becomes fully turbulent prior to separation is termed the transcritical, i.e., beyond critical, region. Some controversy concerning the naming of the super- and trans- critical regions has occurred in the literature but because of historical precedence and to avoid confusion we shall use the terms as defined here.

Figure 3 is a compilation of drag data plotted against Re . The large amount of scatter in the data are due, probably, to effects of transition which is very sensitive to surface roughness and freestream turbulence, particularly in the critical regime. In the transcritical region when the boundary layer is already turbulent, the surface roughness will have the major influence on the boundary layer behavior. Since transition has already occurred, freestream turbulence will not have much effect on the boundary layer or the near wake.

The Strouhal number variation with Re , Figure 4, does not exhibit the wild gyrations as the base pressure coefficient. As Re increases from about 50 where periodic vortex shedding first appears, S increases until about 0.2 and stays nearly constant until the critical regime where it begins to increase with Re through the supercritical regime and appears to settle to a somewhat higher value of about 0.3 in the transcritical regime. Generally, S , does not vary significantly with Re as does the base pressure coefficient. It is important to recognize that S

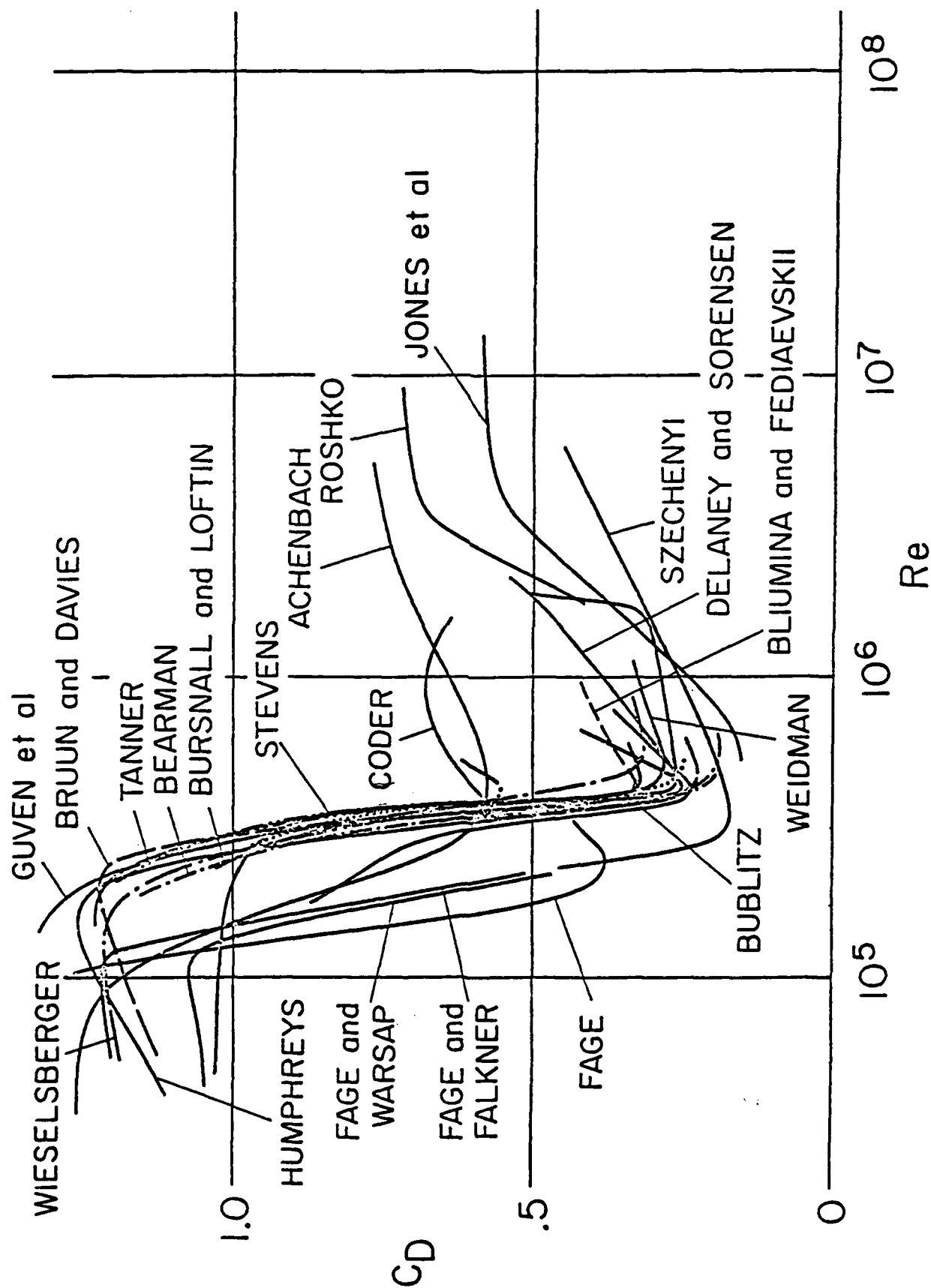


FIGURE 3. Review of Cylinder Drag Coefficients

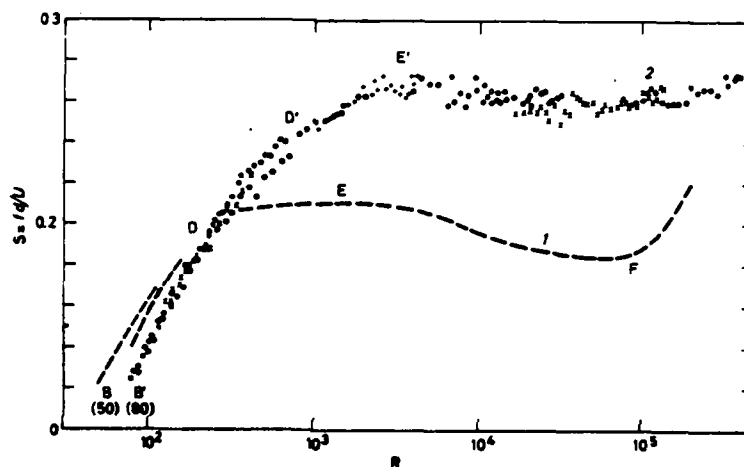


FIGURE 4. Vortex Shedding Frequency for Circular Cylinder (1) and 11-1/4 Degree Wedge (2)

is a local property which may or may not persist along the entire cylinder span whereas the drag coefficient is a global, usually sectional, integrated quantity. Existing measurements do not indicate the strength of the vortices as they are shed locally. This is particularly true in the critical Re regime where vortex shedding along the cylinder is less coherent and measurements of Strouhal frequency along the cylinder may not yield correlated results.

Much of the scatter in the plots versus Re can be reduced by some simple cross plots of, e.g., C_D vs S, C_{pb} vs S or C_D vs C_{pb} . These may be useful correlations and should be further examined particularly in the transcritical regime where one might expect Re dependence becoming less important except in the stagnation region laminar boundary layer before transition. Roughness becomes one of the more important parameters. As an example of an alternative plot consider Figure 5 of C_D vs C_{pb} comparing free streamline theory predictions and some experimental points. The important point is that there appears to be two branches to the curve: one for separation forward of 90 degrees and one for separation aft of 90 degrees with the cross over point at 90 degrees. Although at present there is no data, it is conjectured that a maximum in C_D occurs corresponding to a base pressure coefficient minimum. This is a double sheeted problem in free streamline theory. Each of these two branches map onto a different sheet in the hodograph plane. For the branch with forward separation, the minimum drag coefficient is about 0.5 with a separation point of 55 degrees. Separation upstream of this is unlikely. For aft separation, conceivably, if the boundary layer did not separate, the drag coefficient would go to zero on the other branch.

Other parameters have been plotted to determine if some correlation may be achieved. In particular, from the work of Naumann and Morsbach presented at the 1972 Karlsruhe Flow Induced

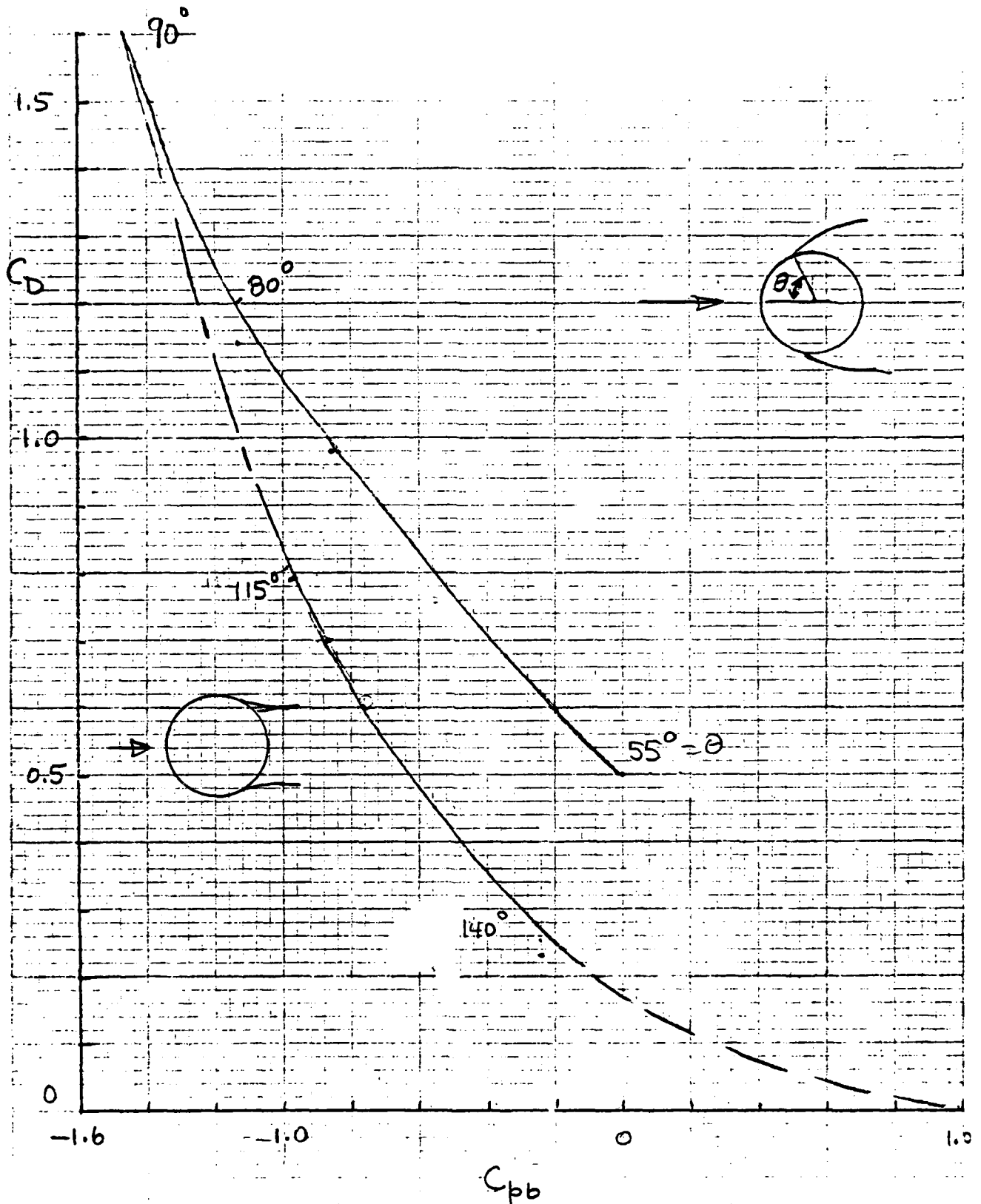


FIGURE 5. Drag Coefficient Correlation with Base Pressure Coefficient (Roshke)

Vibrations Conference, correlations of their experimental data with other parameters were attempted. They forced transition on the cylinder with trips at various locations on the cylinder and determined if correlations existed. Figure 6 is a plot of C_D vs S and SC_D vs S which is nearly constant. There does not appear to be a double sheet for this plot. A correlation of S vs the separation angle, α , is shown in Figure 7a. The correlation for bare cylinders as well as ones with the separation wires seem to indicate independence of how separation occurred. Another experiment using two wires as shown in Figure 7b was performed to study the influence of the relative wire location on coherent vortex shedding. Placement of the wires was important since flow reattachment would occur if, for example, they were placed too far upstream of the natural separation point. Their work was performed in the critical-supercritical Reynolds numbers range where separation angle is sensitive to surface conditions. The circumferential location of the separation wires and the spanwise extent were controlled in the experiments. Coherent vortex shedding could be stopped by placing the wires far apart along the span as governed by the parameter, $2a/t$. When $2a/t$ is one (see Figure 7b), the flow would be two-dimensional, and when zero, the disturbance was zero. The minimum circumferential separation angle of the wires to stop coherent vortex shedding is shown in Figure 7c for various wire lengths plotted as a function of the circumferential location of the first wire. On the basis of results in Figure 7c, the change in circulation required to stop coherent shedding was deduced and is shown in Figure 7d where $\sqrt{2}$ is the circulation in the shed vortex. These experiments are important relative to reducing the effects of flow-induced oscillations with a lesser drag penalty than with, say helical strakes. In fact roughness strips may produce the same effect although no study was made of the scaling with wire or roughness size. These results are found in Morsbach's thesis published in 1966. The planned ONR/NASA experiments should be a test of

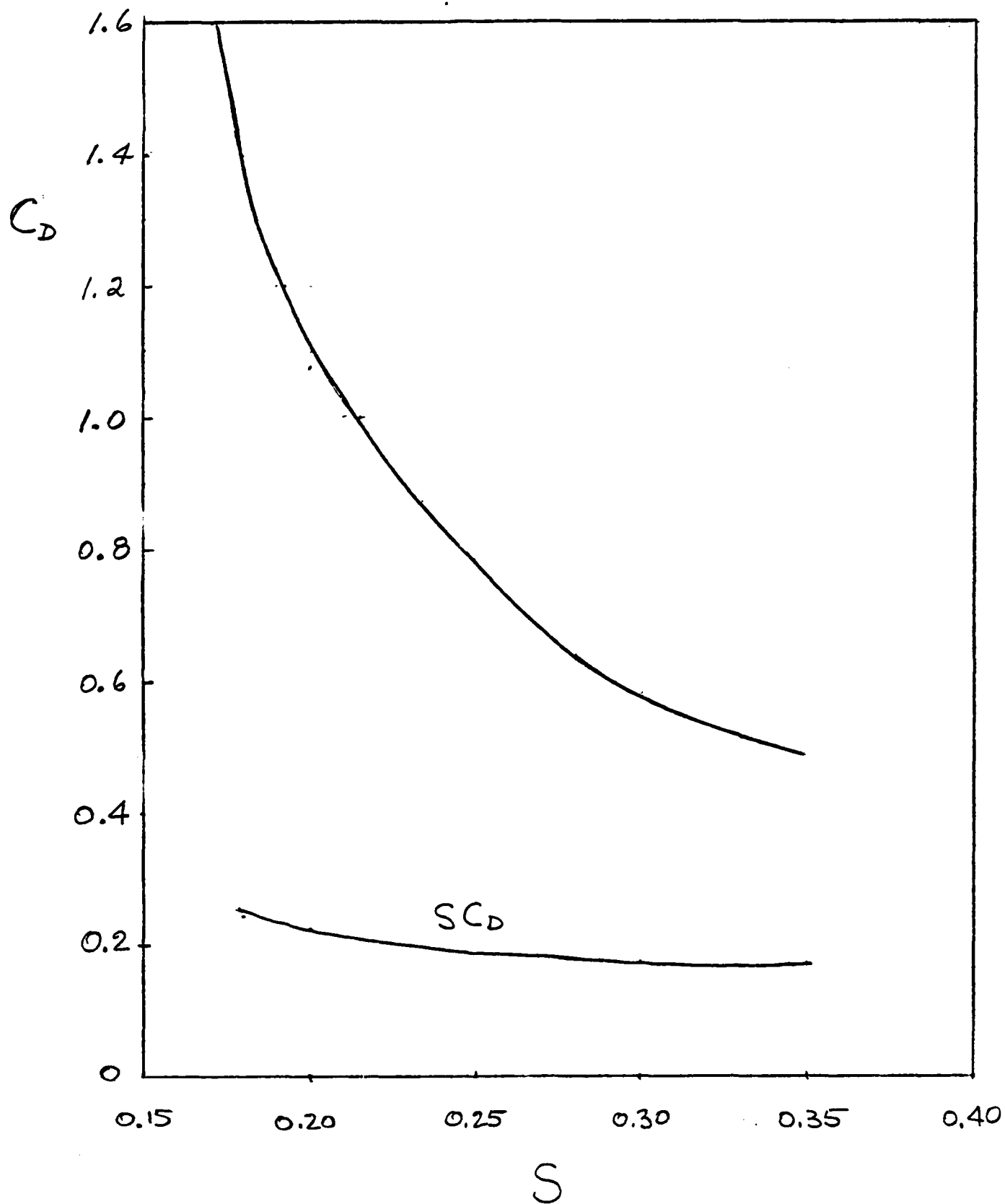


FIGURE 6. Drag Coefficient - Strouhal Number Correlation (Naumann-Morsbach)

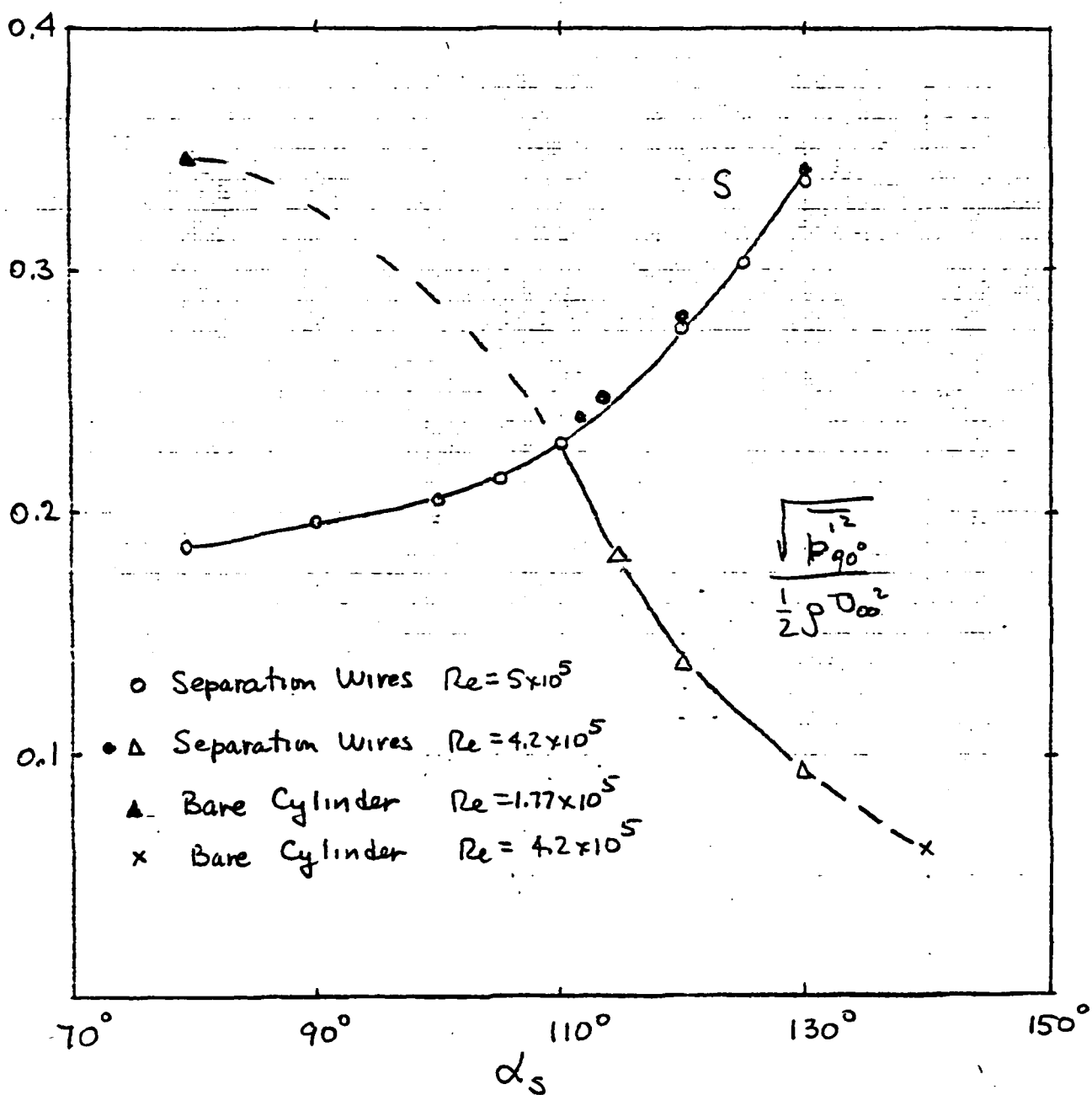


FIGURE 7a. Strouhal Number, Pressure Fluctuation-Separation Angle Correlation (Naumann, Quadflieg)

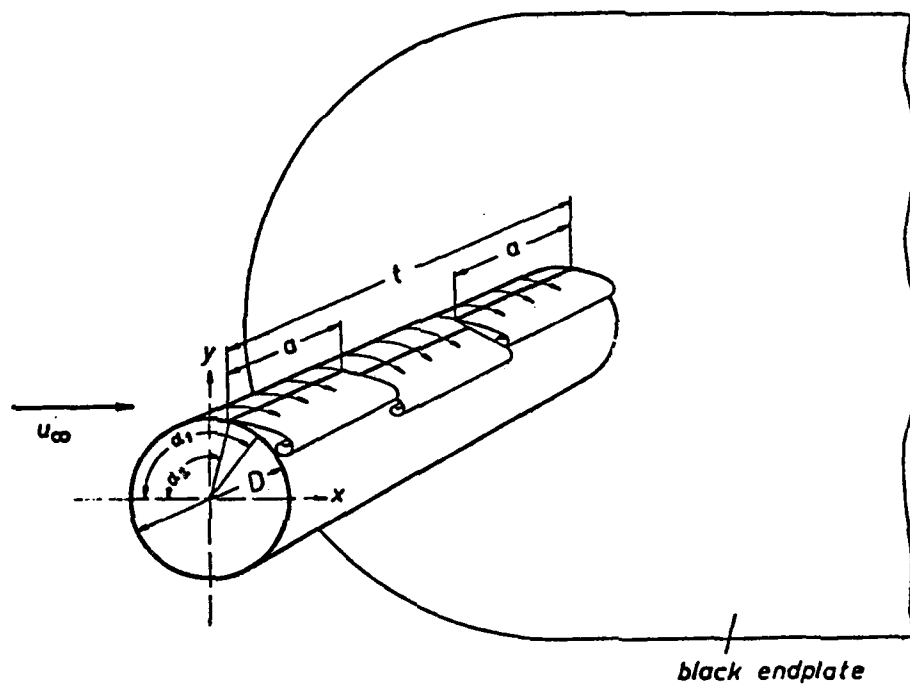


FIGURE 7b. Arrangement for Measuring the Value of Critical Circulation (Naumann, Morsbach)

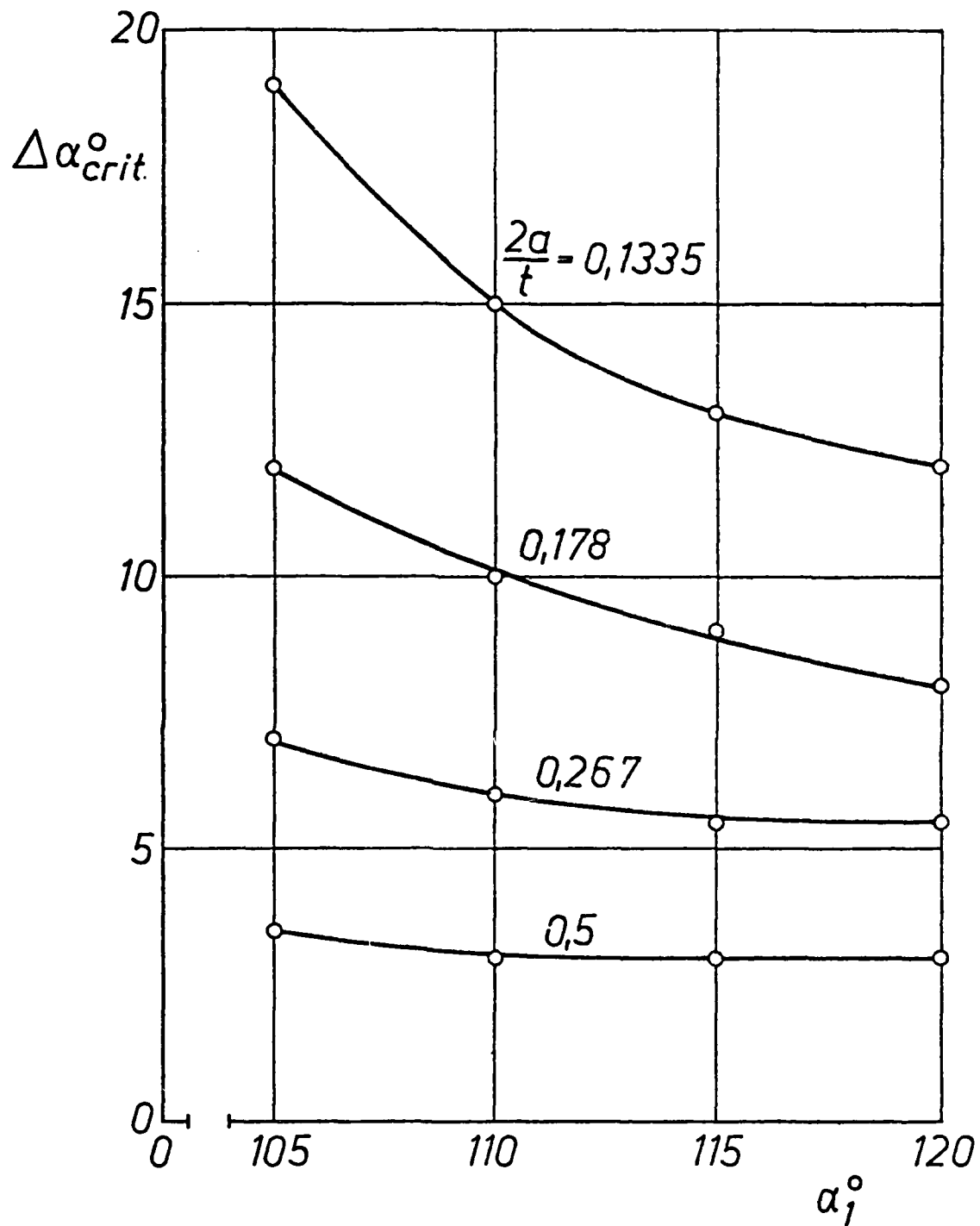


FIGURE 7c. The Critical Angle Difference to Stop Coherent Vortex Shedding (Naumann, Morsbach)

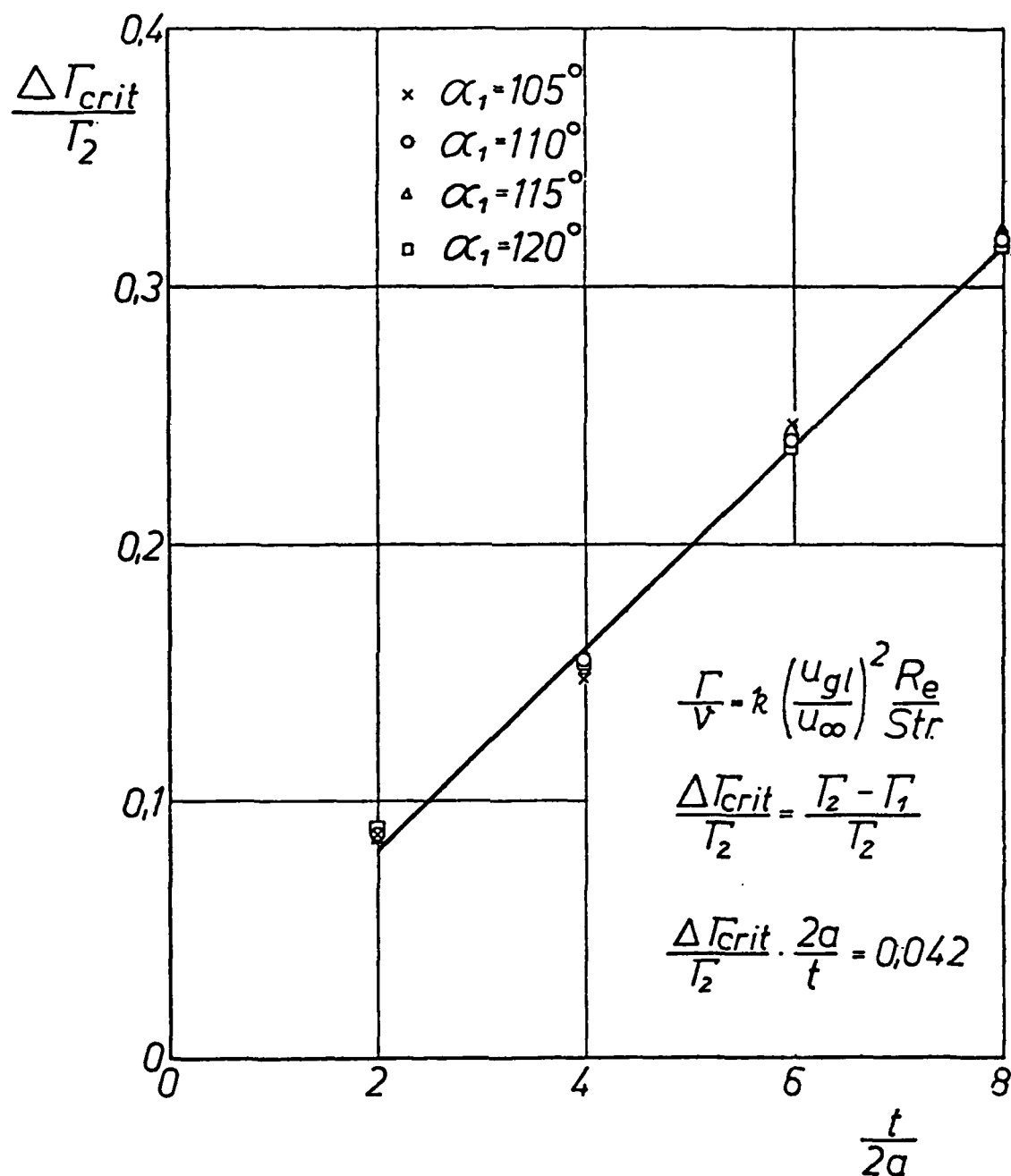


FIGURE 7d. The Critical Amounts of Admissible Circulation Required to Prevent Coherent Vortex Shedding (Naumann, Morsbach)

these correlations particularly with respect to roughness effects. It would also be of interest to determine the separation point for the very smooth, ideal, cylinder in the absence of any disturbances.

The fluctuating lift coefficient vs Re is shown in Figure 8. The scatter in the data is quite large particularly in the sub-critical-critical regime. The values in the transcritical region appears to be about 0.1. The predictions of Chen do not seem too reliable in the transcritical region. The pressure fluctuations at 90 degrees is a measure of the lift and were correlated with separation angle as shown, along with S , in Figure 7a. Whether or not the correlation is valid requires more data. In fact, fluctuating pressures all around the cylinder is also needed. Cantwell's data in the critical region showed that the envelope of the peak fluctuations have the same shape as the mean with a mean base pressure coefficient of -1.2, and a variation between 0 and -3.5.

NASA/ISU Experiments

G. Malcom presented the results of the cylinder flow experiments conducted at Ames by James of Iowa State University who was unable to attend the Workshop. These results have been published as AIAA Paper 79-1477 at the 12th Fluid and Plasma Dynamics Conference, July 23-24, 1979, Williamsburg, VA. The tests were conducted in the 12-foot Pressure Wind Tunnel with its operating range shown in Figure 9. Three different diameter cylinders of 6", 12", and 18" were used. The 12" model will also be used in the forthcoming tests. The typical model design and instrumentation locations are shown in Figures 10 and 11. Integrated sectional drag coefficient vs Re data are shown in Figure 12 along with previous data. The machine roughnesses which are circumferential grooves are the same for all three models, so that the relative roughness for the 6" cylinder is

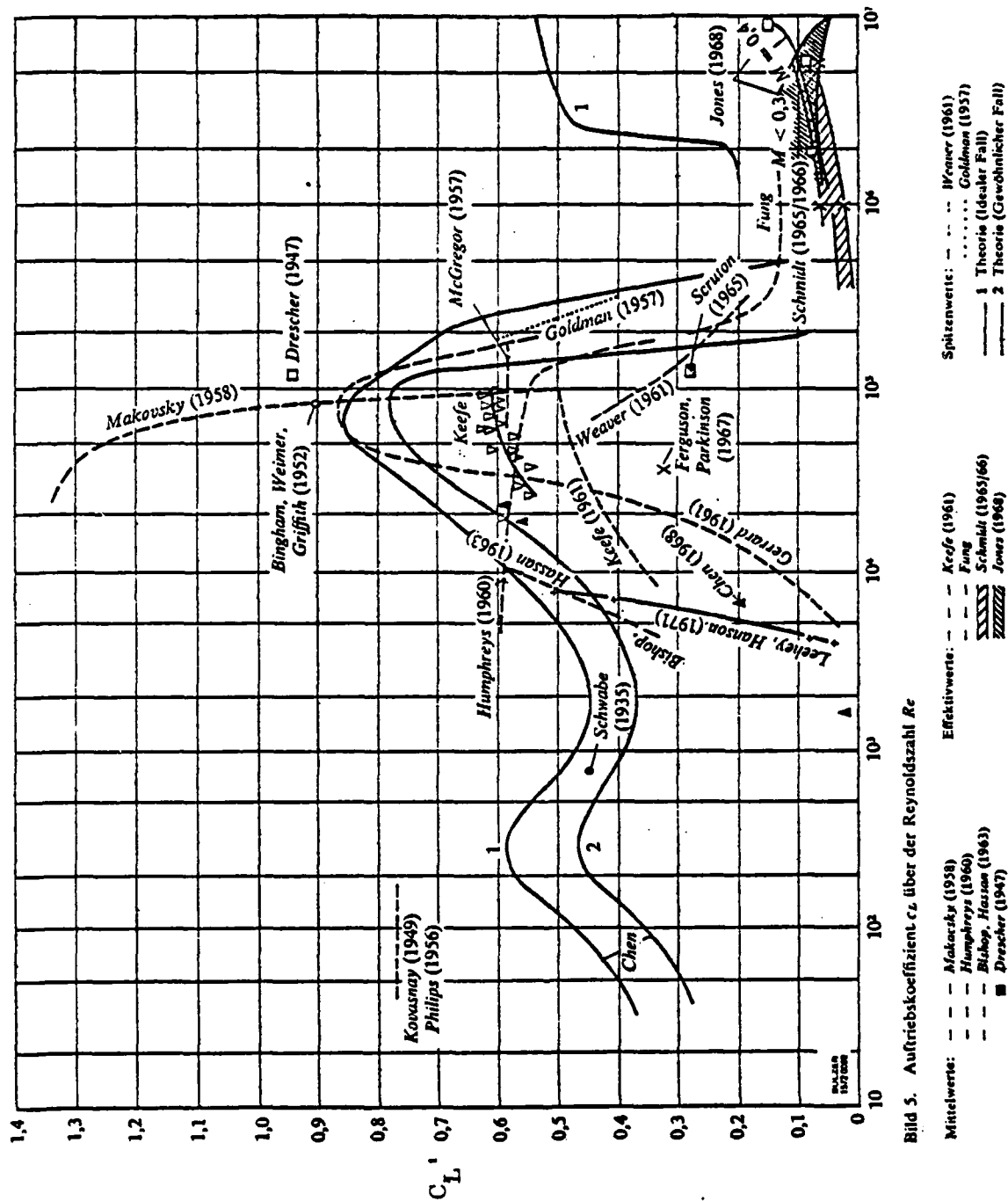


Bild 5. Auftriebskoeffizient c_L über der Reynoldszahl Re

FIGURE 8. Fluctuating Lift Coefficient

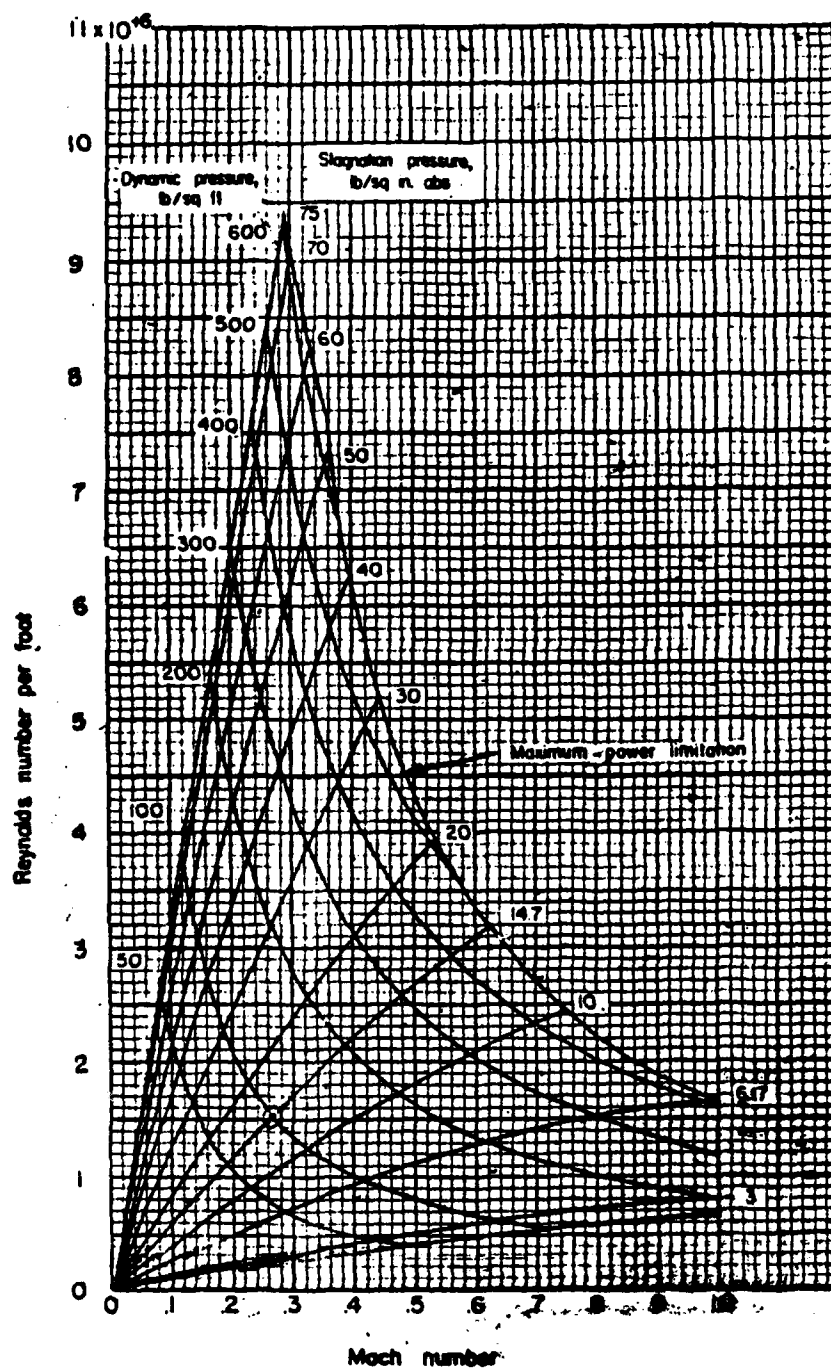


FIGURE 9. Operating Characteristics of the Ames 12-Foot Pressure Wind Tunnel

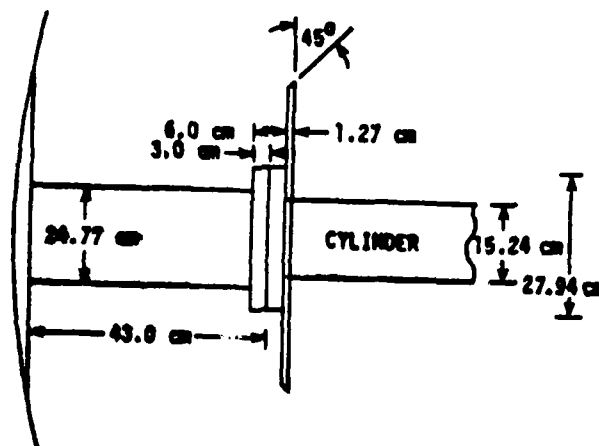


FIGURE 10. Model Support and End-Plate Location for 15.24 cm Circular Cylinder

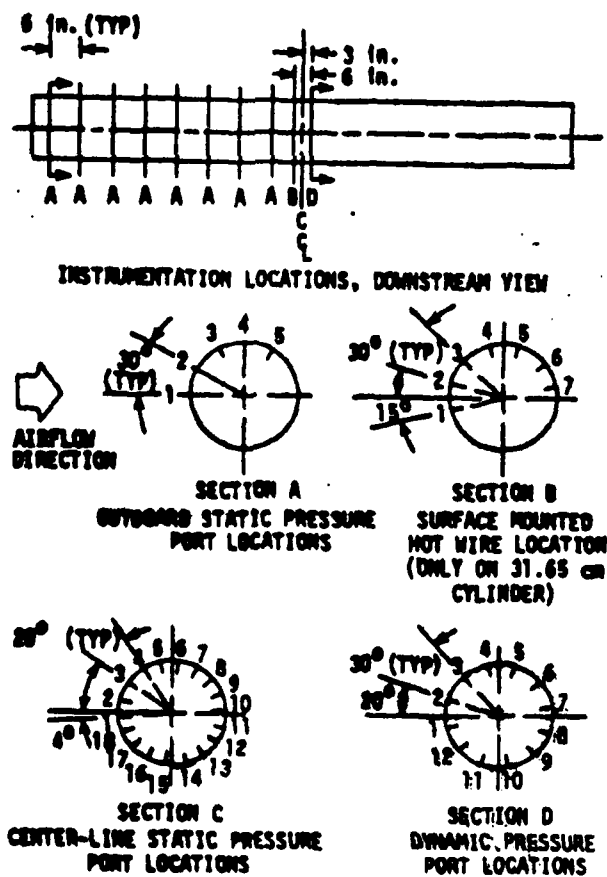


FIGURE 11. Location of Instrumentation on the 31.65 cm Circular Cylinder

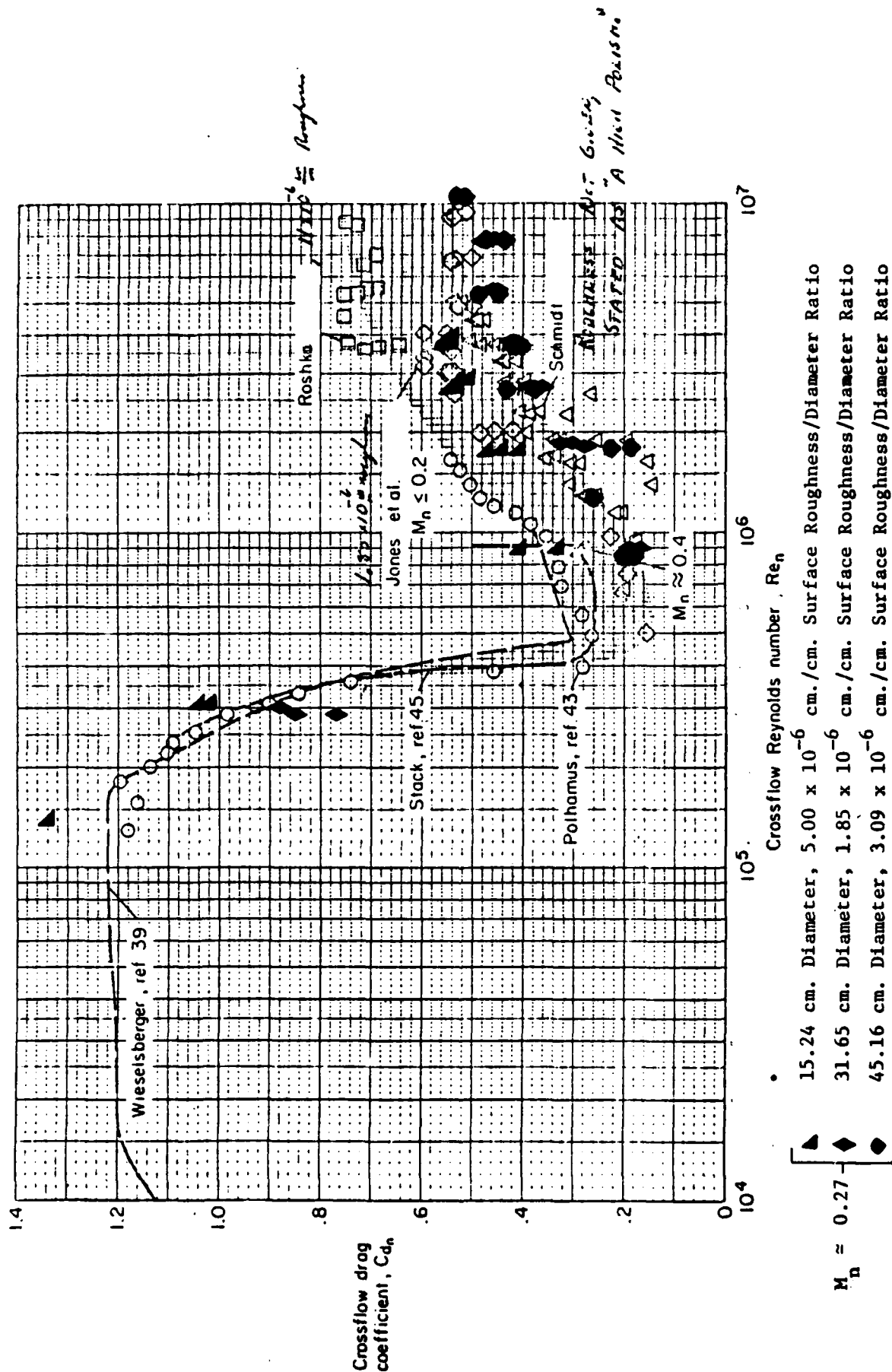


FIGURE 12. Variation of Crossflow Drag Coefficient With Crossflow Reynolds Number for Circular Cylinders at Crossflow Mach Numbers ≤ 0.4 .

larger than the others. This may account for the higher value of C_D for that model. Blockage corrections using Maskell's method have been used.

Changes in the pressure coefficient distribution with Re for the 18" diameter cylinder from subcritical in nature to transcritical is apparent in Figure 13. Spanwise distribution of the pressure coefficient are shown in Figures 14-16. The large variations in the aft region of the cylinder is indicative of the non-two dimensional nature of the flow. Use of different size end plates did not seem to have any significant effects. Elongated end plates with the major portion of the plate in the downstream, location in the wake region is thought to be more effective than the circular plates used in the ISU experiments. A discussion of this will be presented later in the Workshop.

Unsteady pressure data were obtained using Kulite gauges. Fifteen second scope traces at different cylinder angles are shown in Figure 17. The fluctuating pressure coefficients are shown in Figures 18a-18e and the oscillations are seen to decrease as the flow regime varies from critical to transcritical. More details are to be found in the AIAA Paper.

Near Wake Measurements

Experiments were conducted in the Ames 2x2 foot wind tunnel by K. Owen and D. Johnson. Time average and time dependent flow structure in the near wake at an Re of 10^5 were made using LDV techniques. The tunnel Mach number was about 0.6 which means that local velocities were supersonic and shock waves existed which would tend to organize the flow. Although interesting, the work is not too relevant to the incompressible cases of interest here except the techniques may be applicable if necessary.

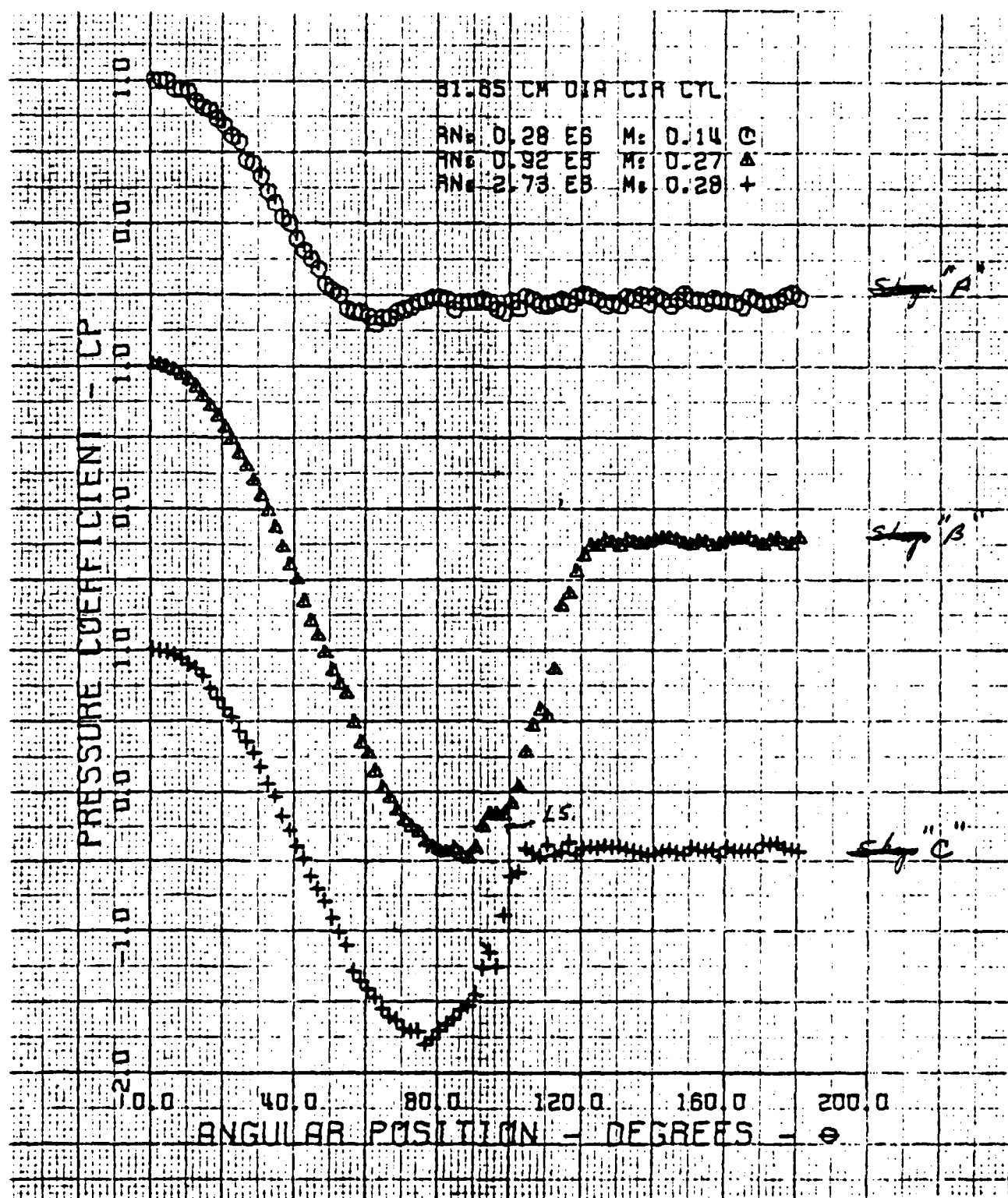


FIGURE 13. Pressure Coefficient Distribution

CPPL OUTBOARD ARRAYS

SYMBOL THETA
 ○ .000
 ◊ 30.000
 △ 60.000
 ▲ 90.000
 ▼ 120.000

Open symbols indicate 60.96 cm. diameter end-plates
 Closed symbols indicate 45.72 cm. diameter end-plates

$R_1 = 0.86 \times 10^6$
 $M = 0.27$

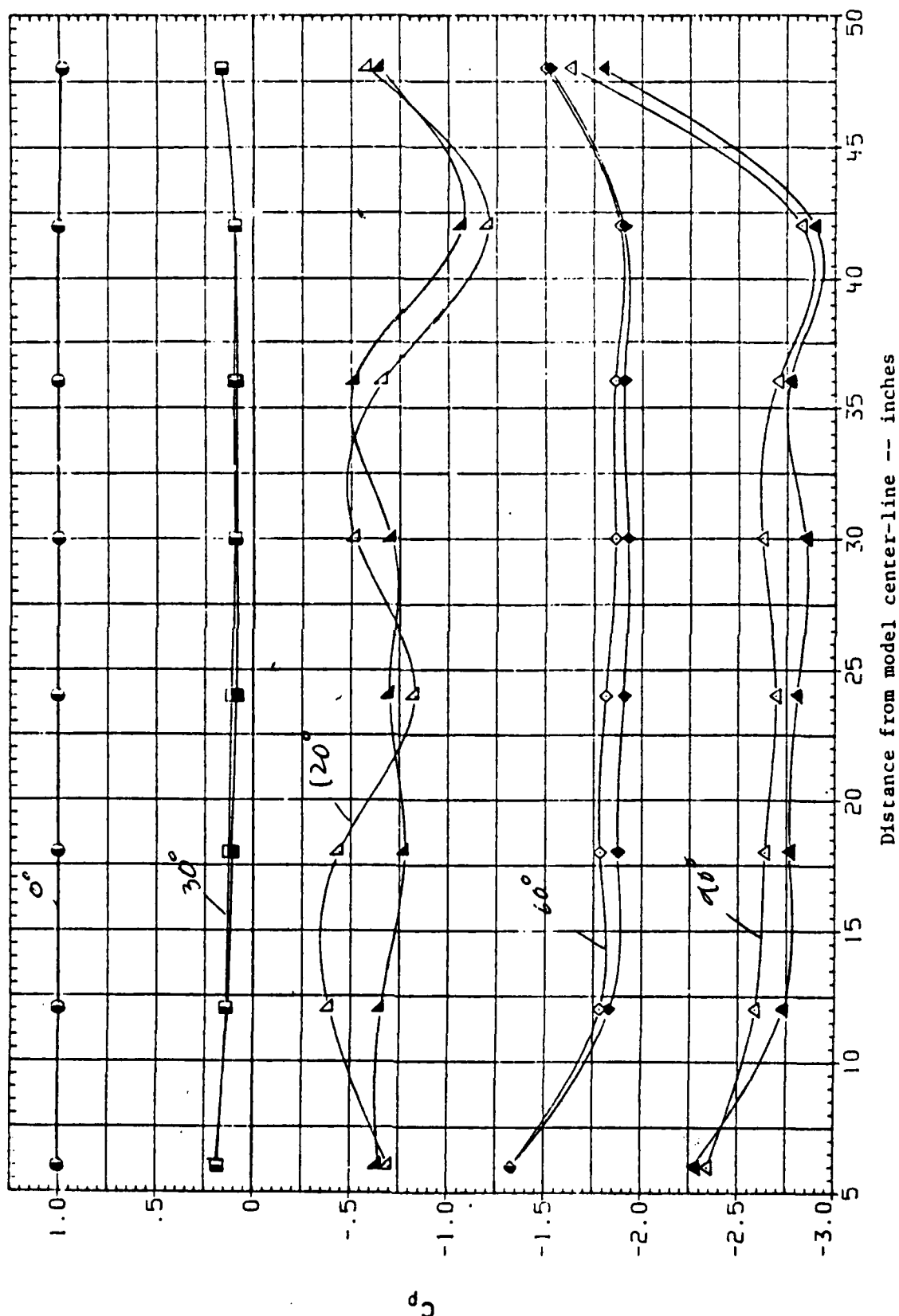


FIGURE 14. Outboard Pressure Distribution on 15.24 cm Circular Cylinder With End-Plates

CPPL OUTBOARD ARRAYS

SYMBOL
 THETA
 .000
 30.000
 60.000
 90.000
 120.000

Open symbols indicate 45.72 cm. diameter end-plates
 Closed symbols indicate 60.96 cm. diameter end-plates

$R_n = 2.72 \times 10^6$
 $M = 0.27$

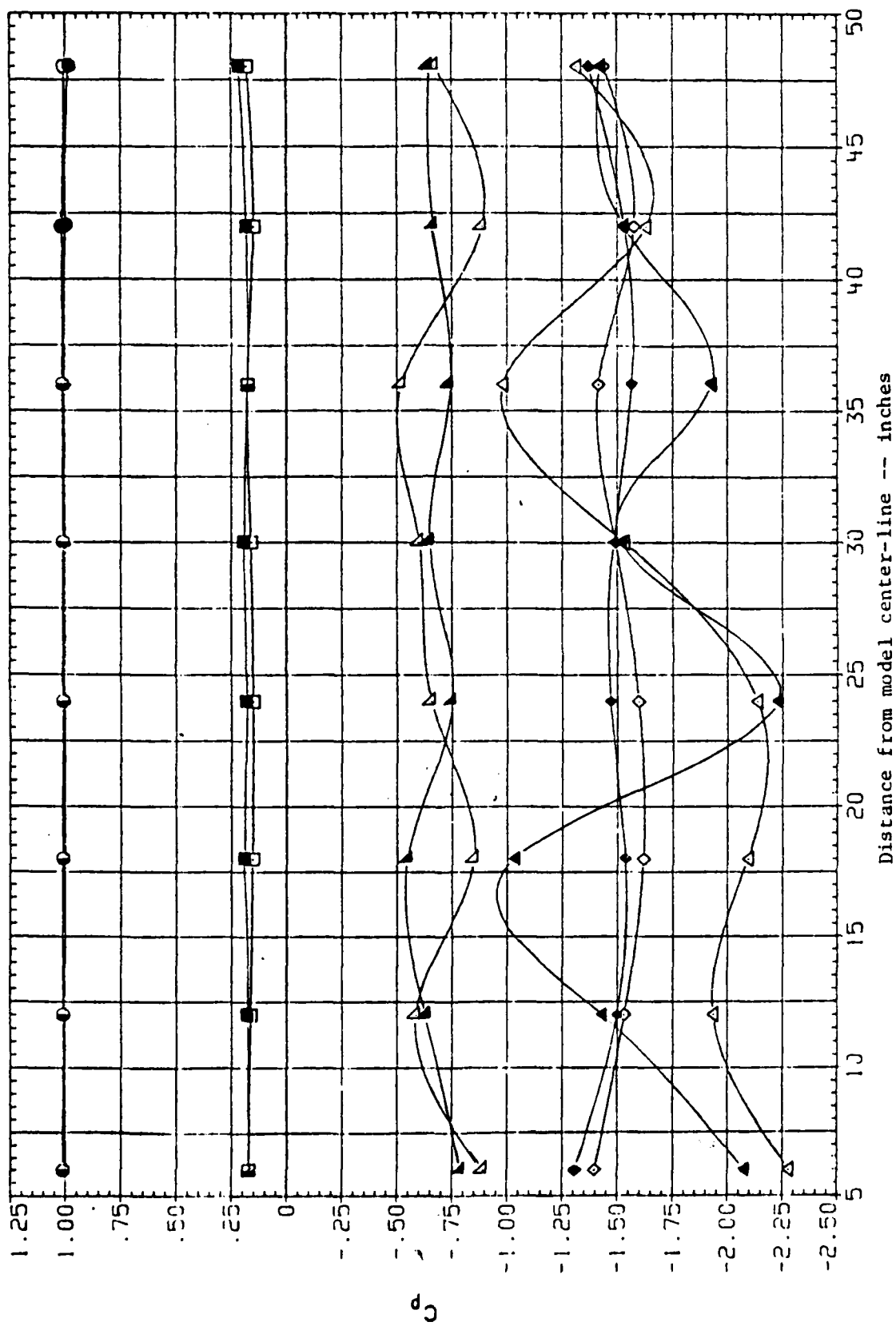


FIGURE 15. Outboard Pressure Distribution on 15.24 cm. Circular Cylinder with End-Plates.

CPPL OUTBOARD ARRAYS

SYMBOL THETA
 O 0.000
 □ 30.000
 △ 60.000
 ◇ 90.000
 ◆ 120.000

Open symbols indicate 45.16 cm. diameter cylinder
 Closed symbols indicate 31.65 cm. diameter cylinder

$R_n = 2.70 \times 10^6$
 $M = 0.28$

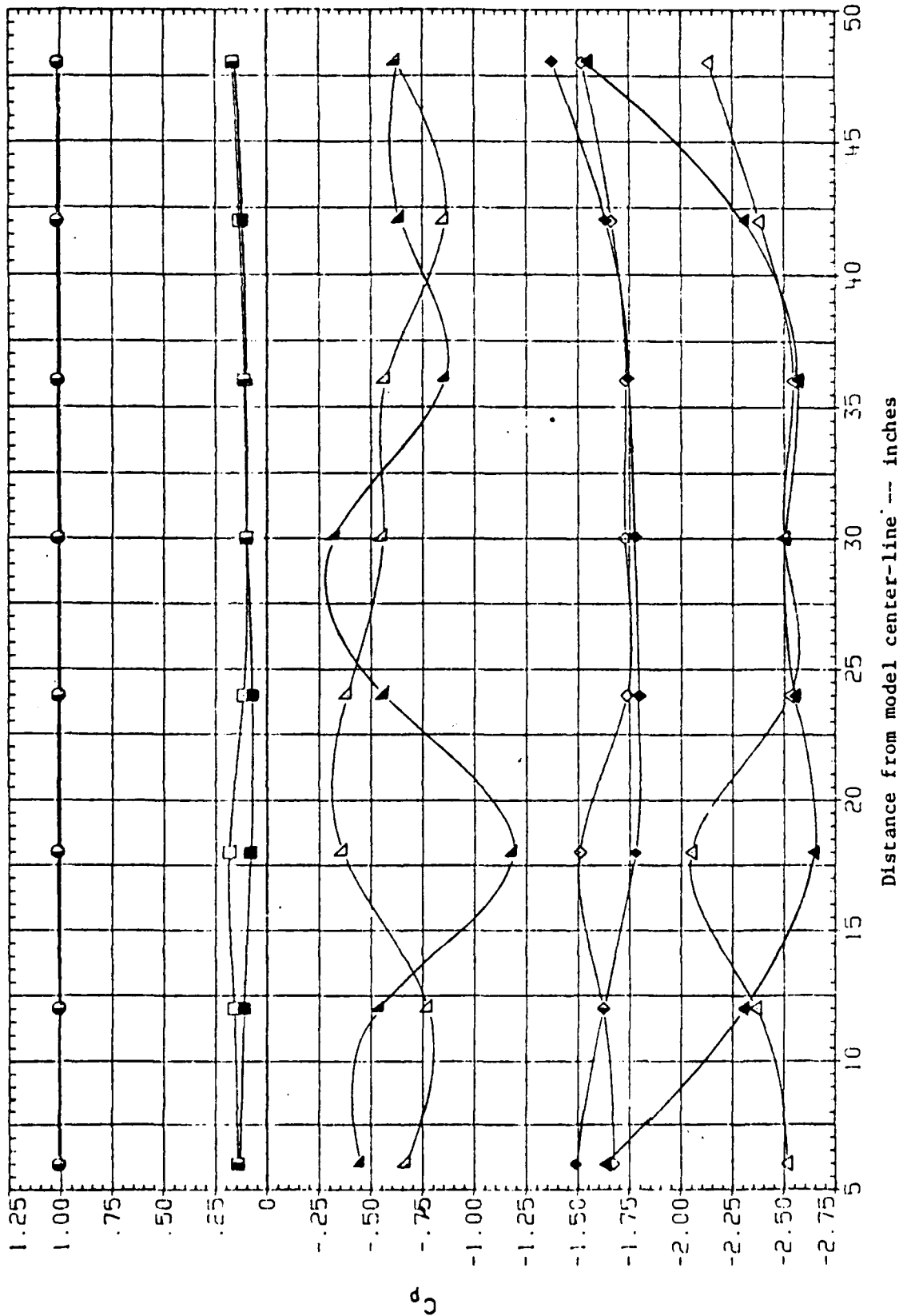
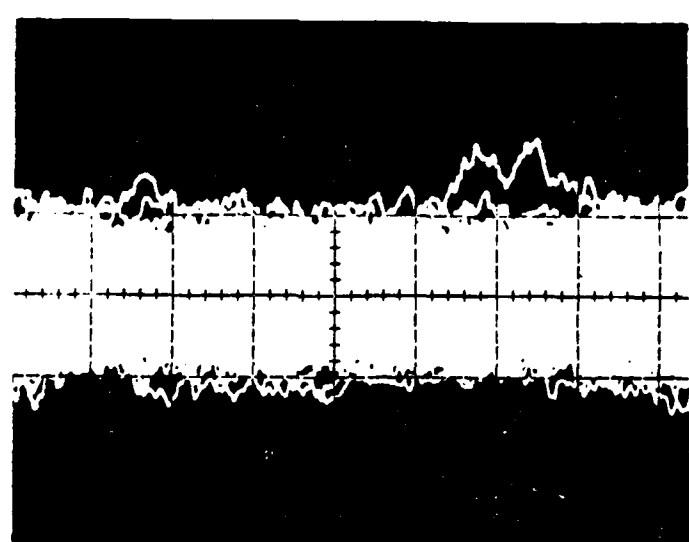
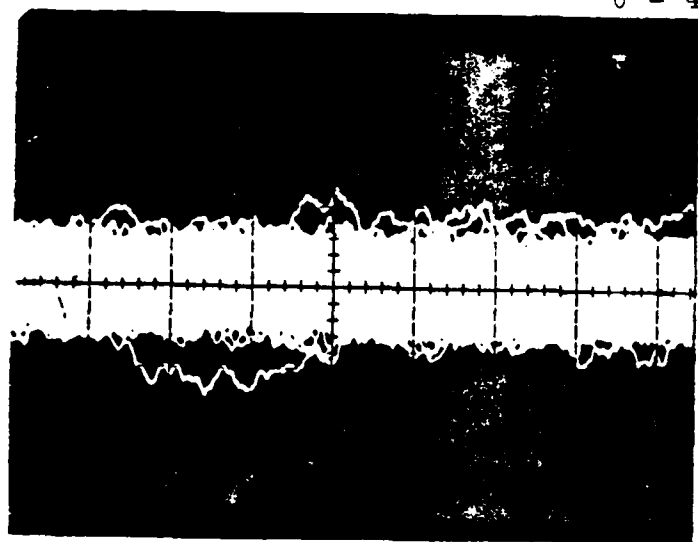


FIGURE 16. Outboard Pressure Distributions on 31.65 cm and 45.16 cm. Diameter Circular Cylinders

44°
θ = 44

K-3

= 50°

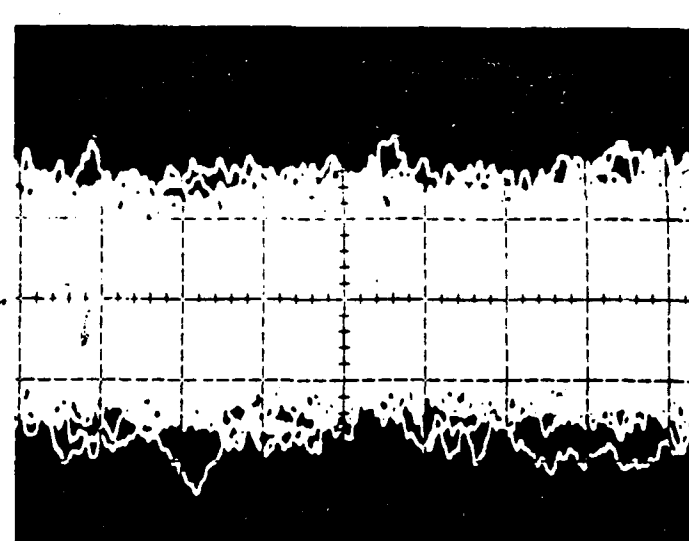
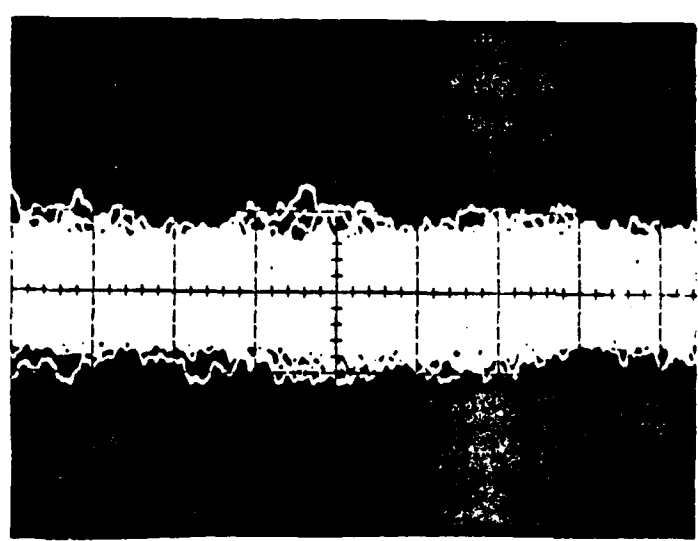


K-2

= 52°

K-3

= 58°



K-3

= 66°

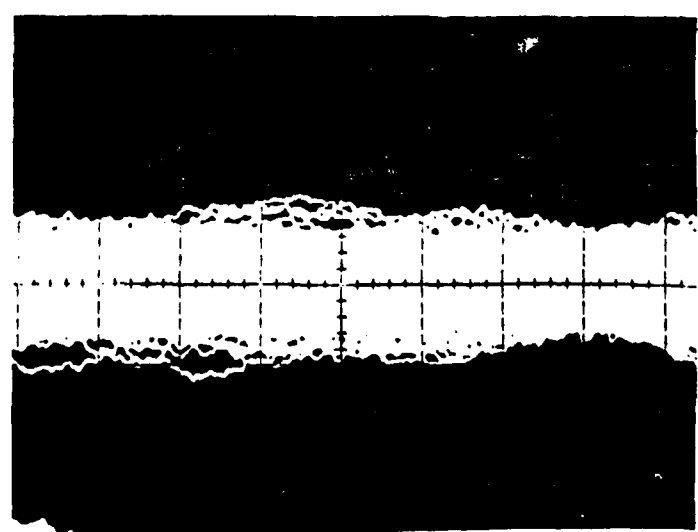


FIGURE 17. 15 Second Scope
Traces of
Kulite Output

FOR AN 6 IN. DIA. CIR. CYLIND.
 $Re(PL) = 0.14E+6$ $M(PL) = 0.1$
 SURFACE ROUGHNESS/DIA. = $5.00E-6$

STATIC PRESSURE COEF. +
 MAXIMUM SURFACE CP ○
 MINIMUM SURFACE CP △
 NORMAL WIDTH OF CP |
 OSCILLATIONS

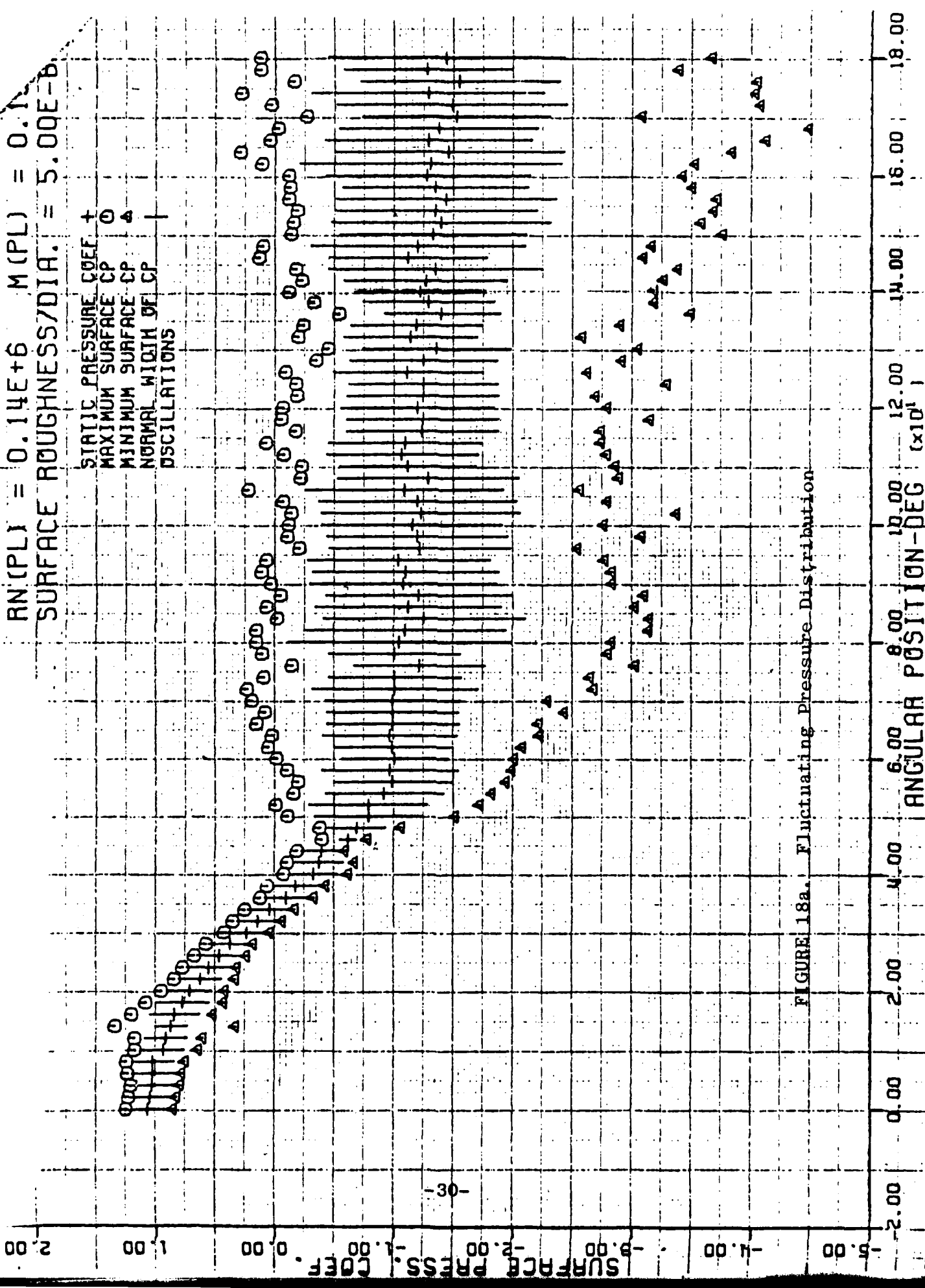


FIGURE 18a. Fluctuating Pressure Distribution

SURFACE CP VS. ANGULAR LOCATION
 FOR AN 6 IN. DIA. CIR. CYLINDER
 $Re(PL) = 0.31E+6$ $M(PL) = 0.270$
 SURFACE ROUGHNESS/DIA. = 5.00E-6

STATIC PRESSURE COEF +
 MAXIMUM SURFACE CP ○
 MINIMUM SURFACE CP ▲
 NORMAL WIDTH OF CP
 OSCILLATIONS

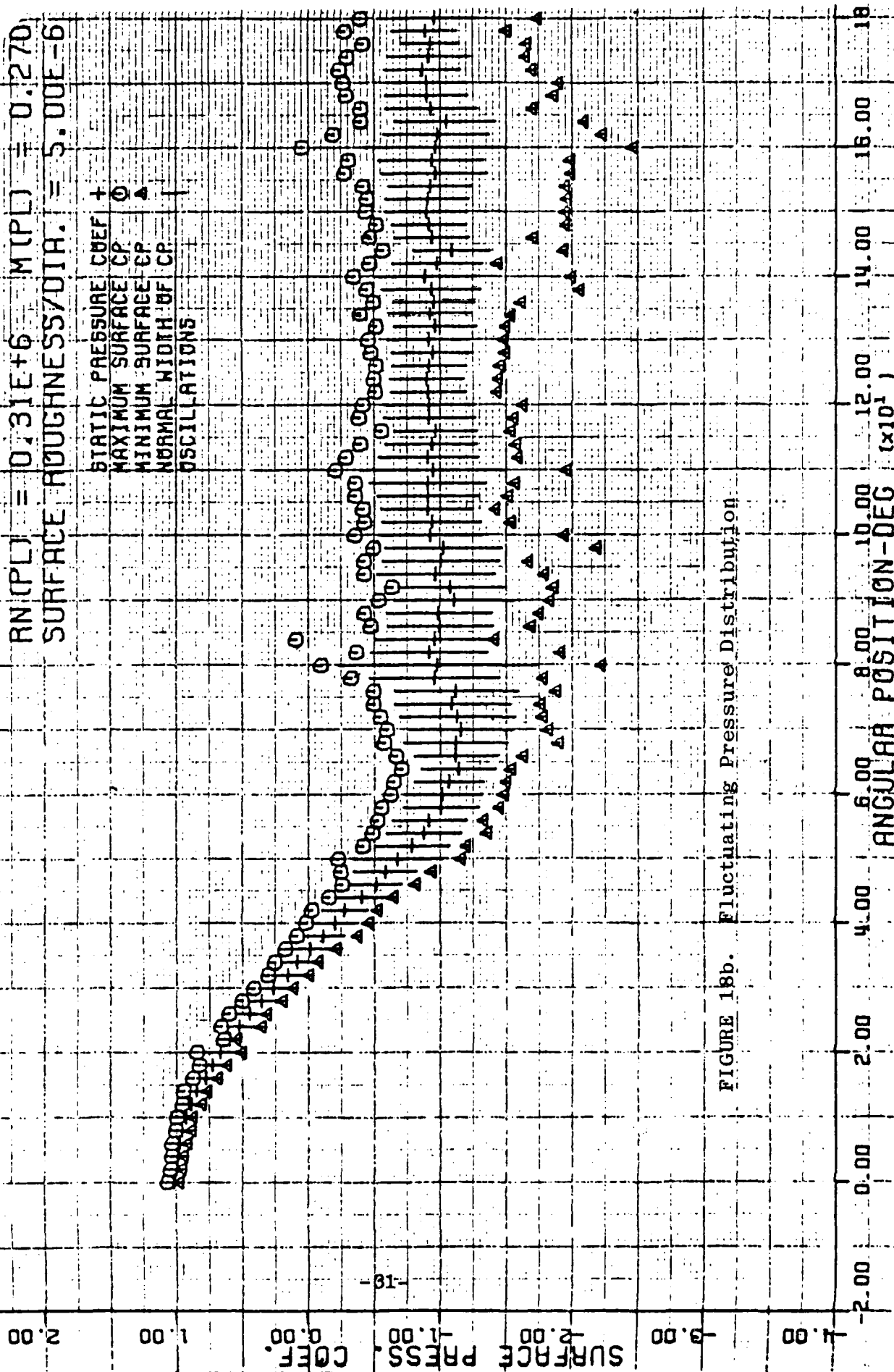


FIGURE 18b. Fluctuating Pressure Distribution

SURFACE CP VS. ANGULAR LOCAT.
 FOR AN 6 IN. DIA. CIR. CYLINDE.
 $Re(PL) = 0.87E+6$ $M(PL) = 0.274$
 SURFACE ROUGHNESS/DIA. = $5.00E-6$

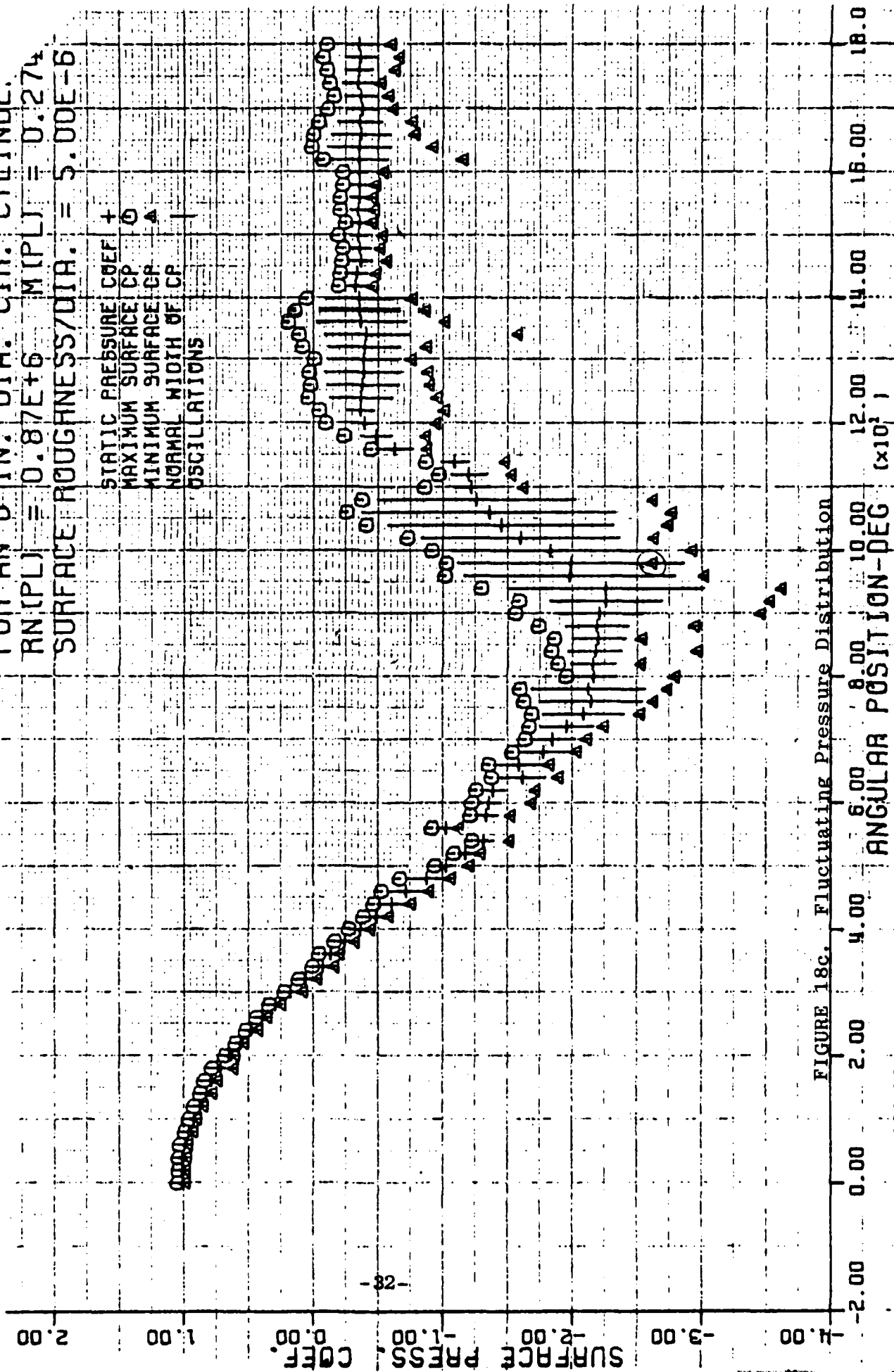


FIGURE 18c. Fluctuating Pressure Distribution

SURFACE CP VS. ANGULAR LOCA.
 FOR AN 6 IN. DIA. OIR. CYLIND.
 $Re(PL) = 2.81E+6$ $M(PL) = 0.2$,
 SURFACE ROUGHNESS/DIA. = $5.00E-6$

STATIC PRESSURE COEF +
 MAXIMUM SURFACE CP ○
 MINIMUM SURFACE CP ▲
 NORMAL WIDTH OF CP |
 OSCILLATIONS

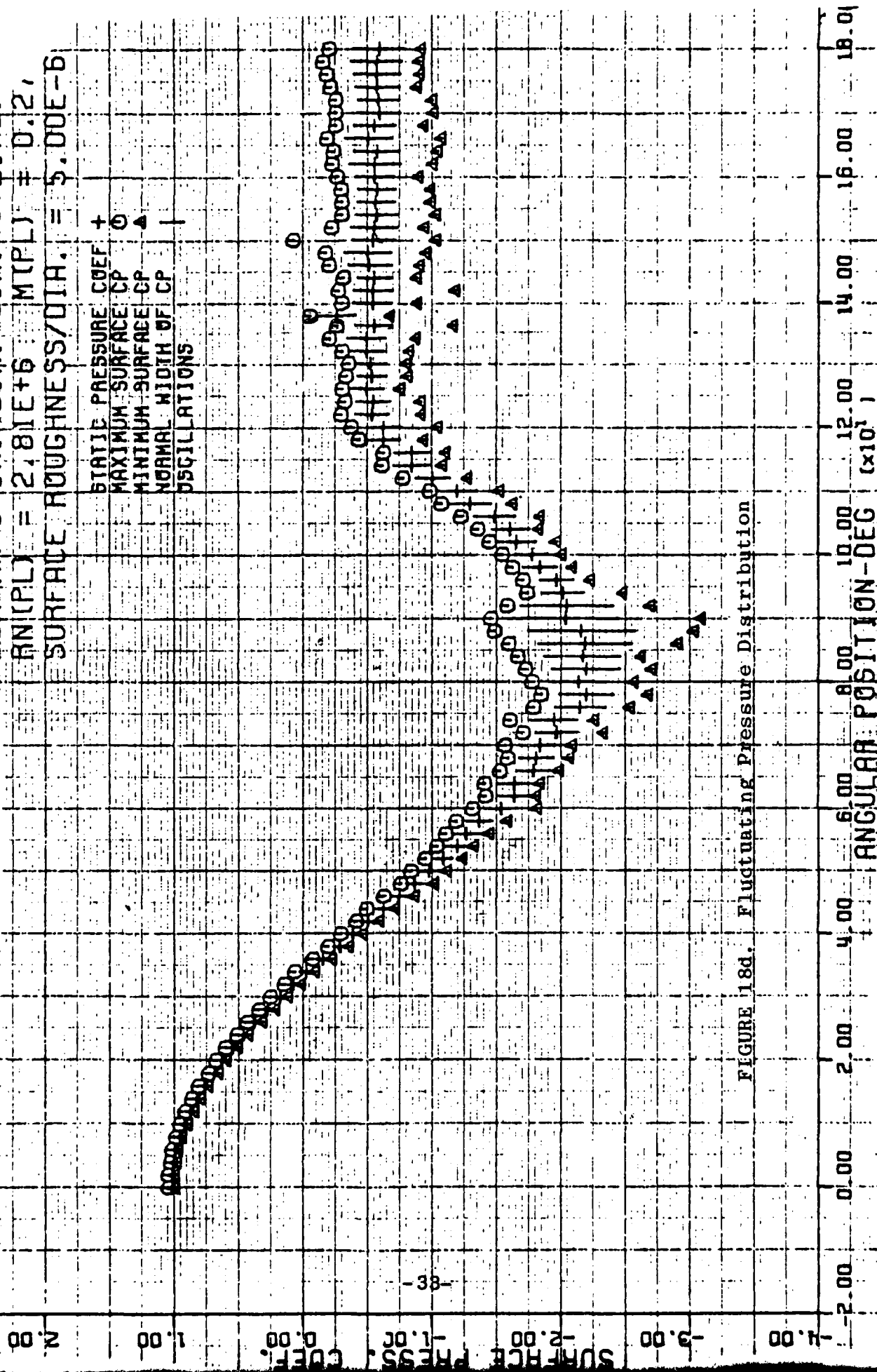


FIGURE 18d. Fluctuating Pressure Distribution

SURFACE CP VS. ANGULAR LOC
 FOR AN 18 IN. DIA. CIRC. CYLIND
 $Re(PL) = 10.9E+6$ $M(PL) = 0.27$
 SURFACE ROUGHNESS/DIA. = $3.08E-6$

STATIC PRESSURE COEF +
 MAXIMUM SURFACE CP 0
 MINIMUM SURFACE CP
 NORMAL WIDTH OF CP
 OSCILLATIONS

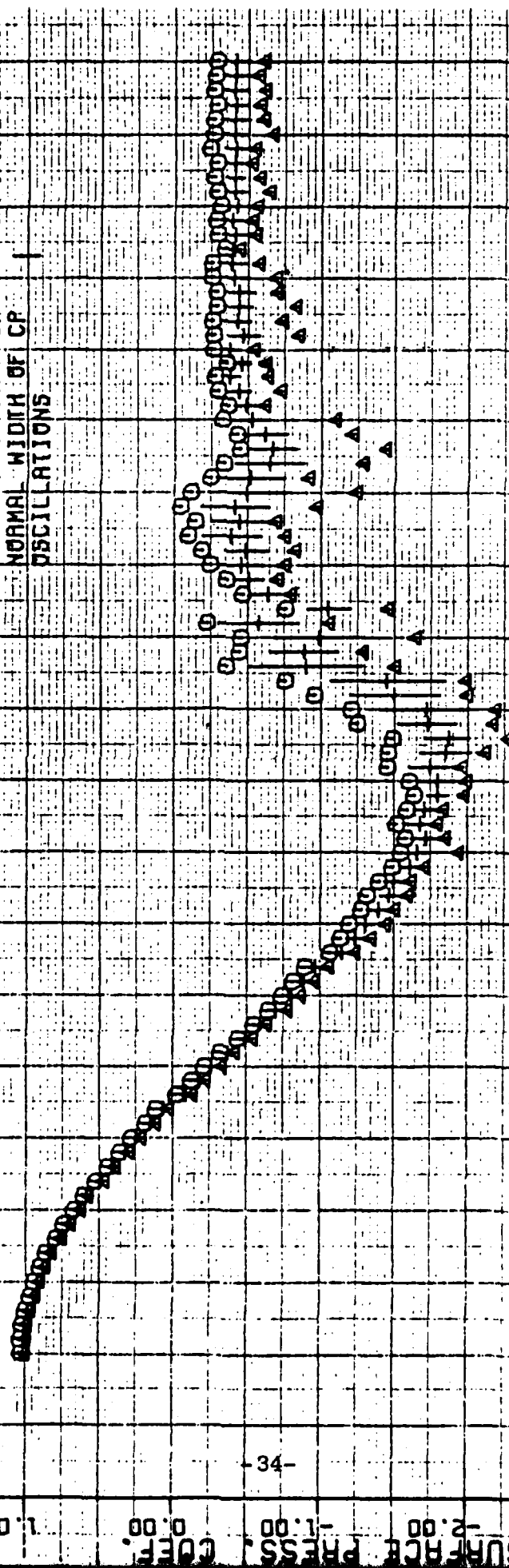


FIGURE 18e. Fluctuating Pressure Distribution

Skin Friction Measurements

W. Rose presented some results from measurements made by himself and S. Murthy in conjunction with the NASA/ISU tests at Ames and the SAI tests at CalTech. Buried hot wires near the surfaces of the cylinder were used to obtain skin friction data and other flow field information. Additional results have been reported in NASA TM 78-454. The results are for both smooth and rough wall cylinders. Photographs of two types of gages are shown in Figure 19. The three wire gage was intended to sense direction of flow in order to determine flow separation, but this did not work. Skin friction measurements along with the measured pressure distributions are shown in Figures 20a-20c for Reynolds numbers corresponding to laminar separation, Figure 20a, to fully turbulent flow in the boundary layer, Figure 20c. The significant scatter in the data may be due to the different gages used as the cylinder is rotated or due to some flow phenomena, but the precise interpretation of these data is as yet uncertain. However, some qualitative as well as quantitative information can be obtained from the data, and these are:

1. Shedding frequencies
2. Transition location
3. Separation and reattachment locations
4. Quantitative skin friction on smooth surfaces
5. Qualitative skin friction on rough surfaces

Accordingly, surface phenomena that has been inferred from the data are plotted in Figure 21. Comparisons were made with Achenbach's data which does not show the increase in skin friction prior to the apparent separation location. Trends are consistent, but quantitative comparisons show significant deviation. Figure 22 shows results for a rough cylinder which used a fine-meshed screen for the roughness elements on the surface. There is large scatter in the data which can be due to the presence of the

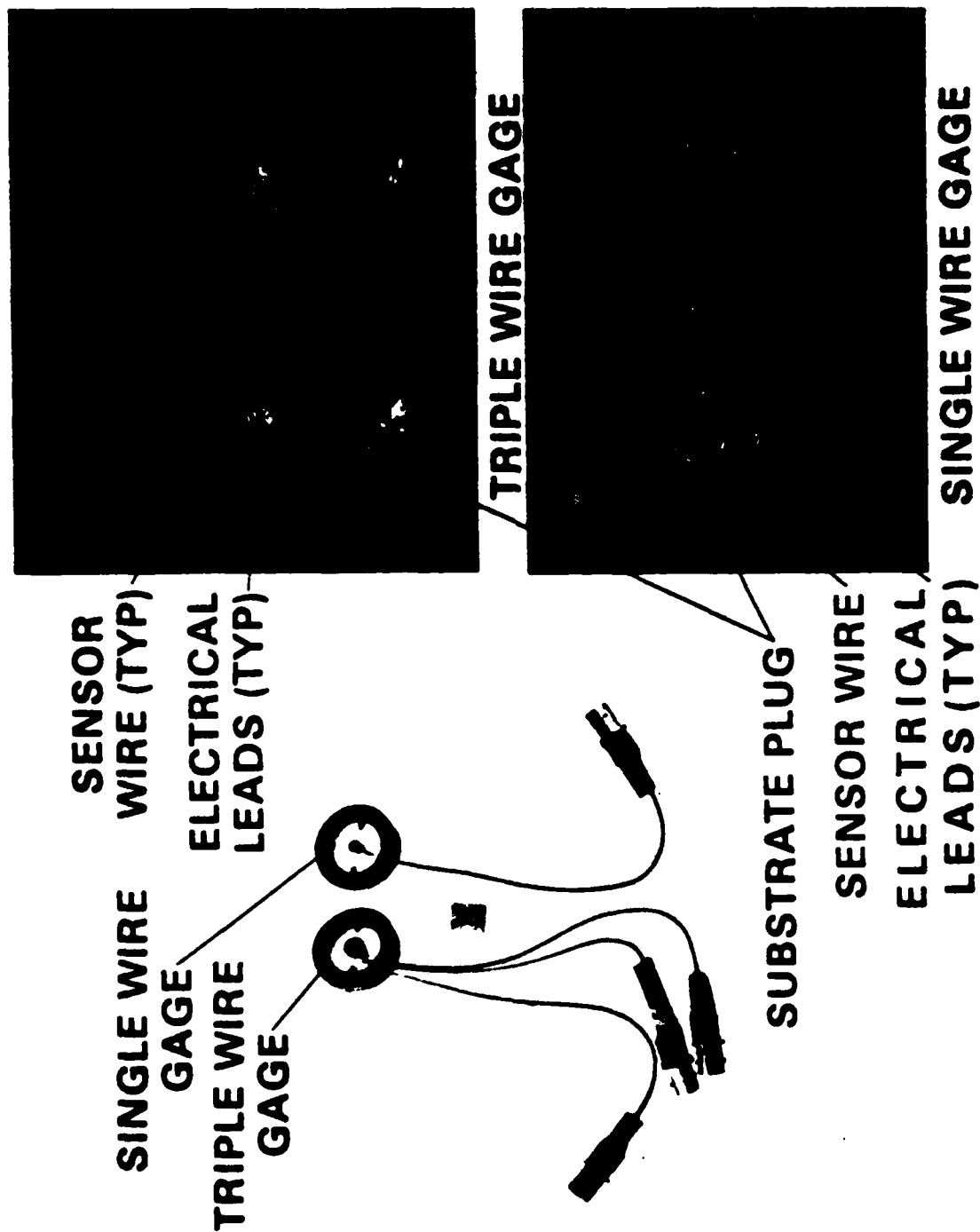
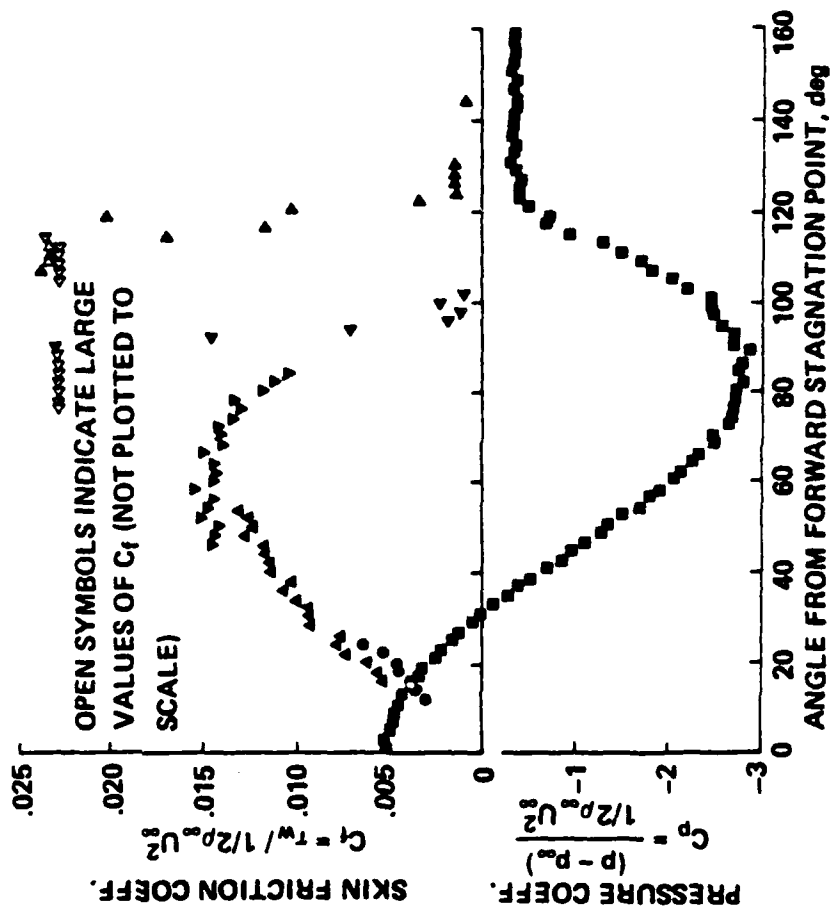


FIGURE 19. Photos of Buried Wires

Re NO. (diam) = 0.84×10^6

MACH NO. = 0.26

\bullet SKIN FRICTION MEAS.
 Δ WITH BURIED WIRE GAGES
 \circ MEASURED PRESSURE DISTRIBUTION



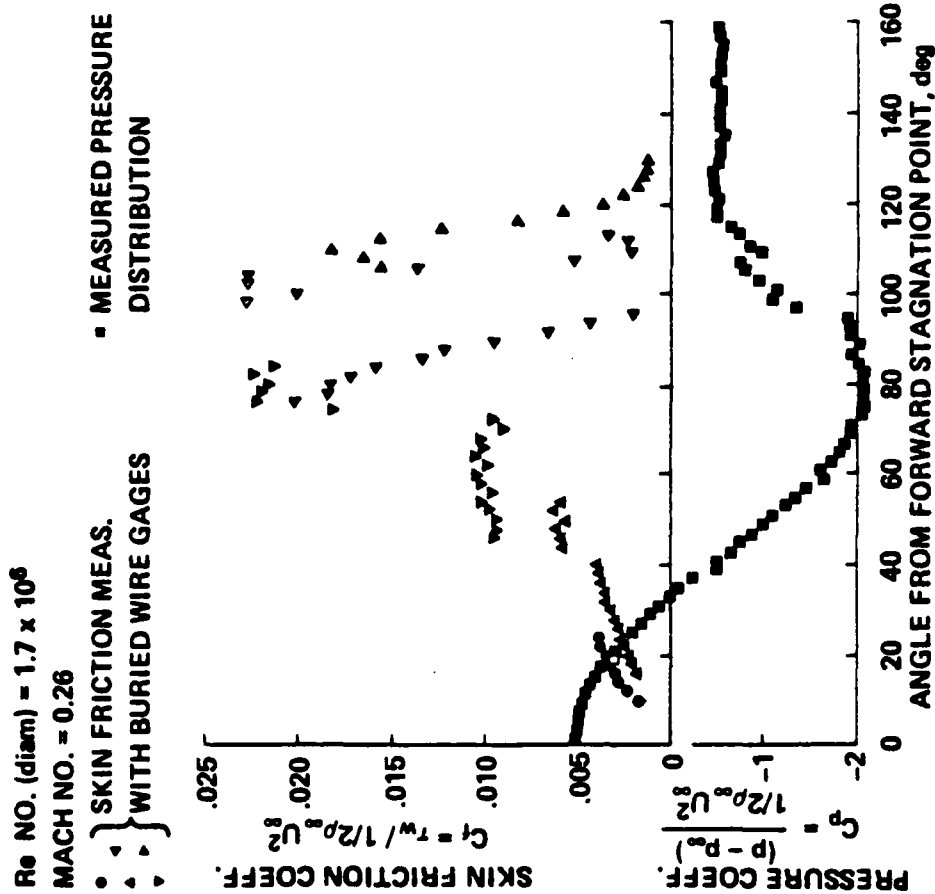


FIGURE 20b. Example of Data Obtained in Turbulent Flow

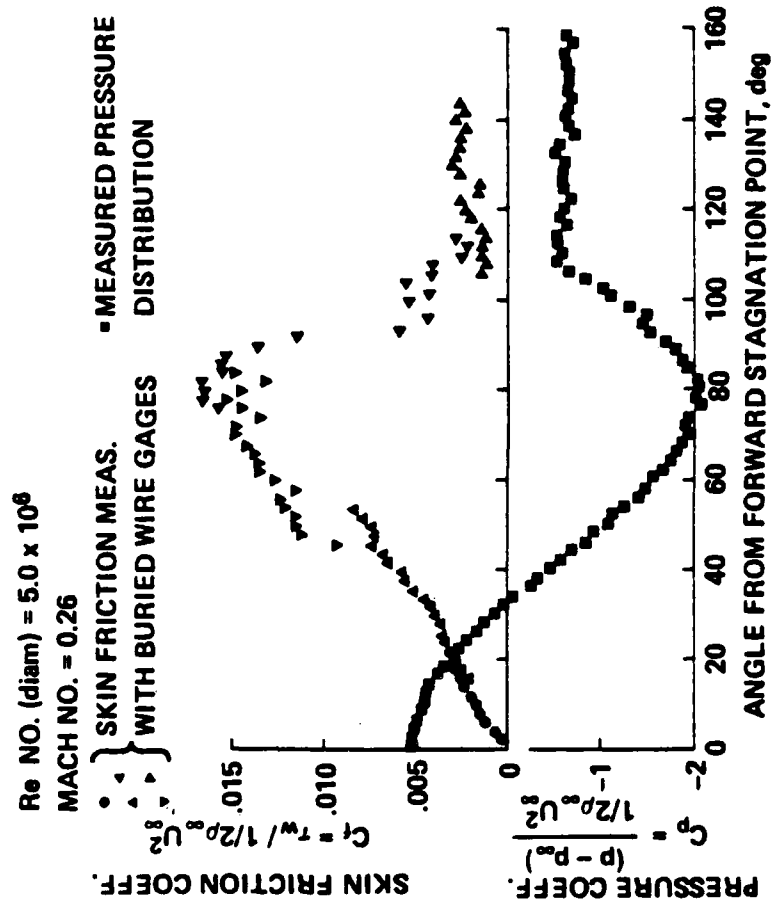


FIGURE 20c. Example of Data Obtained in Turbulent Flow

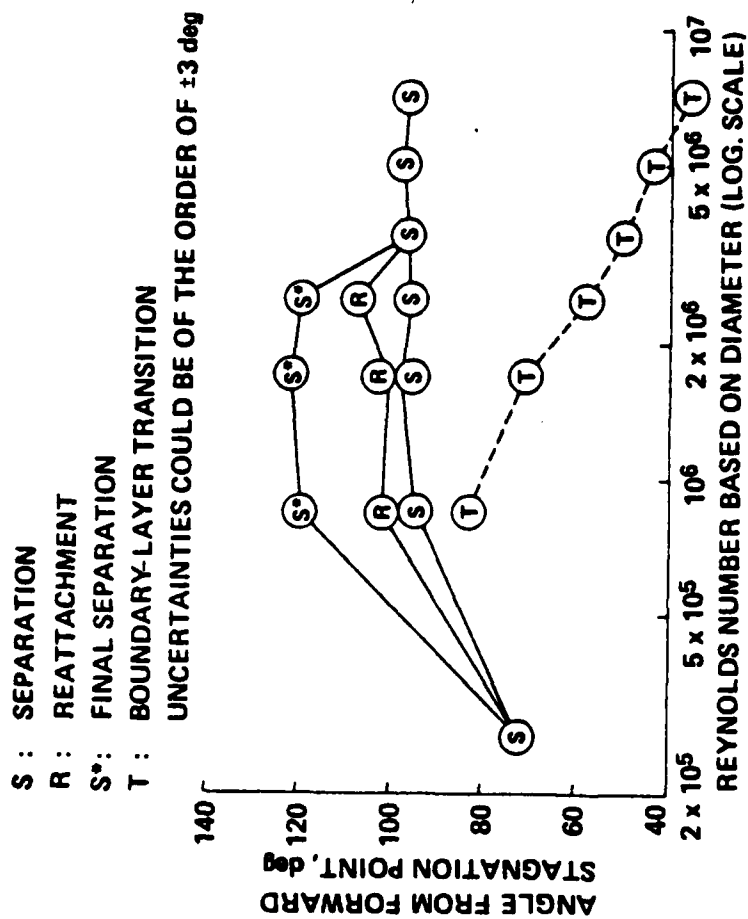


FIGURE 21. Surface Phenomena Inferred from Data

Re NO. (diam) = 1.25×10^6
 MACH NO. = 0.19
 SKIN FRICTION MEAS.
 WITH BURIED WIRE GAGES
 -SMOOTH CYLINDER
 SKIN FRICTION MEAS.
 WITH BURIED WIRE GAGES
 -WITH ROUGHNESS
 K/D = 0.001
 MEAS. PRESSURE DISTRIBUTION
 -SMOOTH CYLINDER
 MEAS. PRESSURE DISTRIBUTION
 -WITH ROUGHNESS, K/D = 0.0011

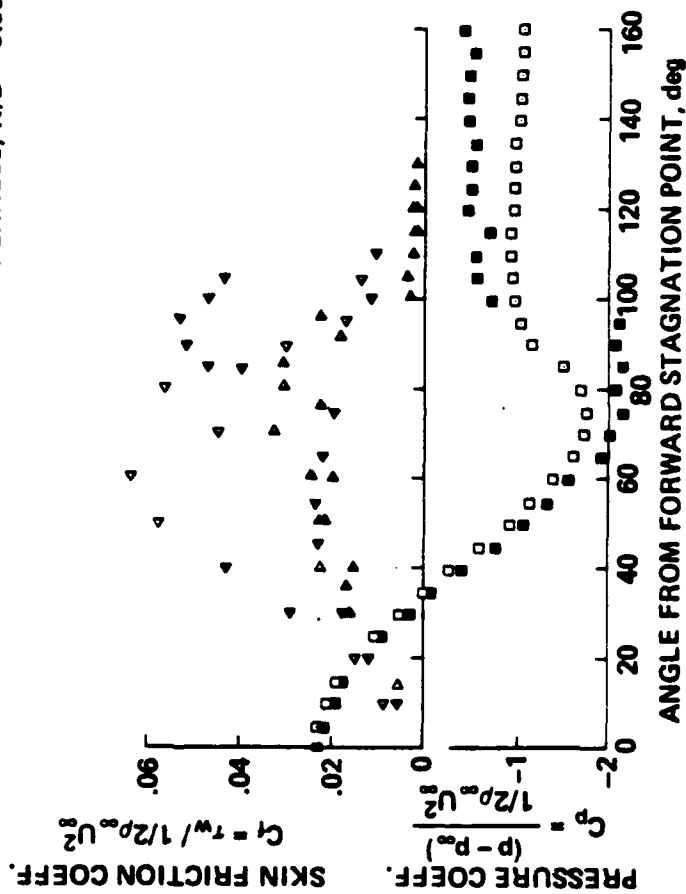


FIGURE 22. Example of Rough Surface Data


screen, however, additional work is necessary to determine the validity of such measurements for rough as well as smooth surfaces.

Effects of Roughness and Stream Turbulence

W. Shih presented some results that were obtained in the 10-foot tunnel at CalTech using the 1-foot cylinder from the NASA/ISU tests. Well-defined stainless steel screens were used to simulate surface roughness, Figure 23. The run matrix is shown in Table 1. The smooth cylinder is in the critical to super critical flow regime and the rough cylinder is in the transcritical regime for both roughnesses. The distribution of pressure coefficient is shown in Figure 24. Data from other sources at similar conditions are also included to show consistency with previous results. The slight asymmetry shown for the smooth cylinder may indicate some surface imperfections causing early transition on one side of the cylinder. Such conditions should be carefully monitored in the forthcoming tests at Ames. Pressure distributions along the cylinder generators are indicative of the two-dimensionality or lack of it on the cylinder as shown in Figure 25. The smooth cylinder data show significant variation along the span as characteristic of the non-coherent nature of the shedding from cylinders in the critical flow regime. On the other hand, roughness on the cylinder tend to organize the shedding process and produces the relatively constant spanwise pressure distributions as is evident from the rough cylinder data in Figure 25.

A rational means was needed to extend lower Reynolds number data to higher Reynolds numbers. The method developed by Guven et al. at the University of Iowa has been used as seen in Figure 26 and 27. Data from a variety of sources including the CalTech results indicate a reasonable correlation by the model. The Reynolds number independent region which indicates dependence only on the relative roughness is shown in Figure 26. The data

TABLE 1. Run Matrix

RUN NUMBER	CONFIGURATION	REYNOLDS NUMBER
6-8	Smooth	1.3×10^6 
19-22	Rough ($K/D=10^{-3}$)	
26-29	Rough ($K/D=10^{-2}$)	

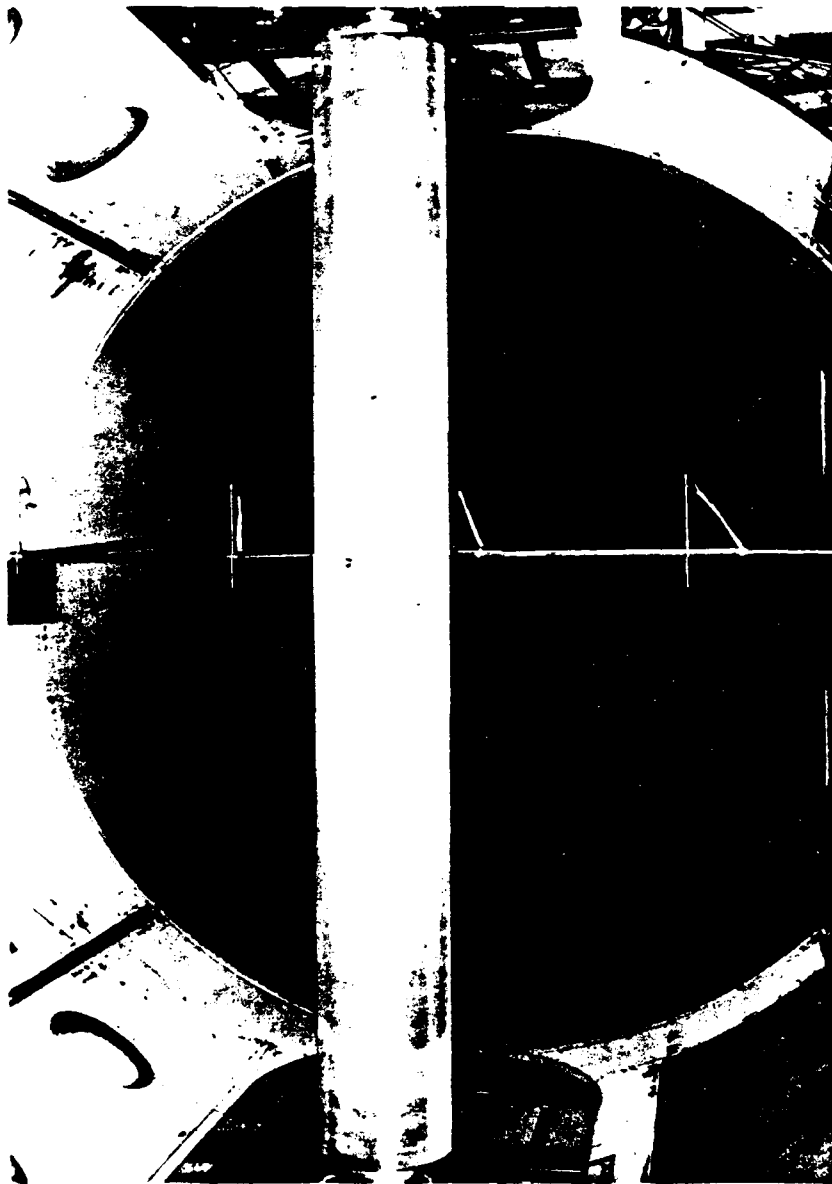


FIGURE 23. Circular Cylinder Model in CalTech 10 Foot Tunnel

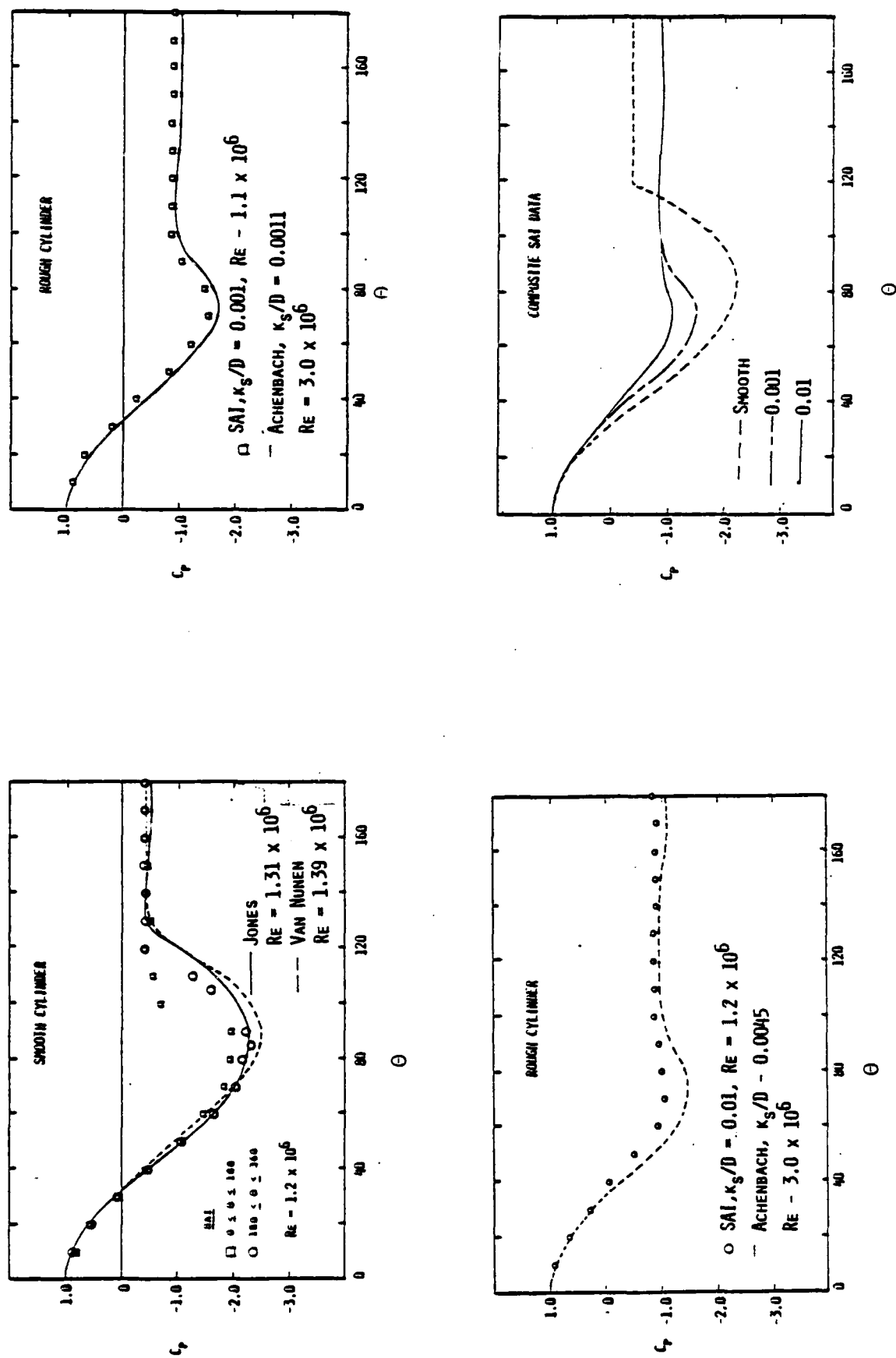
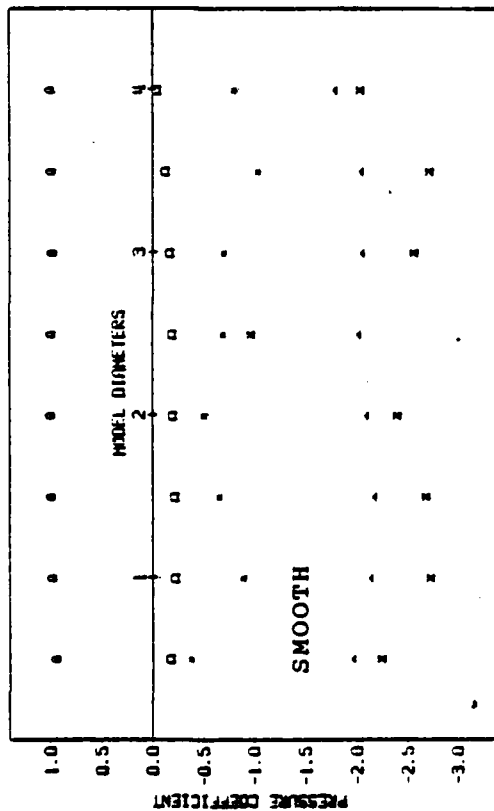
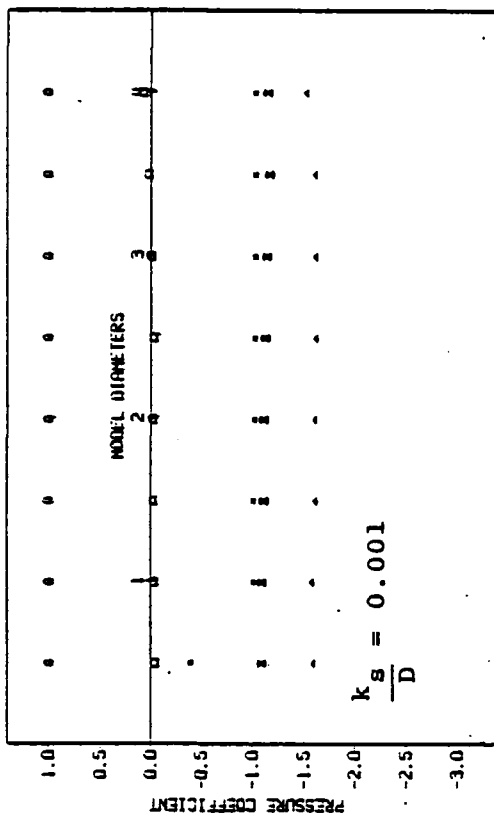


FIGURE 24. Pressure Distributions From CalTech Tests

RUN 6 GENERATOR DATA



RUN 10 GENERATOR DATA



10

RUN 26 GENERATOR DATA

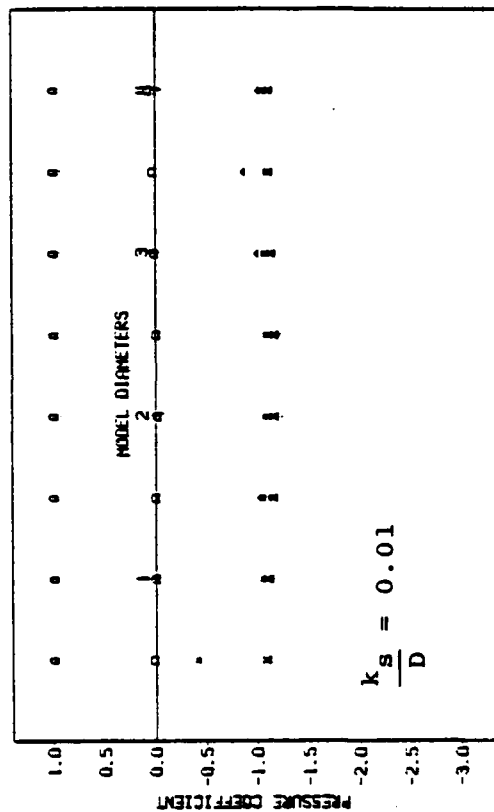


FIGURE 25. Cylinder Spanwise Pressure Distributions From Caltech Tests

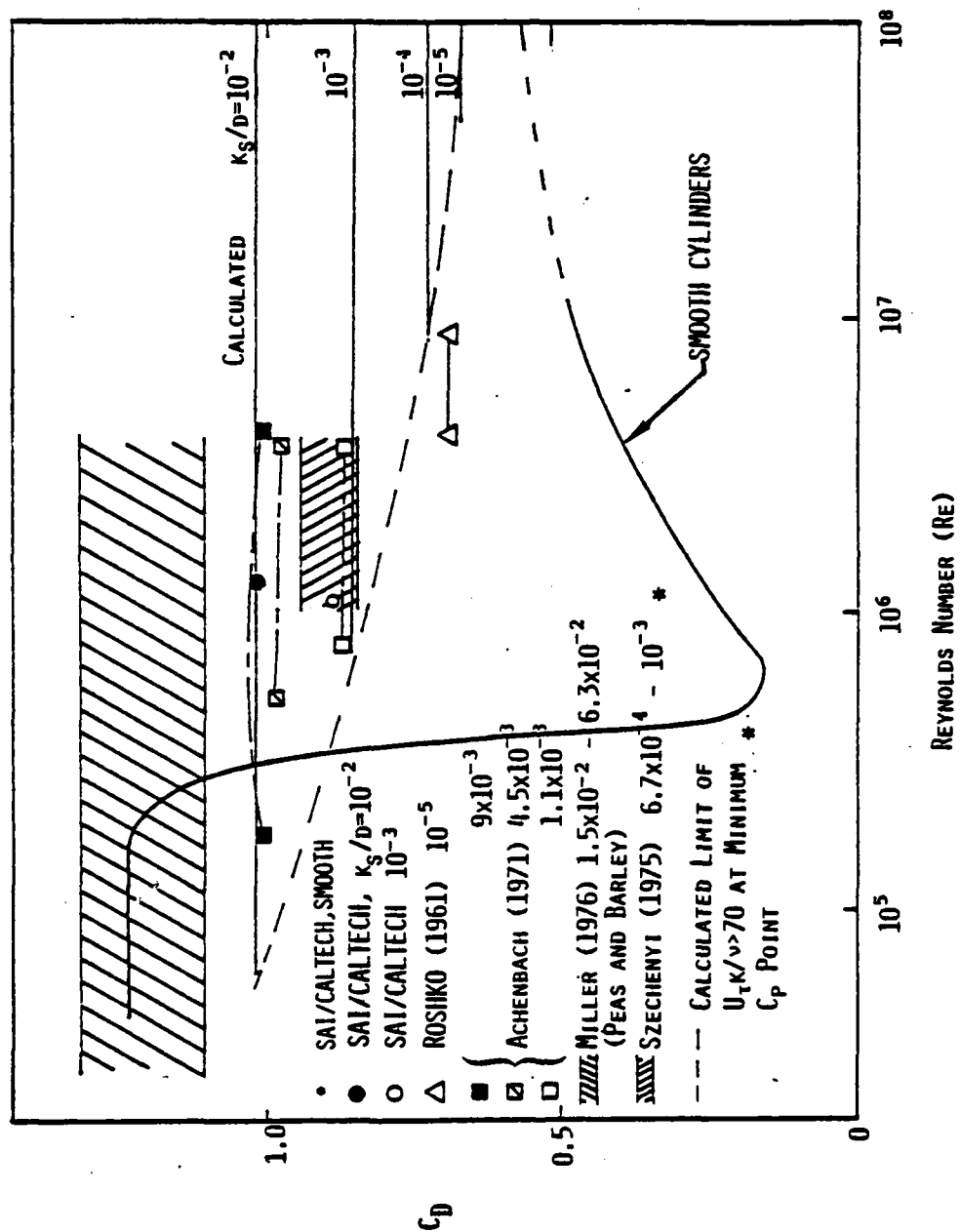


FIGURE 26. Drag Coefficient

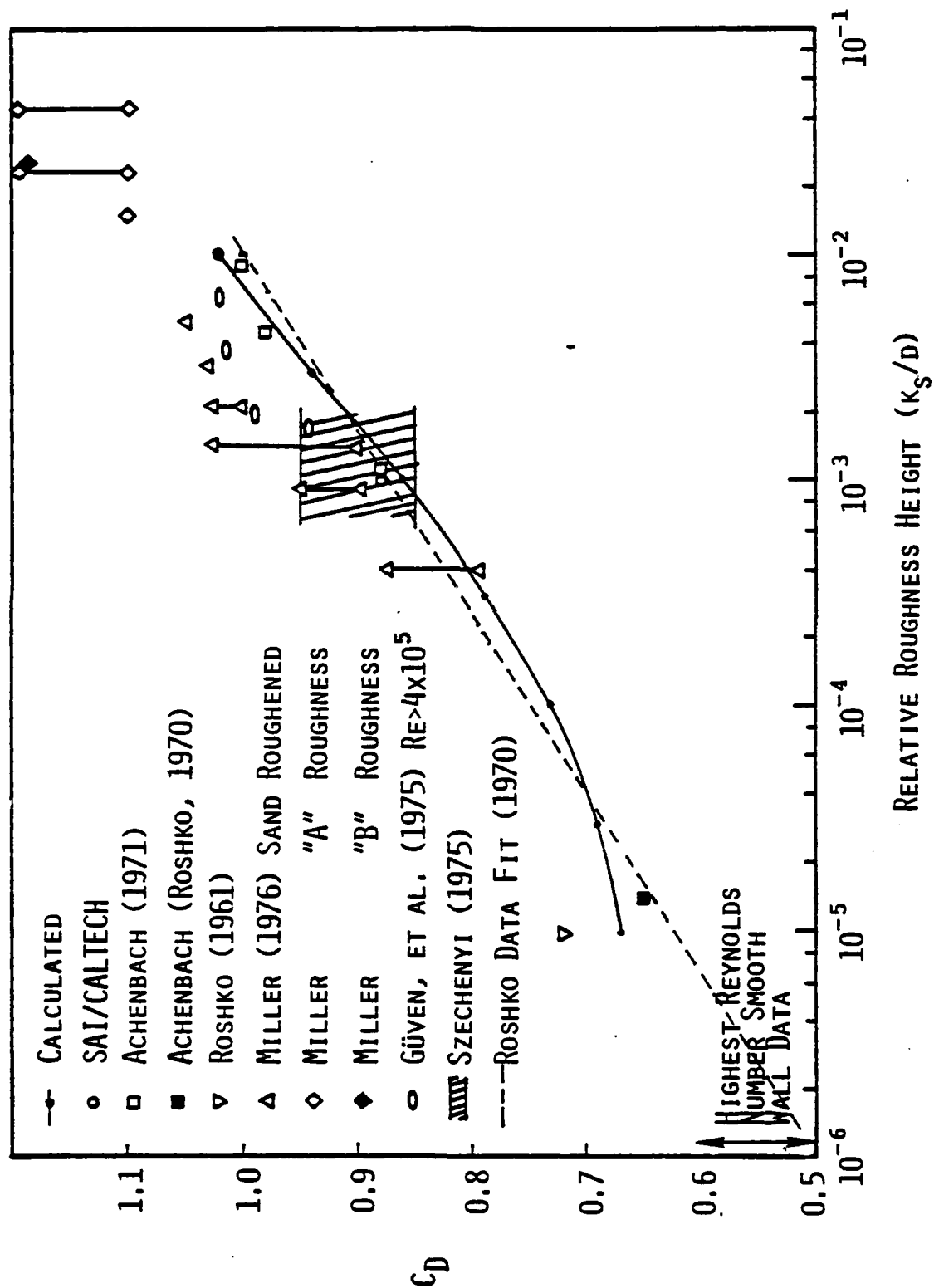


FIGURE 27. Roughness Effect on Drag Coefficient

and the model does not support the contention of Szechenyi that C_D is only a function of the Reynolds number based on roughness. Morkovin suggested that we obtain the Szechenyi data through ONERA and reexamine the results more carefully.

Power spectral density plots of the lift coefficient were obtained from the Kulite pressure gage data and are shown in Figure 28 for the three different surface conditions. The coherent shedding as a result of the presence of roughness on the cylinder is evident. A model for the Strouhal number based on Roshko's universal Strouhal number ideas and the wake source model is shown in Figure 29. It is seen to be only a function of k/D and decreases slightly with increasing roughness. Although the value of S shown in Figure 28 is closer to 0.2, the small decrease with roughness is seen as predicted by the model. This is expected due to the opening of the cylinder wake with roughness.

Freestream Turbulence in the 12-Foot Tunnel

K. Owen presented some hot wire and acoustic pressure data made before and after the settling screens in the NASA 12-foot tunnel. Typically, the velocity fluctuations over the whole Reynolds number regime is less than 0.1%, and the integral scales were several inches in length.

Morkovin indicated that during his stay in the USSR, he was shown data taken by Kovalenkov in a very low turbulence, <0.04%, wind tunnel which suggested that freestream turbulence has the effect of smearing things out. In the very low turbulence environment, onset of critical phenomena was very abrupt and sudden with the formation of the separation bubble all along the cylinder. The data will be published in the open literature in the near future. In this case, the critical Re would be a well-defined number.

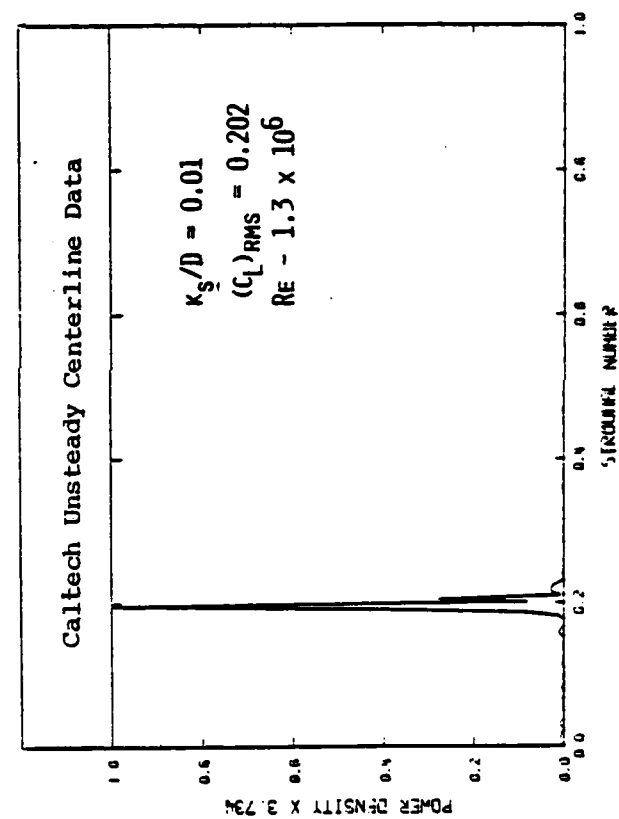
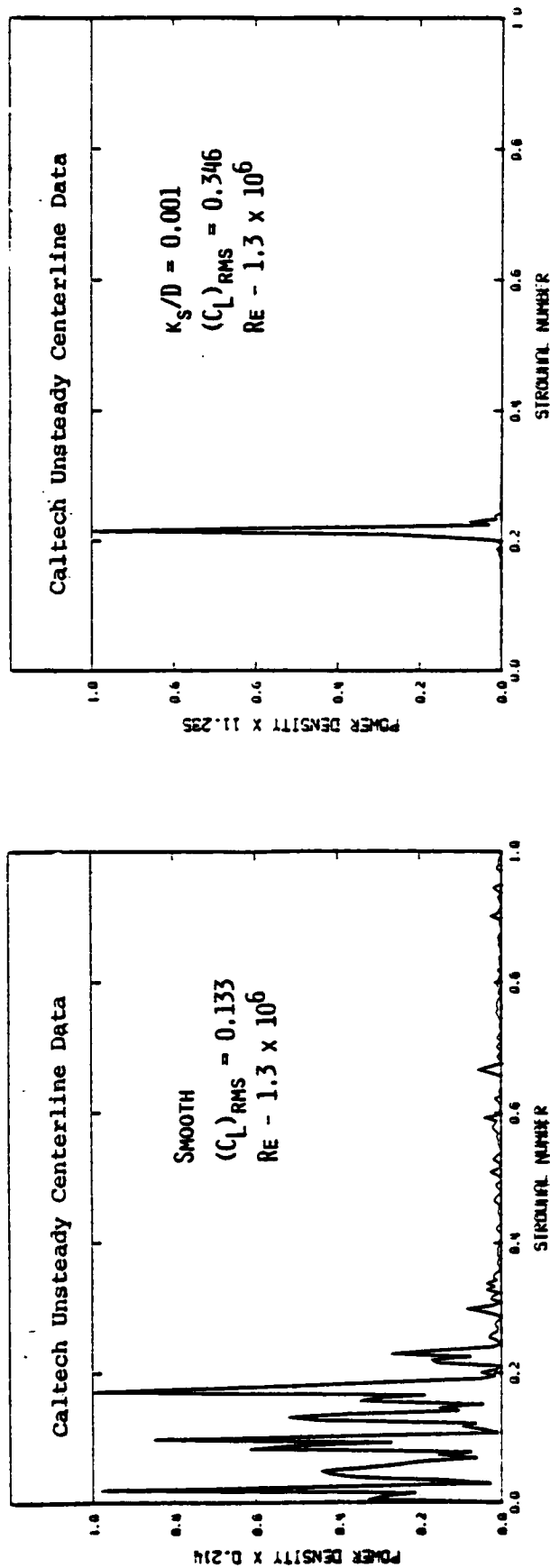


FIGURE 28. Power Spectral Density Plots of the Lift Coefficient

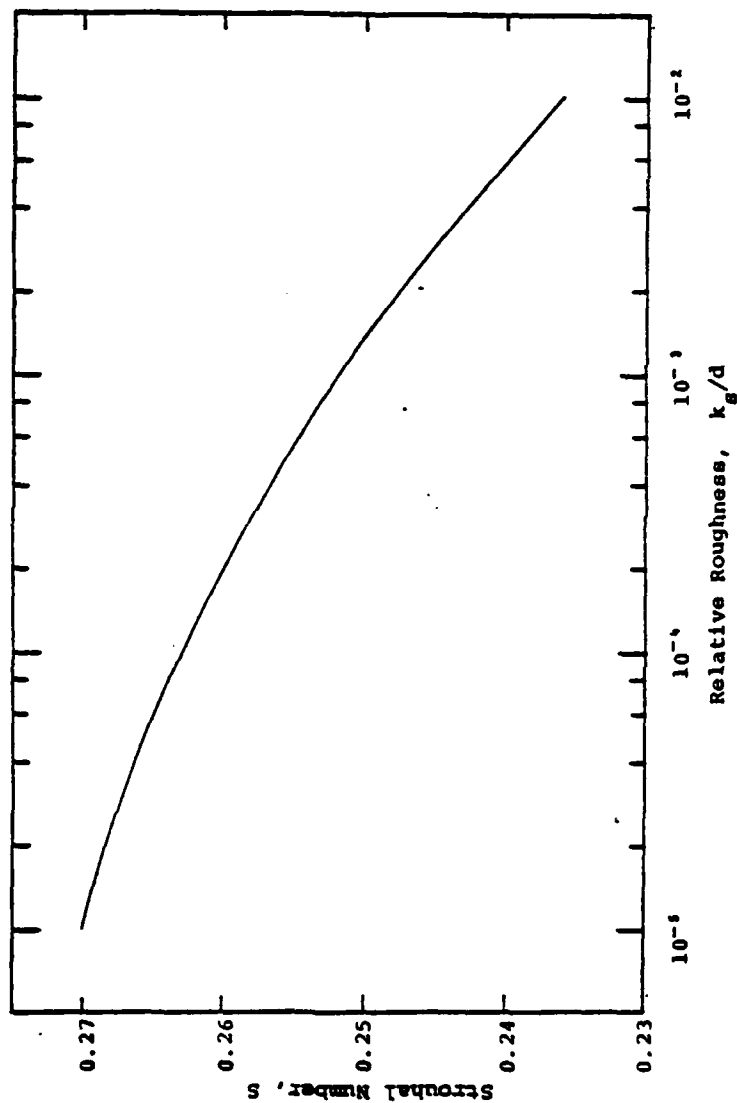


FIGURE 29. Effects of Relative Roughness on Strouhal Number in Reynolds Numbers Independence Regime

Unsteady Flow About Bluff Cylinders

G. Toebe presented a movie that showed in detail the unsteady flow field at and near the rear of bluff non-circular cylinders. The process of alternate vortex formation was clearly portrayed. The effect of non-circular cylinder orientation on fluidelastic stability was shown.

Flow field-force correlation was portrayed by simultaneous showing of the vortex formation and an X-Y recorder tracing the oscillatory lift. Shown also were the effects of splitter plates and of flow confinement or "blocking" on vortex formation. The essentially stochastic character of the phenomenon was illustrated by the lift-drag correlation traces or "Lissajous figures."

Analytical Models

D. Deffenbaugh prefaced his discussions of analytical methods with a brief description of some ocean tests of large scale flexible cylinders performed by TRW off Catalina Island. Intent was to observe hydrodynamically driven motions of the cylinder. Qualitative information was obtained and appeared consistent with previous observations of O. Griffin and small scale tests performed at CalTech.

A review of numerical methods for predicting the flow around the circular cylinder was presented. These include discrete vortex techniques as well as finite difference solutions to the Navier-Stokes equations. Most of the finite difference techniques reviewed used the non-conservative form of the equations, are explicit and use a circular expanding grid. Majority of the work is for low Reynolds numbers of a few hundred, but one solution at 3×10^5 using an upwind differencing technique gave pressure distributions within 20% accuracy, but took many hours on the computer and did not address the turbulence question. The integral-differential method of Thompson and Wu involves placing vorticity on the surface of the cylinder and summing the induced

velocity elsewhere in conjunction with the governing equations of motion. This method uses much computer time and is not competitive with finite difference methods for two-dimensional problems. Due to requirement for grid points only regions of vorticity, this method may be useful for three dimensional problems.

Discrete vortex-wake models are basically inviscid in nature. Vorticity in the wake is represented by discrete vortices and their motion in the flow is followed using the appropriate equations of motion. Sarpkaya developed a method by which vorticity in the boundary layer was convected into the wake, but this is still, basically, an inviscid formulation. Deffenbaugh introduced a viscous boundary layer on the cylinder. An integral-momentum solution was used for the early times of the cylinder motion and for later times, used the Stratford separation criteria. At separation, a vortex is allowed to leave the cylinder and the resulting flow is calculated with the appropriate boundary conditions imposed. Results obtained for an impulsively started cylinder are shown in Figures 30a and 30b as the flow develops around the cylinder and in the wake. The separation angle is shown in Figure 31. Figure 32 shows representative pressure coefficient distributions for various times. Examples of drag and lift as functions of time are shown in Figures 33 and 34. One difficulty with the method is how to handle the loss of 40% vorticity from the boundary layer to the vortex in the wake that has been experimentally determined. The Strouhal number calculated was 0.19. Whether or not this value would be 0.3 if the separation point is moved downstream is not known, but might be an interesting exercise.

Effects of Spanwise Nonuniformities

D. Coles presented some comments on the effects of spanwise nonuniformities on cylinder flows. The following is a revised set of comments that were sent after the Workshop.

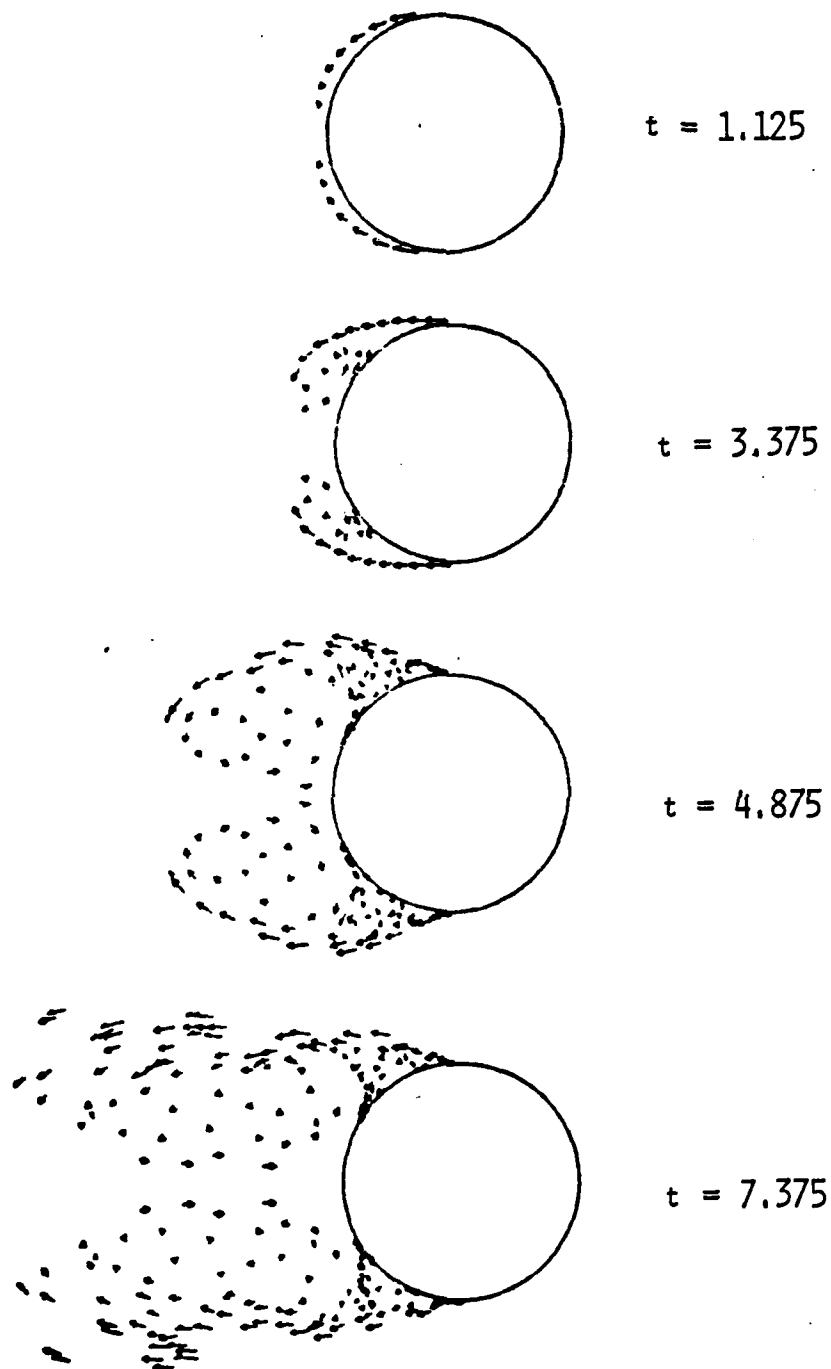


FIGURE 30a. Discrete Vortex Model Early Time Flow Field Development (Deffenbaugh)



FIGURE 30b. Discrete Vortex Model Wake Development $t = 25.0$ (Deffenbaugh)

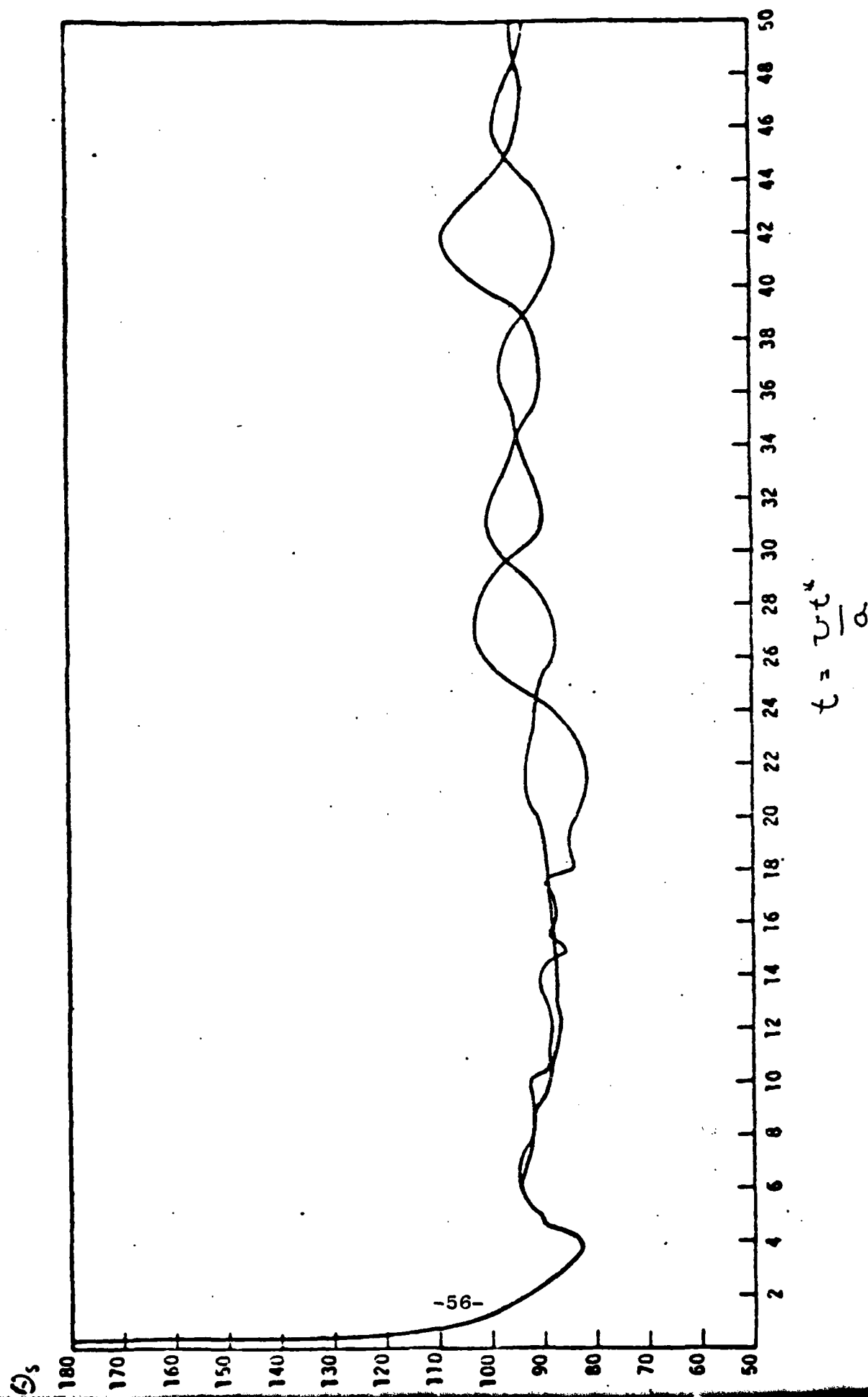


FIGURE 31. Discrete Vortex Model, Boundary Layer Separation Angle

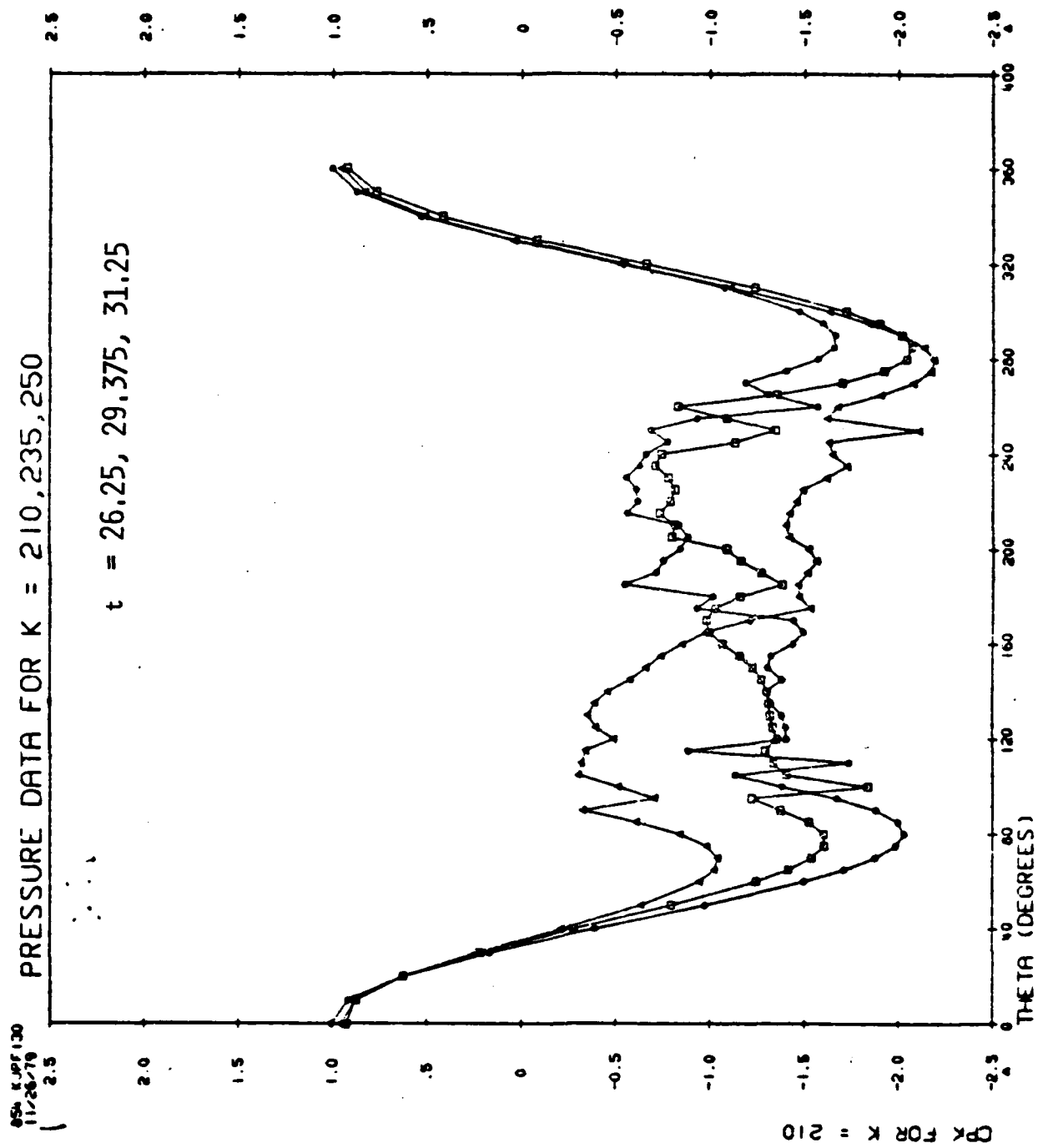


FIGURE 32. Discrete Vortex Model, Pressure Coefficient

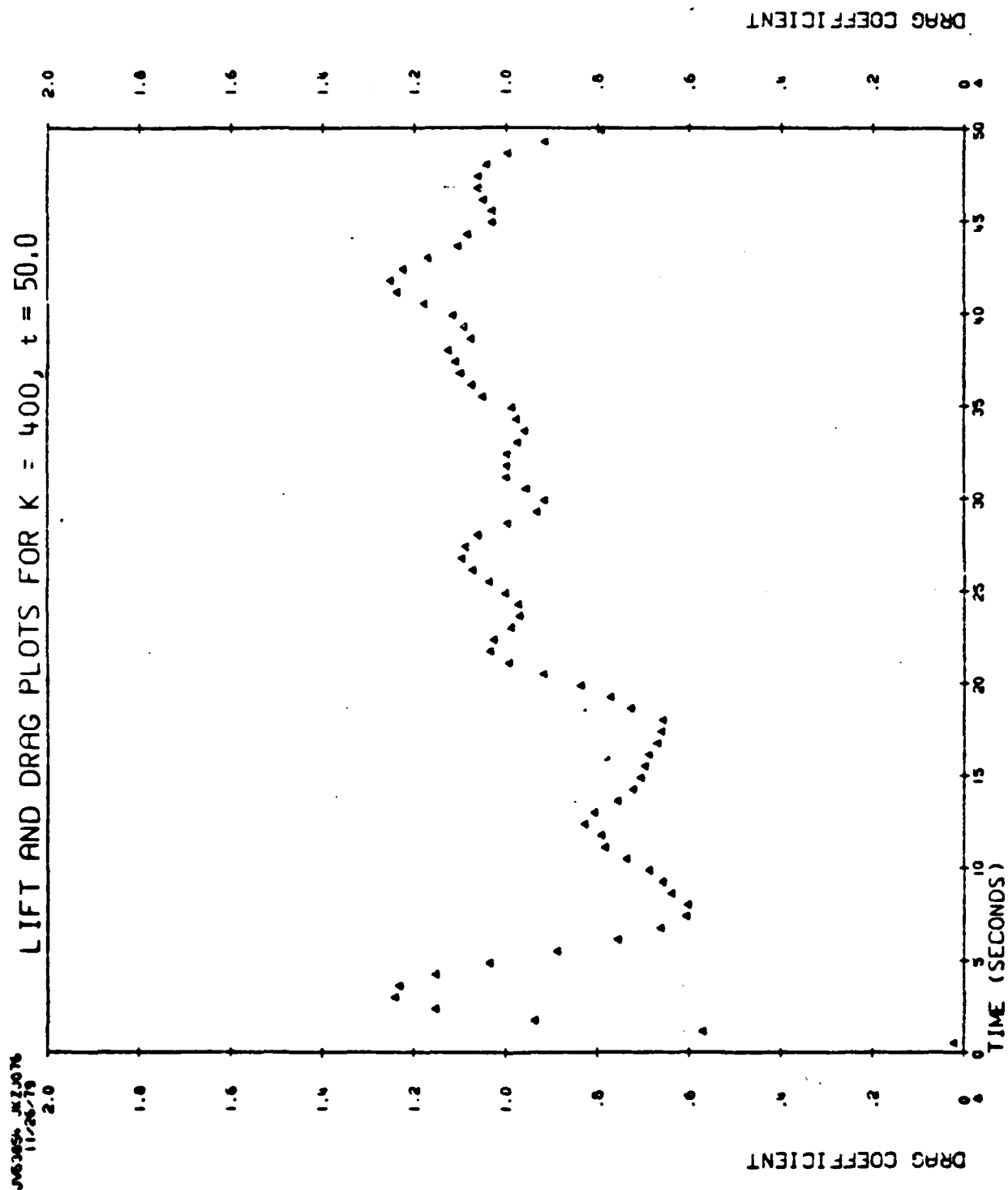


FIGURE 33. Discrete Vortex Model, Drag Coefficient

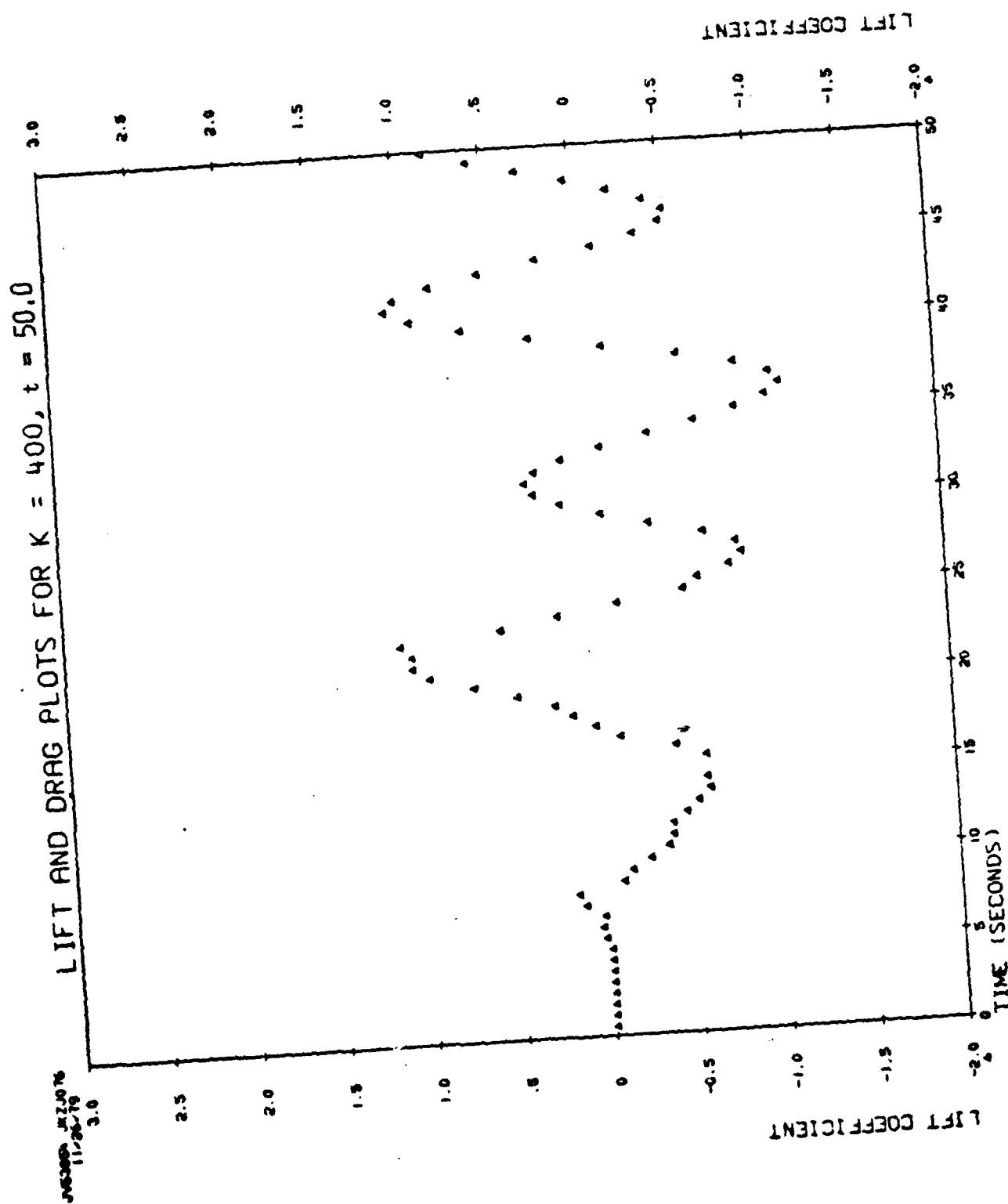


FIGURE 34. Discrete Vortex Model, Lift Coefficient

Free end - Interest in flow past finite cylinders arises in part from structural and air-pollution problems connected with stacks, towers, and high-rise buildings. In the early 1960's, some emphasis was also put on the problem of wind loads on rockets in the launching position.

It has been known since the early measurements by Wieselsberger (1921; see also McKinney 1960) that the drag of a cylinder of finite length in a uniform stream is less than the drag of an equal length of an indefinitely longer cylinder. The reasons are not obvious, and involve some complicated three-dimensional flow patterns near the free end.

Several studies of cantilevered cylinders have been made at Reynolds numbers in the range 10^4 to 10^6 for the simplest possible geometry, which is a uniform solid circular cylinder cut off normal to its axis. Etzold and Fiedler (1976), working at $Re = 30,000$ with a high turbulence level, used flow visualization to establish the presence of an end bubble bounded in the forward region by a shear layer which connects boundary-layer vorticity from one side of the cylinder to the other. Measurements by Sykes (1962) and others show that the low drag for a finite cylinder is caused primarily by high base pressure in the first several diameters near the tip, slightly reinforced by a low forward stagnation pressure in the last fraction of a diameter near the tip. This low pressure is associated with a strong deflection of the approaching flow toward the free end, with an axial velocity at the corner comparable to or larger than the free-stream velocity. In fact, the only available measurements of pressure on the end of the cylinder, by Farivar (1975), show the pressure coefficient over the upstream half of the end surface at $Re = 70,000$ to be constant at about -1.4 , rising to -0.5 toward the rear. The general spanwise deflection, especially at the sides of the cylinder, generates streamwise vorticity which turns into two nearly stationary trailing vortices near the tip,

as noted by Sykes and by Etzold and Fiedler. These vortices have the same sense as for a wing lifting toward the free end. Application of free-streamline considerations to the end bubble promises to be a difficult matter.

Above and downstream from the free end, according to Etzold and Fiedler, fluid having initially high stagnation pressure moves toward the root of the cylinder due to induction by the two trailing vortices, and is entrained into the base region. Part of this fluid close to the cylinder reverses direction and flows back toward the low-pressure region on the end surface. If the cylinder is sufficiently long, the backflow occupies about two diameters. The more downstream part of the entrained fluid flows generally away from the tip in the base region, in a mildly adverse pressure field. It is presumably this latter flow which raises the base pressure and reduces the drag.

Another influence of a free end is to disrupt locally any regular vortex shedding. Schmidt (1963), Blackiston (1963), and Spitzer (1965) found very short coherence lengths for section lift and drag near the end of a flat-faced cylinder. However, their measurements were made in a range of Reynolds numbers (380,000 to 750,000) where coherence is normally poor. Much of their attention eventually turned to a study of the effect of various disturbances in producing local transition, unsymmetrical flow, and finite static lift.

Gould, Raymer, and Ponsford (1968) were interested in flow past tall chimneys. They worked at much higher Reynolds numbers, as high as 5.4×10^6 . In this range also the section drag coefficient was reduced by the presence of the free end, and surface oil-flow visualization showed the trailing vortices already mentioned. These tended to be weakened when there was efflux from the end (the case of influx was not considered). Surface-pressure correlations around the cylinder indicated that non-steady pressure loads would be quite conducive to ovaling a distance of a few diameters from the tip.

In general, at both subcritical and transcritical Reynolds numbers, the effects of a closed free end seem to be manifested in fixed streamwise vortices which modify the normal shedding phenomenon over the last several diameters of the cylinder, and which also deflect high-energy fluid into the base region and thus reduce the drag. Addition of shear to the stream does not have a large additional effect (Gould et al. 1968, Maull and Yound 1972, Farivar 1975). Very little is known about effects of flow into or out of the cylinder, although it is clear from work on the launch problem (e.g., Buell, McCullough, and Steinmetz 1963) that aerodynamic loads can be strongly affected by minor changes in geometry.

Shear Flow - Interest in sheared flow arises from a need to establish coherence lengths for use in design of cylindrical structures exposed to wind or water forces. For sheared flow past a uniform cylinder, and also for uniform flow past a tapered cylinder, there is general agreement that the local Strouhal number is nearly the same function of local Reynolds number as in two-dimensional flow. At CalTech, our first experience with the problem involved some hot-wire measurements in the wake of a slightly tapered cylinder in a uniform stream at Reynolds numbers of a few hundred (unpublished lab-course report, 1958). Given that S is independent of Re , the streamwise pitch of the vortex street must be proportional to local diameter, and there is some difficulty in visualizing the configuration of vorticity in the wake. A flow-visualization study was carried out to resolve the difficulty. The technique, suggested by H. W. Liepmann, was to cool the model in a bath of liquid nitrogen before insertion in the tunnel. Moisture in the tunnel air condensed near the cold model and made the wake structure visible. Some photographs from this study (unpublished lab-course report, 1960), depicting the wake of a uniform cylinder, of a tapered cylinder, and of a cylinder with a 2:1 discontinuity in diameter, all at a Reynolds number of about 200, are shown as Figures 35a, 35b and



FIGURE 35a. Wake Structure For Uniform Cylinder (Coles)

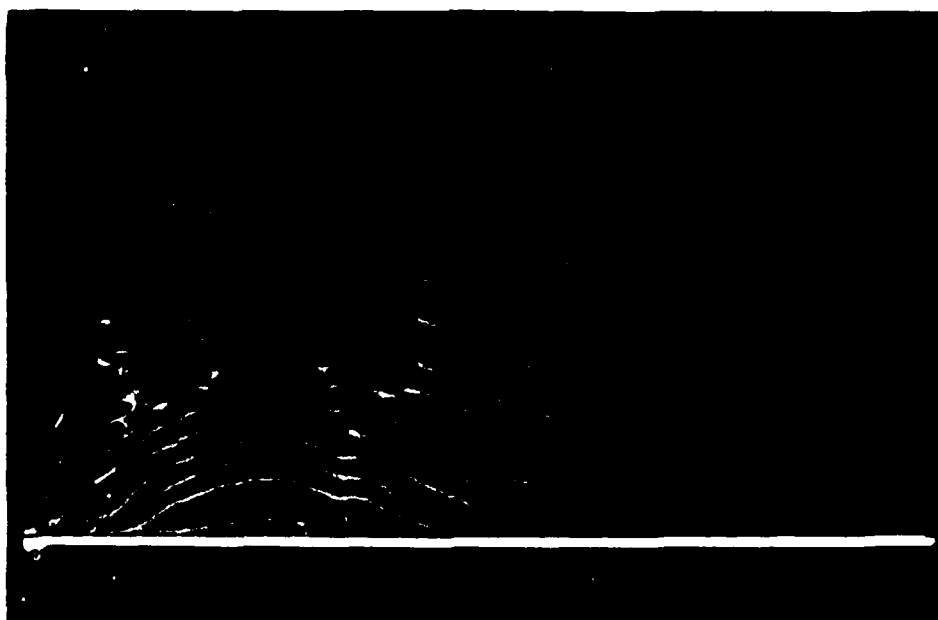


FIGURE 35b. Wake Structure For Tapered Cylinder

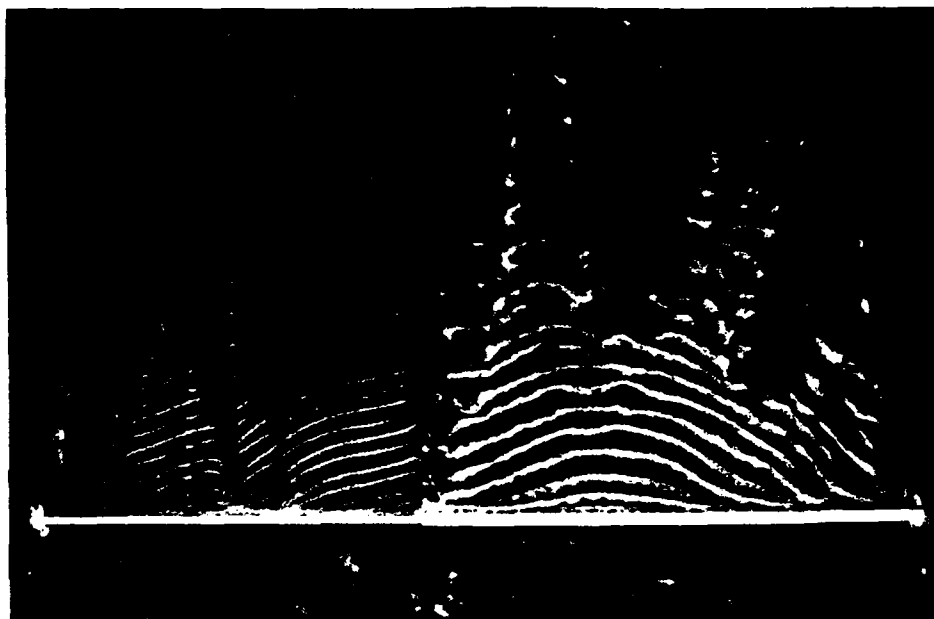


FIGURE 35c. Wake Structure for Cylinder with a 2:1 Discontinuity in Diameter

35c. Our conclusion was that the conventional vortex laws govern the situation. The shed vortices do not end in the fluid; typically a vortex from one side of the street (or just possibly part of this vortex) crosses over and joins with a vortex from the other side. The same conclusion was reached by Gerrard (1966), who suggested that three-dimensionality associated with random vortex crossover (which he characterized as flapping of the wake) is probably the main source of the amplitude and frequency modulation commonly observed in the subcritical range of Reynolds numbers. A paper by Gaster (1969) outlines an alternative interpretation of modulation for the case of a tapered cylinder, but begs the question of vortex continuity.

This work in flow at low Reynolds numbers indicates that the typical vortex structure in a real wake, particularly far downstream, is likely to be an elongated, distorted loop rather than a line vortex. The mechanisms are mostly kinematic, and the Reynolds number is important only to the extent that local disturbances determine the axial scale of these loops and thus determine the axial coherence length, particularly in the critical range of Reynolds number. Naumann and Quadflieg (1968) discuss the problem in terms of the circulation differences associated with a non-uniform separation line, and give estimates of the differences which can be tolerated without serious disruption of the vortex street.

There are several reasons why the effect of shear in the free stream cannot be equated to the effect of variations in diameter, except for the common property just described. As emphasized by Maull and Young (1973), a sheared stream contains vorticity oriented normal to the cylinder axis. This vorticity becomes wrapped around the cylinder and appears as streamwise vorticity in the wake; it will deflect the approaching stream by induction and it may also be concentrated by non-uniformities and amplified by stretching. Moreover, suppose that the diameter

is constant and the local drag coefficient and Strouhal number are nearly independent of Re , as in the subcritical and transcritical range. Two conclusions then follow. First, the nominal pitch of the vortex street in a sheared flow will be essentially constant (at roughly 5 diameters, say, if $S = 0.2$) along the length of the cylinder. Second, the surface-pressure distribution around the cylinder will scale in an affine way with the local dynamic pressure, as indicated in particular by some data for base pressure by Mair and Stansby (1975). But it can be shown that the flow of vorticity into the base region at a separation line is proportional to the net pressure change measured from the front stagnation line to separation, * and thus to the local dynamic pressure. If the vortex pitch is constant, the vortex strength must vary, as noted (with some aberrations in the argument) by Gerrard. The vortex laws again suggest a configuration of closed loops. These loops may be shed with a large initial inclination, as observed by Maull (1969), by Maull and Young (1972) and by Bradbury and Moss (1975); in any case they will be continuously rotated in the plane of the wake by the shear in the free stream, and will contribute to concentrations of streamwise vorticity. One consequence in a severely constrained flow may be the appearance of fixed shedding cells along the cylinder length, as observed by Maull and Young and by Davies (1975). Finally, suppose again that local pressures around the cylinder scale roughly linearly with local stagnation pressure. The resulting axial pressure gradient in the base region, where the pressure is everywhere lower than ambient static pressure, ought to produce a strong spanwise flow from the low-speed end of the cylinder toward the high-speed end, although this flow will be opposed to some extent by induction by the trailing vorticity. Axial velocities in the base region of the order of one third of the local free-stream velocity were measured by Bradbury and Moss for a narrow plate normal to a sheared stream.

* This observation comes under the heading of common knowledge; i. e., it does not seem to be written down anywhere, at least in general form. In the notation of Lagerstrom (1964), the momentum equation for an incompressible fluid is

$$\frac{D\vec{u}}{Dt} = -\frac{1}{\rho} \text{grad } p + \begin{cases} \nu \text{ div grad } \vec{u} \\ \text{or} \\ -\nu \text{ curl curl } \vec{u} \end{cases}$$

Taking the curl yields the vorticity equation for $\vec{\Omega} = \text{curl } \vec{u}$,

$$\frac{D\vec{\Omega}}{Dt} = (\text{grad } \vec{u}) \vec{\Omega} + \begin{cases} \nu \text{ div grad } \vec{\Omega} \\ \text{or} \\ -\nu \text{ curl curl } \vec{\Omega} \end{cases}$$

and integration in a fixed control volume gives, after a little manipulation of the integrals,

$$\frac{d}{dt} \int \vec{\Omega} dV = - \int \vec{\Omega} (\vec{u} \cdot \vec{n}) dS + \int \vec{u} (\vec{\Omega} \cdot \vec{n}) dS + \begin{cases} \nu \int (\text{grad } \vec{\Omega}) \vec{n} dS \\ \text{or} \\ \nu \int (\text{curl } \vec{\Omega}) \chi \vec{n} dS \end{cases}$$

where \vec{n} is the outward unit normal. Use of the original momentum equation gives finally

$$\frac{d}{dt} \int \vec{\Omega} dV = - \int \vec{\Omega} (\vec{u} \cdot \vec{n}) dS + \int \vec{u} (\vec{\Omega} \cdot \vec{n}) dS + \begin{cases} \nu \int (\text{grad } \vec{\Omega}) \vec{n} dS \\ \text{or} \\ - \int \frac{D\vec{u}}{Dt} \chi \vec{n} dS - \frac{1}{\rho} \int \text{grad } p \chi \vec{n} dS \end{cases}$$

The first version of the last term represents diffusion of vorticity across free boundaries. At a solid boundary, where $\text{grad } \vec{\Omega}$ may not be explicitly known, the second version of the last term provides an alternate means for evaluation. It is clear that a pressure gradient at a wall continuously generates vorticity; this vorticity lies in the wall and is normal to and proportional to $\text{grad } p$. The term involving $D\vec{u}/dt$ is zero if a no-slip condition applies, but is displayed here because it represents, for example, a concentrated vorticity source at the leading edge of a flat plate in Blasius flow, for which $\text{grad } p \neq 0$.

Note that the equations are independent of any particular coordinate system and that the flow need not be steady, two-dimensional, or even laminar.

These arguments indicate that the main effect of shear, other things being equal, must be to decrease the coherence length associated with vortex shedding. This effect of shear works in opposition to effects of surface roughness and of cylinder vibration, and is therefore important for structural design. It needs to be better understood than it is at present.

A little should be said about devices which have been used to generate sheared flow in wind tunnels. One such device is a curved screen or gauze; another is a non-uniform turbulence grid; a third, which has special problems, is a sheared honeycomb. If such a device operates on an initially uniform stream, as is usually the case, it is required to have two effects. One is to produce a non-uniform decrement in total pressure, or more properly in dynamic pressure. The other is to deflect the entire flow toward the high-speed region. The desired result is a parallel flow having a constant static pressure but a gradient in velocity. Some design rules are available (Elder 1959, but see Maull 1969 for an error in Elder's analysis), but cut-and-try methods are sometimes required.

Production of sheared flow at very high Reynolds numbers has its own special difficulties. Structural loads on the device may preclude the use of curved screens in favor of a turbulence grid, whose higher stream turbulence levels may or may not be desirable. If the Reynolds number for a cylindrical test model is 10^7 , say, the Reynolds number for the grid elements will probably be at least 10^6 , and these elements, if they are circular cylinders, will themselves be operating at supercritical Reynolds numbers. One consequence is that tunnel power will be less at the operating condition than on the way to this condition, with possible unstable tunnel operation during the passage. The problem was encountered during the grid-turbulence measurements at high Reynolds numbers in the Cooperative Wind Tunnel by Kistler and Vrebalovich (1961). The grid elements should therefore

probably have a square or rectangular or triangular cross section rather than a circular one, to fix separation and avoid the problem of a critical Reynolds number. Even so, the tunnel may have to operate with say 30 percent of the test section occupied by grid elements having a drag coefficient near unity, and the required pressure ratio may not be available even if the required power can be achieved, if necessary by reducing the dynamic pressure.

A method proposed elsewhere for producing sheared flow is use of a circular towing tank, with the towed model lying along a radius. The local stream velocity will vary linearly along the model, as desired. However, curvature effects seem to disqualify the method. For fluid in the base region at rest with respect to the model, the shear produces a base pressure which decreases quadratically with increasing radius, as required by an affine pressure field. However, the pressure gradient required to prevent axial motion increases quadratically because of the curvature of the flow. A reasonable conjecture is that spanwise velocities in the base region and perhaps elsewhere would be abnormally large compared to the case of shear alone.

Effects of Cylinder Motion

W. Shih presented a few comments on the effects of cylinder motion of flows around cylinders since T. Sarpkaya was unable to attend the meeting. The comments are based on the work of Owen Griffin which is more structural response oriented but does have some interesting implications relative to the flow phenomena. Since all structures to some degree are elastic in nature, the question of cylinder motion is a practical one. Specific answers we seek are what are the consequences of cylinder motion on the following: (1) delineation of the traditional cylinder flow regimes; (2) resonance of the cylinder with the shedding frequency or lock-on phenomena; (3) lift and drag augmentation; (4) organization of spanwise coherence. Additional parameters governing the structural response are introduced and are the reduced

velocity which is just $1/S$ when the oscillation is at the vortex shedding frequency; and the reduced damping defined by:

$$k_s = \frac{2m\delta}{\rho D^2}$$

where m is the equivalent cylinder mass per unit length including the internal water mass and the added mass; D is the cylinder diameter; δ is the log decrement of oscillation; and ρ is the fluid density.

As the fluid velocity is increased from zero, the first mode of oscillation to occur is the unsteady drag-driven in-line motion as shown in Figure 36. The initial excitation is a result of symmetric shedding of the vortices from the back of the cylinder. With further increases in the reduced velocity, the more familiar alternating vortex shedding occurs. Typical observed maximum displacements in the in-line direction are about 10-12 percent of the cylinder diameter. At still higher flow velocities, cross flow induced vibrations become important as seen in Figure 37. The rigid cylinder value of the inverse Strouhal number at these conditions is about 5, but the cylinder motion is seen to lock the shedding frequency on to the cylinder oscillation frequency over a considerable range of flow velocities. The maximum half amplitude of oscillation is 60-70 percent of the cylinder diameter. Figure 37 applies to both forced as well as flow induced oscillations. Higher mode responses have also been observed provided the reduced velocity corresponds to one of the higher normal modes as shown schematically in Figure 38.

The effect of structural damping on the cylinder displacement is shown in Figure 39. For values of the reduced damping less than about 0.2, damping has very little effect on the amplitude of oscillation and the so-called hydrodynamic damping dominates. A limit to the peak displacements is observed as indicated in Figure 39. This is reasonable since the phase of

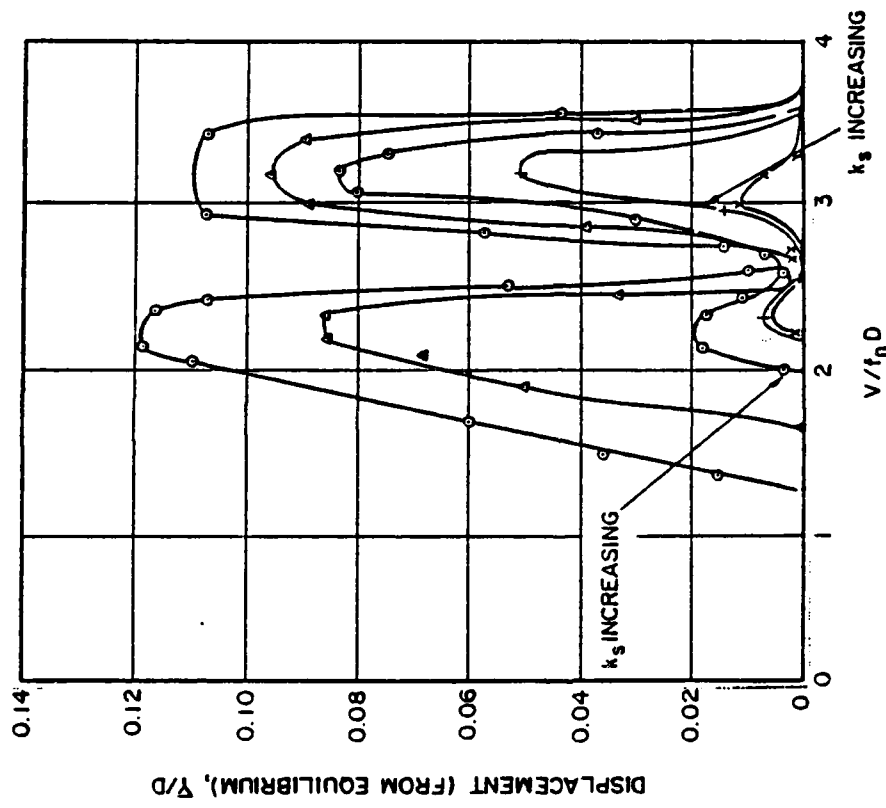


FIGURE 36. Vortex-Excited Displacement Response of a Flexible Cantilever (From Equilibrium) in the In-Line Direction Plotted Against the Reduced Velocity $V/f_n D$. The Reduced Damping of the Structure is Denoted by k_s .
From King (1974).

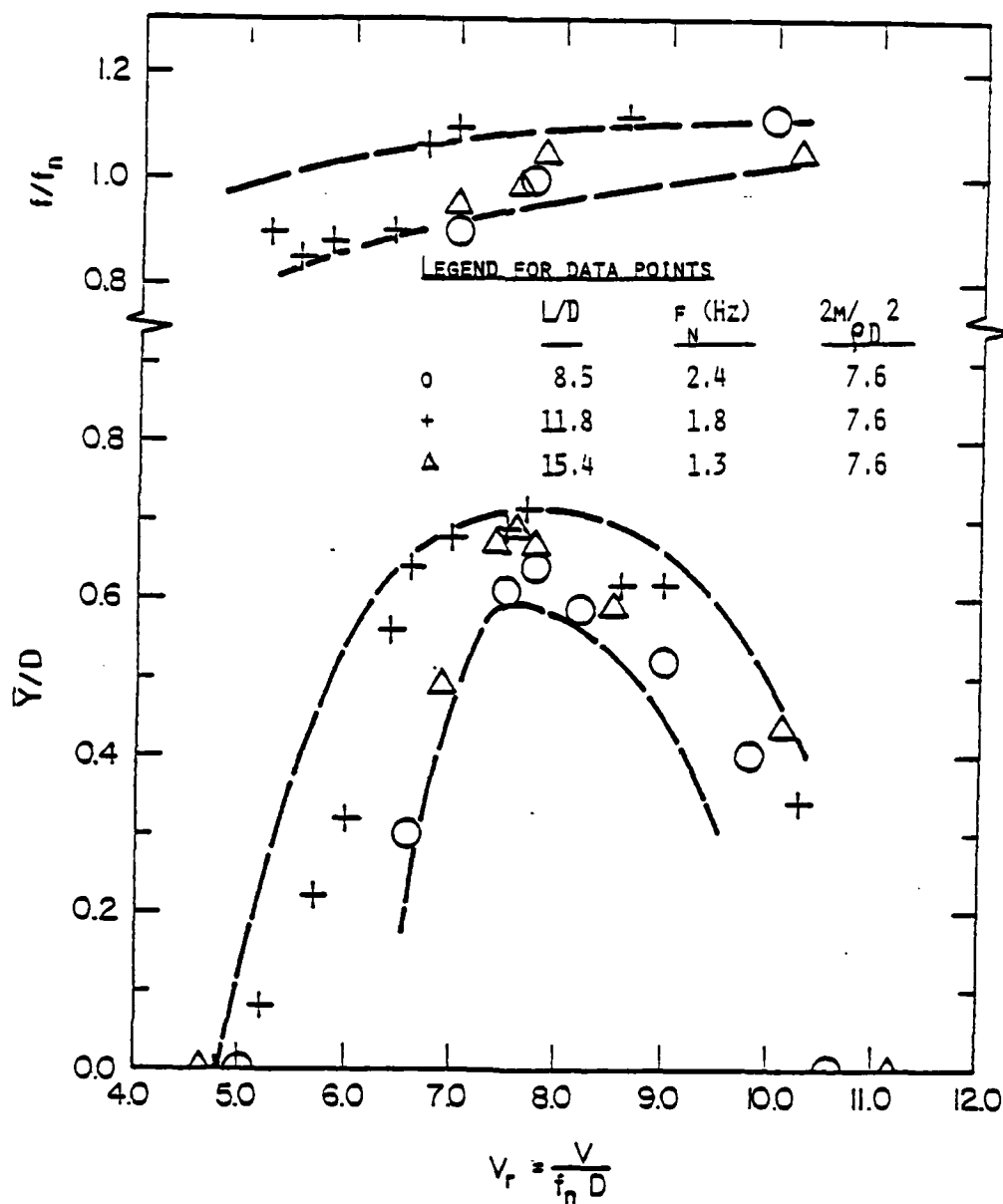


FIGURE 37. Cross Flow-Induced Vibration Displacement E/D and Frequency F of Three Circular Cylinders in Water, Plotted Against the Reduced Velocity V_r . From Griffin (1979).

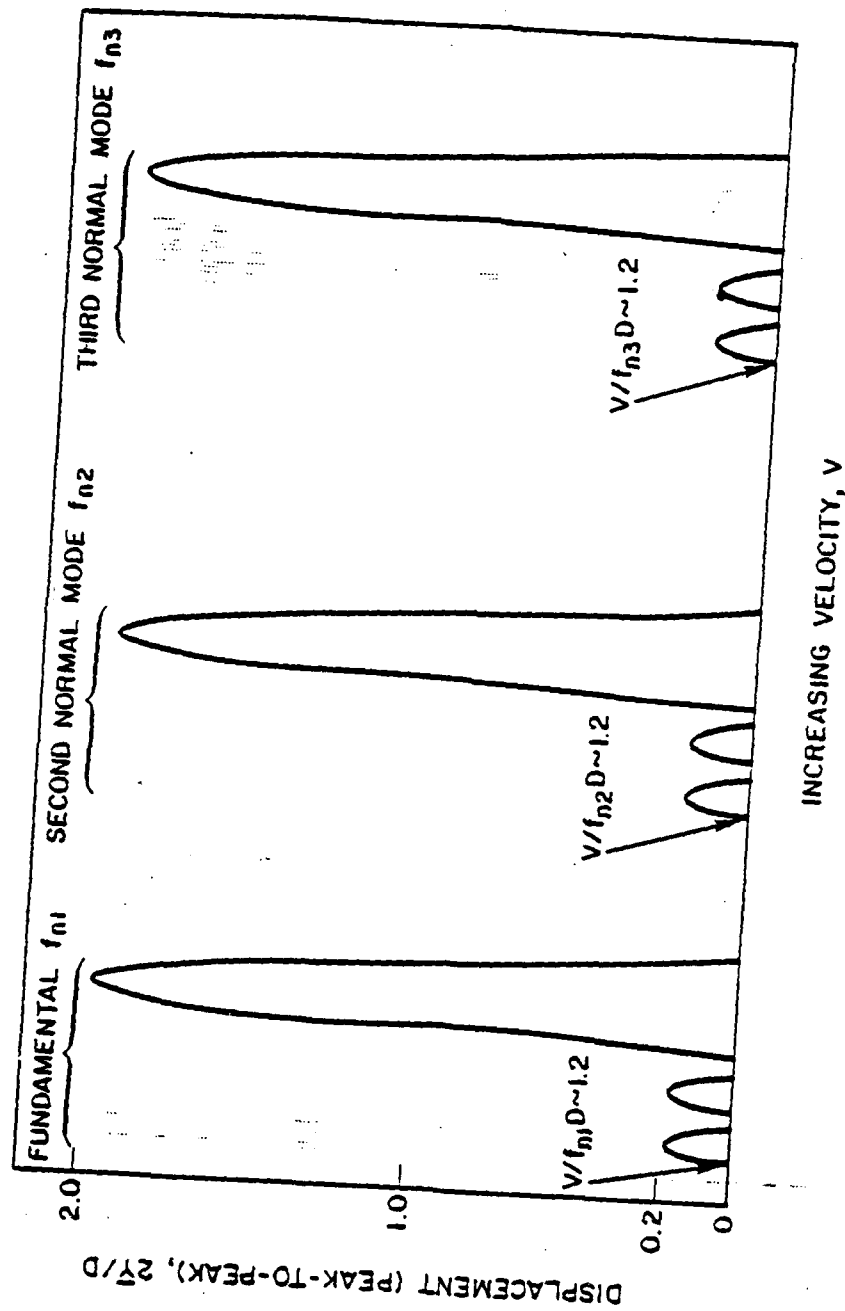


FIGURE 38. Composite Stability Diagram for the First Three Normal Modes of a Flexible, Cantilevered Circular Cylinder as a Function of the Incident Water Velocity. Both In-Line (Small Displacement) and Cross Flow (Large Displacement) Instabilities are Shown. From King (1977).

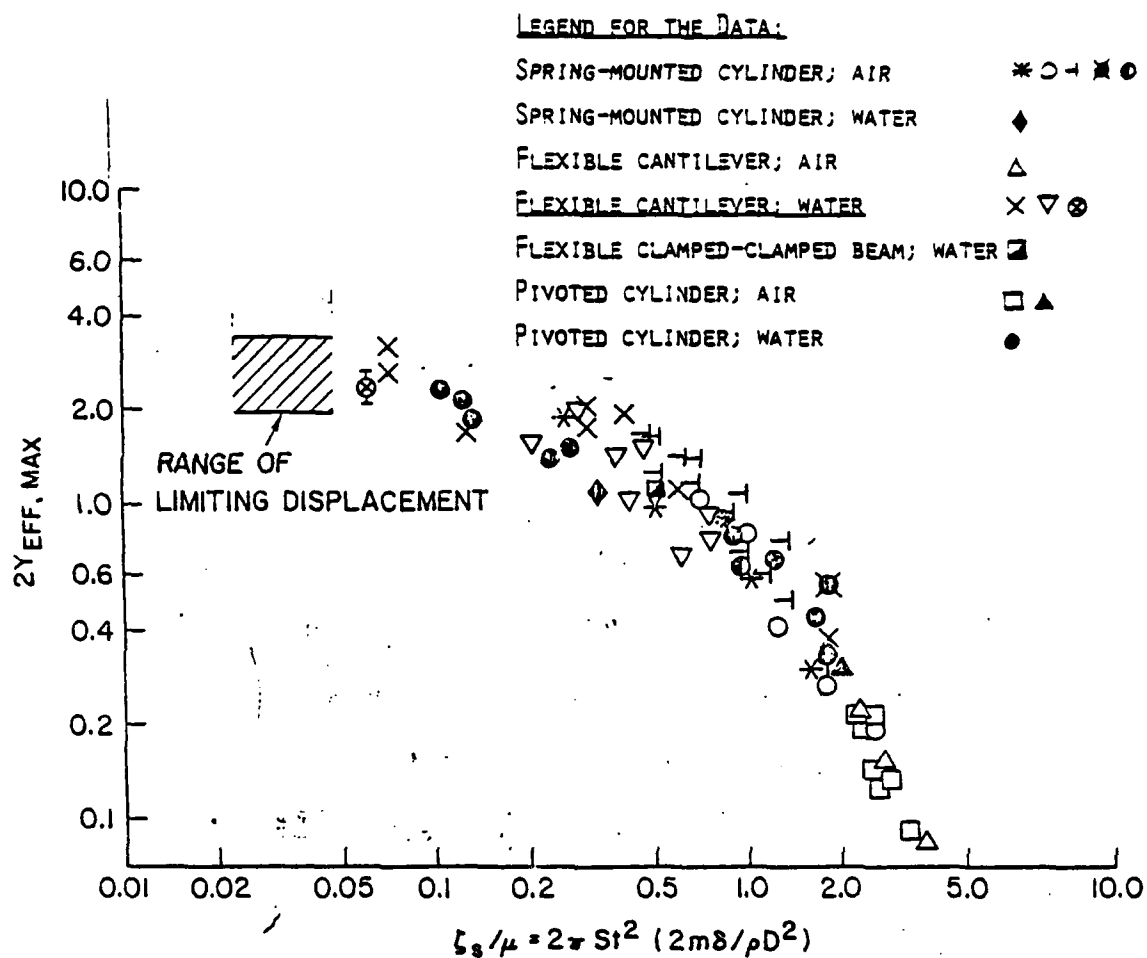


FIGURE 39. Maximum Vortex-Excited Flow Displacement $2Y_{EFF, MAX}$ of Circular Cylinders, Plotted Against the Reduced Damping $\zeta_s/\mu = 2\pi St^2 (2m\delta/\rho D^2)$

the hydrodynamic driving force, i.e., vortex shedding changes 180 degrees during the motion. The data shown represent a variety of cylinder configurations and appears to be universal in nature including higher mode responses. The effective lift coefficient corresponding to the maximum displacements are shown in Figure 40.

Figure 41 shows the close resemblance between scale model and full scale test results. The shift in scale may be the slight difference in Strouhal frequency in the different Re regimes. Thus the results presented appear to be scalable.

A correlation of the effect of cylinder motion on cylinder drag coefficient is given by Griffin based on a least square fit to the data:

$$\begin{aligned} C_D/C_{D0} &= 1.0 + 1.16(W_r - 1)^{0.65} & W_r > 1 \\ &= 1.0 & W_r \leq 1 \end{aligned}$$

$$W_r = (1 + 2Y/D)f/fs$$

Maximum values for C_D could be a factor of two greater than the rigid cylinder value.

Proposed Cylinder Tests

W. Shih presented a review of the proposed cylinder tests at the Ames 12-foot pressurized tunnel. All attendees had received copies of the proposed work and were requested to offer suggestions for conducting the tests. The stated objectives of the tests are (1) to determine steady and unsteady flow properties on smooth and rough cylinders over the maximum achievable Reynolds numbers (up to 8×10^6); (2) to investigate Reynolds number independence regime for rough cylinders. These objectives are to be achieved by using the 1-foot NASA/ISU cylinder using steady

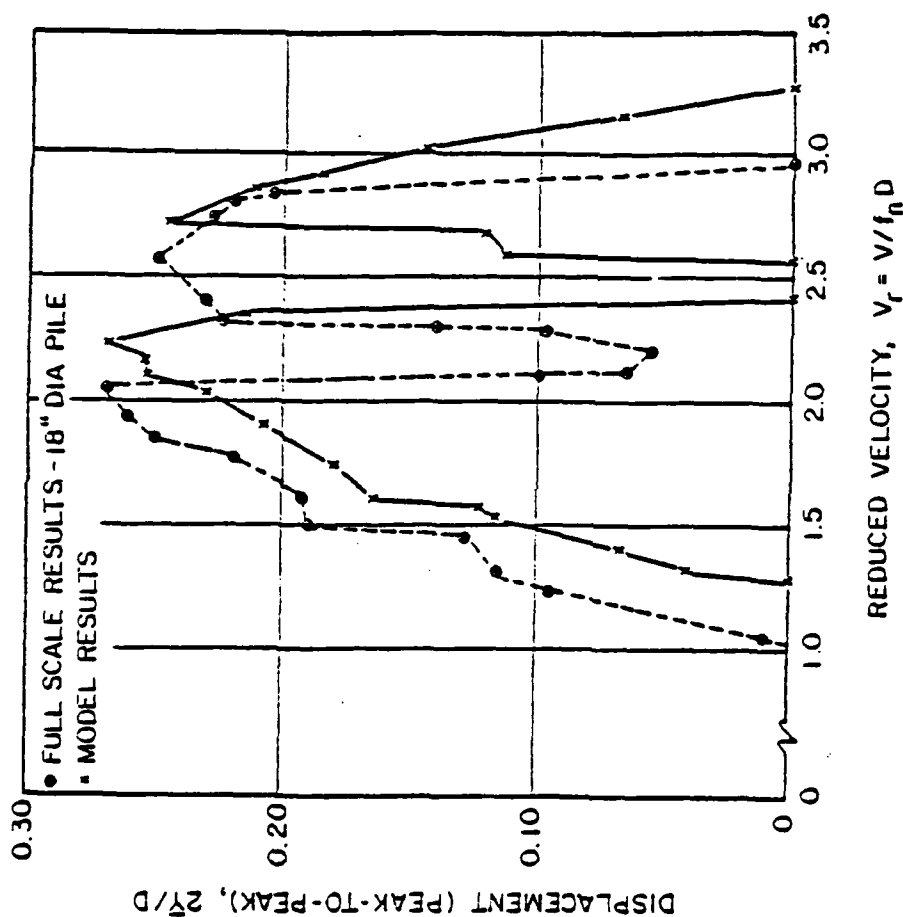


FIGURE 41. A Comparison of the Full Scale and 1/27-Scale Model Results for Vortex-Excited In-Line Oscillations of a Flexible, Cantilevered Circular Cylinder. The Full-Scale Reynolds Number was about 6(105). From King (1974).

and unsteady surface pressure gages distributed circumferentially and longitudinally on the cylinder. Boundary layer and/or surface shear measurements will be made to determine the boundary layer characteristics.

The specifics on the model and instrumentation are as follows:

Model

Diameter = 1.04 feet
Length = 11.3 feet
L/D = 10.9

Surface Finish

Smooth-chrome plated, $d/D \sim 6 \times 10^{-7}$
Rough-screens $3 \times 10^{-4} \leq k/D \leq 10^{-2}$

Instrumentation

Static pressures:

Mean-Statham PM121TC/scani-valve
Instantaneous-Kulite XCQL-7A-093-4D;
SCQL-17-093-4D

Boundary layer, shear:

Pitot traverse
Surface shear-imbedded hot wires

Detail design of some of these items are yet to be performed. Also whether or not the buried hot wires are to be used depends on the validity of the results in the presence of the screens. Calibration of the gages can be made in conjunction with the boundary layer probe measurements. The mounting of the surface hot wires is critical since the presence of the probe may influence the flow itself.

A schematic of the instrumentation ports on the cylinder is shown in Figure 42 for zero roll angle. A maximum rotation of 38 degrees can be achieved during the tests so that a good reso-

lution of the circumferential pressure distribution in the center section of the cylinder can be obtained. Such resolution is not available in the outboard sections but sufficient instrumentation is present to permit spot checks and to obtain spanwise correlations along several generators. However, the separation bubble in the critical regime may be difficult to resolve with the available outboard ports. It was suggested that a full section of additional Kulite gages one or two diameters away from the center section would be useful to obtain correlations of the entire section lift rather than just along one generator. In any case, the spanwise variations of vortex shedding is very important relative to the definition of the critical region and understanding coherence. One of the measurements should be a careful consideration of coherence length and what influence parameters such as roughness has on it. It was suggested that we should concentrate on the $Re = 10^6$ to 10^7 range, i.e., the super-transcritical regime since the critical region is dependent on too many uncontrollable parameters such as freestream turbulence which vary from tunnel to tunnel. A Kulite instrumented generator on the bottom of the cylinder was thought to be desirable so that correlation between the top and bottom of the cylinder may be determined.

Boundary layer measurements are useful in determining their characteristics in the fully rough regime and also as inputs into the analytical models such as that developed by Guven et al. The design of the traversing mechanism has not been considered in detail but it is thought that it will originate from inside the cylinder which will minimize the interference due to the presence of the probe. However, the limited rotation capability of the cylinder reduces the range of a probe fixed on the model.

A schematic of the surface hot wire mounted on the cylinder is shown in Figure 43 for the smooth cylinder. One concern is how their presence will affect transition and must be investigated. How the plugs will be mounted in the presence of the screens, if at all, have not been decided. The screen mounting scheme is

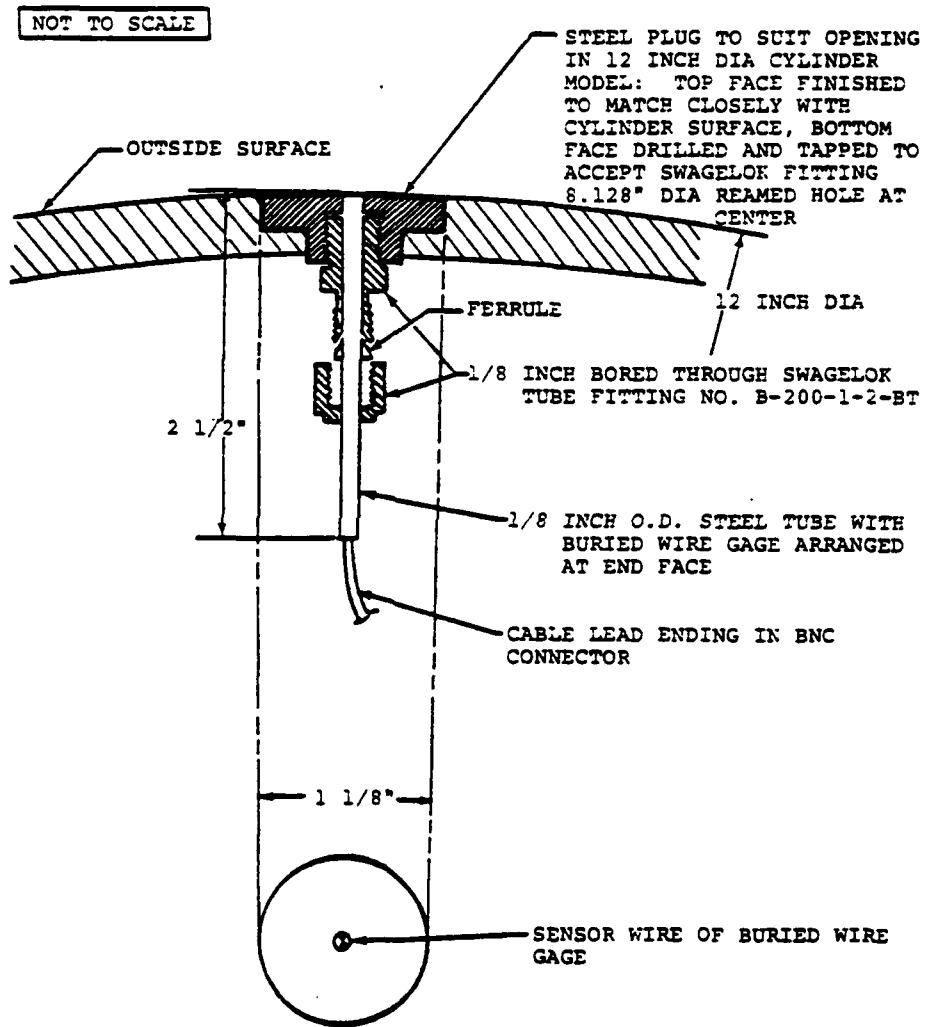


FIGURE 43. Hot-Wire Gauge Mount

shown in Figure 44. The safety wires are attached in the back of the model where they should not interfere with the flow process. The information or reduced data that will be derived from the measurements are summarized here in the order of ease of measuring as well as importance to the current program:

Mean Pressures as Function of Re, k/D:

Circumferential distribution-integrated drag,
Longitudinal distribution, two dimensionality,

Dynamic (Unsteady) Pressure as Function of Re, k/D

Circumferential distribution, lift, drag, power
spectral densities (PSD)
Longitudinal distribution, spanwise coherence,
instantaneous separation angle

Boundary Layer Characteristics as Function of Re, k/D

Velocity profile-boundary layer character,
transition
Surface shear-transition, separation, Strouhal
frequency

The proposed test matrix, Table 2, show the various configurations and run conditions anticipated. If necessary some of the runs can be eliminated; e.g., configuration 5, which investigates the effects of roughness spacing is not absolutely essential and the elimination of one other roughness is possible as well as reducing the number of Re for some of the configurations.

A discussion of end plate design philosophy was conducted by M. Morkovin. Most end plate designs are circular and symmetrical fore and aft of the model. This is not correct since the low momentum region of the cylinder flow should be protected and this is the base region of the cylinder where significant cross flow pressure gradients relative to the low momentum fluid can be

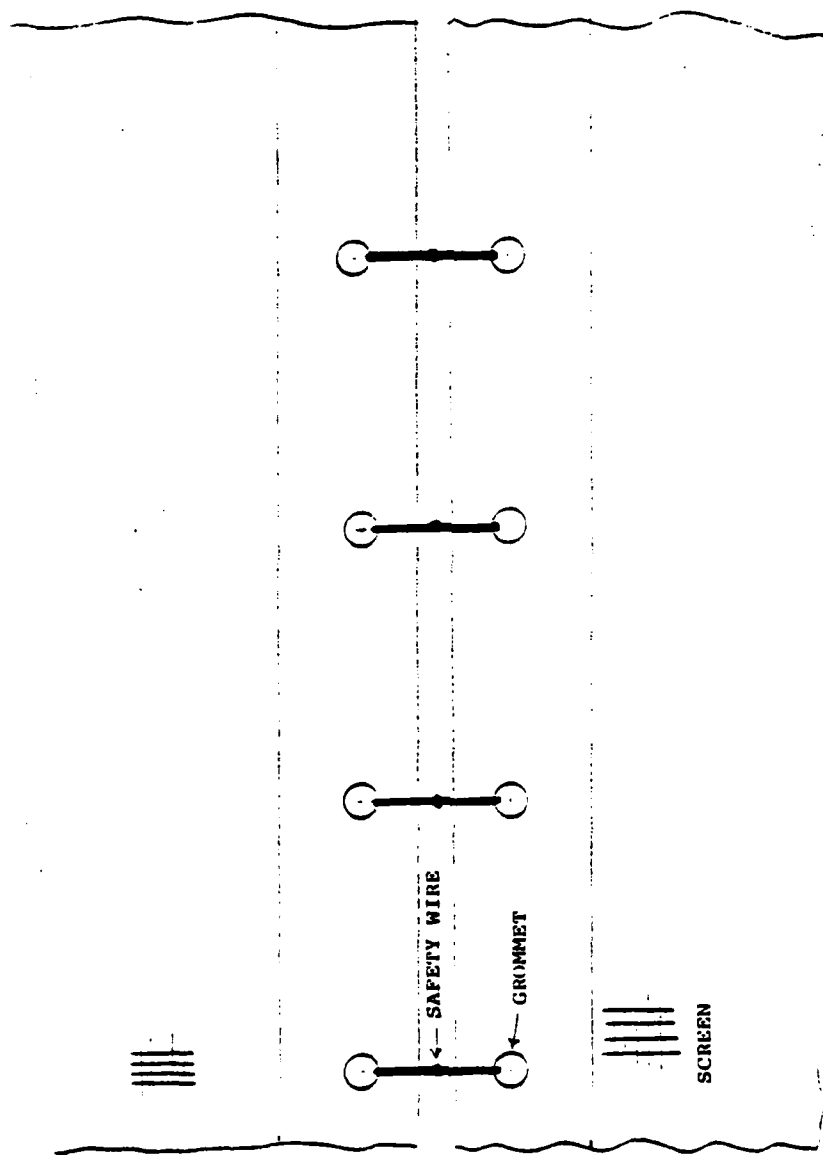


FIGURE 44. Grommet and Safety Wire Screen Attachment Design

TABLE 2. Proposed NASA Ames Test Matrix

CONF. CODE	CONFIGURATION	REYNOLDS NO. (10^6)						MODEL ROTATIONS (EACH REYNOLDS NO.) (DEGREES)	TUNNEL HOURS
		8	6	4	2	1	.3	.1	
1	SMOOTH	X	X	X	X	X	X	X	16
2	ROUGH ($k/d = 3 \times 10^{-4}$)	X	X	X	X	X	X	X	16
3	ROUGH ($k/d = 10^{-3}$)	X	X	X	X	X	X	X	16
4	ROUGH ($k/d = 10^{-2}$)	X	X	X	X	X	X	X	16
5	ROUGH ($k/d = 10^{-2}$) SPACING	X	X	X	X	X	X	X	16

TASK	HOURS
MODEL INSTALLATION/CHECKOUT	32
MODEL CHANGES	32
TOTAL HOURS	144

generated due to the existence of the wall boundary layer. In the front part of the cylinder, the induced gradients have a lesser effect so that there is no actual need to protect the cylinder flow from the wall boundary layer and in fact undesirable since the new boundary layer formed is laminar and experiences an adverse pressure gradient. Thus, the end plate should extend mostly downstream of the cylinder base and be a length such that it extends to the end of a closed recirculating base wake which depends on Re and requires some experimentation to determine. Upstream, the plate should extend no more than a boundary layer thickness or so and have a rounded leading edge. This design philosophy has been used with significant success at IIT.

Summary of Recommendations Made at the Workshop

The following is a summary of several items that were brought up during the course of the Workshop that should be considered during the experiment planning. They are not listed in any specific order.

1. End plate design should follow along the lines of Morkovin's suggestions.
2. Should investigate the question of coherence carefully with regards to the following items:

Surface roughness - isolated as well as distributed.

Additional outboard section instrumented with Kulites

Kulites at -90 and 180 degrees generators as well as at 90 degrees.

Fix separation with isolated stringers, vortex generators

Consult Morsbach thesis

3. Flow visualization using tufted grids, if they can be made to survive, with stroboscopic observations; the uninstrumented side of the cylinder could be used to

evaluate the effects of the pressure orifices and other ports on the flow using some form of flow visualization technique. An additional outboard station on the unused side may be informative.

4. For smooth cylinder, should acquire more data in the region just beyond critical-supercritical where the vortex shedding becomes coherent again in order to observe the transition process.

References for Section on Spanwise Nonuniformities
(By D. Coles)

- Blackiston, H. S. Jr., 1963, Tip effects on fluctuating lift and drag forces acting on a circular cylinder perpendicular to an air flow. AE Thesis, Calif. Inst. Tech.
- Bradbury, L. J. S. and Moss, W. D., 1975, Pulsed wire anemometer measurements in the flow past a normal flat plate in a uniform flow and in a sheared flow. Proc. 4th Int'l. Conf. on Wind Effects on Buildings and Structures, Heathrow, 485-496.
- Buell, D. A., McCullough, G. B., and Steinmetz, W. J., 1963, A wind-tunnel investigation of ground-wind loads on axisymmetric launch vehicles. NASA TN D-1893.
- Davies, M. E., 1975, The effects of turbulent shear flow on the critical Reynolds number of a circular cylinder. NPL (Marine Sciences), Rep. TM 108.
- Elder, J. W., 1959, Steady flow through non-uniform gauzes of arbitrary shape. J. Fluid Mech. 5, 355-368.
- Etzold, F. and Fiedler, H., 1976, The near-wake structure of a cantilevered cylinder in a cross-flow. Z. für Flugwissenschaften 24, 77-82.
- Farivar, D., 1975, An experimental investigation of uniform, and linearly sheared flows around cylinders of finite length, Ph.D. Thesis, Univ. Pennsylvania.
- Gaster, M., 1969, Vortex shedding from slender cones at low Reynolds numbers. J. Fluid Mech. 38, 565-576.
- Gerrard, J. H., 1966, The three-dimensional structure of the wake of a circular cylinder. J. Fluid Mech. 25, 143-164.
- Gould, R. W. E., Raymer, W. G., and Ponsford, P. J., 1968, Wind tunnel tests on chimneys of circular section at high Reynolds numbers. Proc. Symp. on Wind Effects on Buildings and Structures, Loughborough, Vol. I, Paper 10.
- Kistler, A. L. and Vrebalovich, T., 1966, Grid turbulence at large Reynolds numbers. J. Fluid Mech. 26, 37-47.
- Lagerstrom, P., 1964, Laminar flow theory. In "Theory of Laminar Flows", (F. K. Moore, ed.), Princeton Univ. Press, 20-285.
- Mair, W. A. and Stansby, P. K., 1975, Vortex wakes of bluff cylinders in shear flow. SIAM J. Appl. Math 28, 519-540.

AD-A105 088

PHYSICAL RESEARCH INC PALOS VERDES ESTATES CA
HIGH REYNOLDS NUMBER CYLINDER FLOW WORKSHOP, 27-28 NOVEMBER 197--ETC(U)
AUG 81 W C SHIH
PRI-LA-81-R003

F/G 20/4

N00014-79-C-0893

NL

UNCLASSIFIED

2 x 2
1/4 x 1/4
0-000



END
DATE
FILMED
10-81
DTIC

- Mau11, D. J., 1969, The wake characteristics of a bluff body in a shear flow. AGARD CP 48, "Aerodynamics of Atmospheric Shear Flows," 16.1-16.13.
- Mau11, D. J. and Young, R. A., 1972, Vortex shedding from a bluff body in a shear flow. IUTAM-IAHR Symp. on Flow-induced Structural Vibrations, Karlsruhe (Springer), 717-729.
- Mau11, D. J. and Young, R. A., 1973, Vortex shedding from bluff bodies in a shear flow. J. Fluid Mech. 60, 401-409.
- McKinney, L. W., 1960, Effects of fineness ratio and Reynolds number of the low-speed crosswind drag characteristics of circular and modified-square cylinders. NASA TN D-540.
- Naumann, A. and Quadflieg, H., 1968, Aerodynamic aspects of wind effects on cylindrical buildings. Proc. Symp. on Wind Effects on Buildings and Structures, Loughborough, Vol. I, Paper 9.
- Schmidt, L. V., 1963, Measurements of fluctuating air loads on a circular cylinder. Ph.D. Thesis, Calif. Inst. Tech.; see also J. Aircraft 2, 49-55, 1965.
- Spitzer, R. E., 1965, Measurement of unsteady pressures and wake fluctuations for flow over a cylinder at supercritical Reynolds numbers. AE Thesis, Calif. Inst. Tech.
- Sykes, D. M., 1962, The supersonic and low-speed flows past circular cylinders of finite length supported at one end. J. Fluid MEch. 12, 367-387.
- Wieselsberger, C., 1921, Neuere Feststellungen über die Gesetze des Flüssigkeits- und Luftwiderstandes. Phys. Zeitschrift 22, 321-328 (translated as "New data on the laws of fluid resistance," NACA TN 84, 1922). Data are tabulated in "Der Widerstand von Zylindern," Ergebnisse der Aerodynamischen Versuchsanstalt zu Göttingen, II Lieferung, Section IV-3-a, pp. 23-28, 1923.